

Structure Formation with Warm White Noise: Effects of Finite Number Density and Velocity Dispersion in Particle and Wave Dark Matter

Mustafa A. Amin^a, M. Sten Delos^b, Mehrdad Mirbabayi^c

^a*Department of Physics and Astronomy, Rice University, Houston, TX, 77005, U.S.A.*

^b*Carnegie Observatories, 813 Santa Barbara Street, Pasadena, CA 91101, USA*

^c*International Centre for Theoretical Physics, Trieste, Italy*

E-mail: mustafa.a.amin@rice.edu, mdelos@carnegiescience.edu,
mirbabayi@ictp.it

ABSTRACT: We investigate the evolution of density perturbations in dark matter with finite number density and velocity dispersion. Using a truncated BBGKY hierarchy, we derive analytical expressions for the dark matter power spectrum during radiation and matter domination. A component of *warm white noise* emerges in our analysis, which arises due to the finite number density and undergoes scale-dependent evolution because of the velocity dispersion. Although free streaming erases adiabatic initial perturbations on small scales, warm white noise persists below the free-streaming length and grows during matter domination, with growth suppressed below the dark matter Jeans length. Our calculated power spectra agree with N -body simulations in the linear regime and accurately predict halo mass functions in the nonlinear regime. Effects of warm white noise can emerge on observable quasi-linear scales for ultralight dark matter produced after inflation with a subhorizon correlation length. Our formalism is applicable to these scenarios (with de Broglie-scale quasi-particles), to cases in which dark matter includes macroscopic structures (such as primordial black holes), and to traditional warm and cold dark matter scenarios.

Contents

1	Introduction	2
1.1	Notation & Conventions	4
1.2	Summary of Derivation and Results	5
2	Derivation: from Liouville Equation to Power Spectrum Evolution	7
2.1	Evolution of the distribution function	9
2.1.1	Liouville Equation	9
2.1.2	BBGKY Hierarchy	9
2.1.3	Mayer Cluster Expansion	10
2.1.4	Statistical Homogeneity	10
2.2	Power Spectrum Evolution	11
2.2.1	Fundamental Solutions: the Growth Functions for Warm Dark Matter	13
2.2.2	Evolution from Adiabatic Initial Conditions	14
2.2.3	Evolution of White Noise	15
2.3	Power Spectrum Evolution in an Expanding Universe	17
2.3.1	The Main Result	18
2.3.2	Relevant Scales and Range of Validity	20
3	Comparison with N-body Simulations	22
3.1	White Noise in the Linear Regime	23
3.2	White Noise Beyond the Linear Regime	24
3.3	White Noise with Initial Adiabatic Perturbations	26
3.4	Halo Internal Structures	29
4	Generalizations	32
4.1	Warm Wave Dark Matter	32
4.2	Non-gravitational Interactions	33
4.3	Subdominant Fractions	34
4.4	Relativistic Physics	34
5	Summary & Conclusions	35
A	Diagrammatic Interpretation of the Growth Functions	47
B	Numerically Evaluating the Growth Functions	49
C	Fitting Functions and Approximate Evaluation of Power Spectrum	50
D	Example: the Uniform-Sphere Momentum Distribution	51

1 Introduction

There is significant evidence for the existence of dark matter from observations of cosmological structures on large scales (\gtrsim Mpc co-moving) [1, 2]. However, probing structure formation on smaller scales (\lesssim Mpc co-moving) offers a unique opportunity to uncover the microscopic nature of dark matter and its production mechanism. A variety of current and upcoming observations aim to probe the small-scale matter power spectrum [3]. These include analyses of the Lyman- α forest, galaxy satellite populations, gravitational lensing, stellar streams, 21-cm line intensity mapping, dynamical heating of stars, and the abundance of high-redshift galaxies [3–17]. To fully leverage these data, it is beneficial to develop theoretical models that connect the observed small-scale power spectrum to the microscopic properties and initial conditions of the dark matter.

On small scales, the linear matter power spectrum exhibits features that are sensitive to the nature of dark matter. For instance, in models with sufficient velocity dispersion in the early universe ($\gtrsim 10 \text{ km s}^{-1}$ at matter radiation equality), such as those involving “warm” dark matter, the adiabatic power spectrum is suppressed below co-moving scales of \sim Mpc. This “free-streaming suppression” has been extensively studied in microscopic particle dark matter models [18–34], and more recently in wave dark matter models [35–38].

Another universal feature emerges on sufficiently small scales where the Poissonian distribution of the underlying constituents of the dark matter becomes important. These constituents may be particles, quasi-particles in wave dark matter, primordial black holes [39], axion mini-clusters [40], solitons [41] or other bound structures (e.g. [42]). This Poissonian behavior introduces a white-noise component in the power spectrum at small scales. If the co-moving number density of these constituents is $\bar{n} \lesssim 10^8 \text{ Mpc}^{-3}$, then the resulting white-noise spectrum could fall within the reach of observational probes of structure in the quasi-linear regime ($k \lesssim 10 \text{ Mpc}^{-1}$), such as Lyman- α and 21-cm maps and the galaxy distribution. For higher \bar{n} , the white-noise contribution would boost dark matter substructure deep in the nonlinear regime, but the influence of such structure could still be detected. For example, effects on the power spectrum could be detected up to $k \sim 10^2 \text{ Mpc}^{-1}$ with strong lensing [6] and dwarf galaxy structures [12], up to $k \sim 10^3 \text{ Mpc}^{-1}$ with stellar kinematics [43], and up to k in excess of 10^6 Mpc^{-1} with pulsar timing [44–47] and microlensing of high-redshift stars [48, 49].

In this work, we focus on the evolution of this white-noise contribution in the presence of a velocity dispersion. We analytically derive the time evolution of the matter power spectrum during the radiation- and matter-dominated eras. Our result exhibits several key physical effects, which we illustrate in Figure 1. During the radiation era, free streaming erases initial (e.g., adiabatic) density perturbations, but it cannot erase the underlying Poisson distribution. During matter domination, that Poisson distribution can then give rise to gravitational clustering, even below the free-streaming length. The velocity dispersion instead suppresses perturbation growth below the Jeans length, which is smaller than the free-streaming length and shrinks further over time. We find excellent agreement between the analytically calculated power spectrum and N -body simulations. The analytic prediction also leads to accurate halo mass functions.

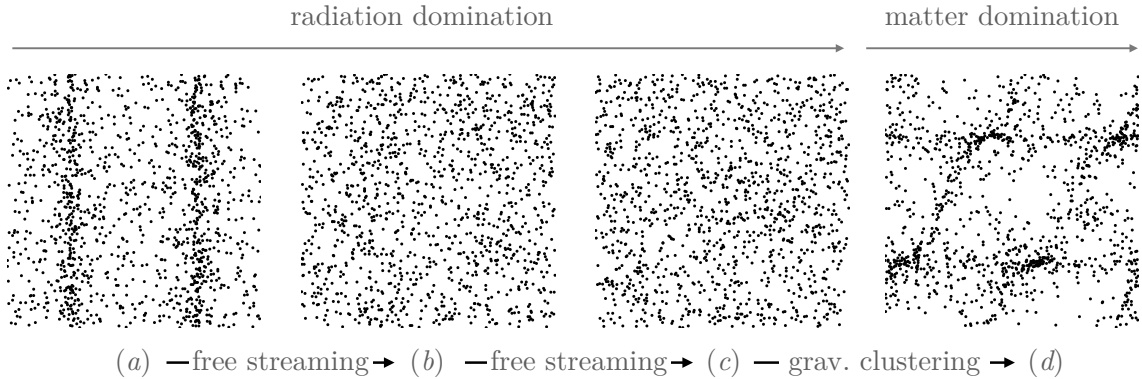


Figure 1: During radiation domination, free streaming erases existing correlations below the free-streaming length, revealing more of the underlying Poisson distribution of particles: (a) \rightarrow (b). However, free streaming cannot change the underlying Poisson distribution: (b) \rightarrow (c). During matter domination, gravitational clustering builds correlations above the Jeans length: (c) \rightarrow (d). The points could represent de Broglie-scale quasi-particles in wave dark matter, composite/macroscopic dark matter (including primordial black holes or substructures) or “usual” particle dark matter.

Our calculation of the power spectrum involves solving a truncated BBGKY (Bogoliubov–Born–Green–Kirkwood–Yvon) hierarchy. The setup, including the truncated BBGKY hierarchy, can be found in textbooks [50, 51]. The result for the free-streaming suppression for the adiabatic part is also well known. However, the form of the solution we are able to write down for the evolution of the white noise part is different from existing literature. In this solution, the connection between the shape of the initial phase space distribution function (DF) and the shape of the final power spectrum is transparent for both the adiabatic and white-noise parts.

Although our formalism rigorously applies to particle dynamics, we expect our results to approximately apply also to wave dark matter as long as we restrict ourselves to scales sufficiently larger than the de Broglie scale. Ultralight wave dark matter is of particular interest because it can simultaneously produce free-streaming suppression and white noise both at a level accessible to observations of quasi-linear structure [35]. For instance, if excitations of the dark matter field are produced after inflation, as in axion models with post-inflation Peccei–Quinn symmetry breaking, their finite correlation length leads to a clumpiness of the density field with an initially white noise spectrum. The same clumpiness also implies a non-trivial velocity dispersion. A simplified model would then be to introduce quasi-particles which represent the coherent patches and whose velocity dispersion that of the underlying wave dark matter field.¹ We expect that our formalism can be also extended to include additional effects present in wave dark matter at small scales.

Our present formalism is also specialized to non-relativistic gravitational dynamics of

¹Clumpiness at the de Broglie scale has been widely studied in the context of halos of ultralight dark matter [52–67]. In this case the velocity dispersion arises due to local gravitational clustering rather than early-universe initial conditions.

single-component dark matter, but it could be extended to include interactions beyond gravity, relativistic effects, and multi-component dark matter. Moreover, in the future, baryonic effects, which have been ignored in the present work, will need to be considered for detailed comparison with observations on small scales.

As an historical aside, the use of the Liouville equation and the (truncated) BBGKY hierarchy has a rich history in gravitational (and plasma) physics. One can derive fluid equations based on the collisionless Boltzmann equation, also called the Jeans or Vlasov equation [68, 69], which can then be solved with relative ease in many circumstances in cosmology (see for example, [70]). In our work, we are going beyond this collisionless equation to include collision terms, but with a simple truncation scheme that works in the linear regime of density fluctuations. For related earlier work, see for example refs. [71–73].

1.1 Notation & Conventions

The background Friedmann–Lemaître–Robertson–Walker spacetime is given by

$$ds^2 = -dt^2 + a^2(t)d\mathbf{x} \cdot d\mathbf{x}, \quad (1.1)$$

where $a(t)$ is the scale factor, \mathbf{x} are co-moving co-ordinates, and we set $c = 1$. We assume a background expansion history dominated by radiation and matter, with the Hubble expansion rate given by

$$H(y) = \frac{k_{\text{eq}}}{\sqrt{2}a_{\text{eq}}} y^{-2} \sqrt{1+y}, \quad \text{where } y \equiv \frac{a}{a_{\text{eq}}}. \quad (1.2)$$

The scale factor at matter-radiation equality is $a_{\text{eq}} \approx 1/3388$, and the co-moving wavenumber associated with the horizon size at that time is $k_{\text{eq}} = a_{\text{eq}}H(a_{\text{eq}}) \approx 0.01/\text{Mpc}$ [74].

Our Fourier conventions for finite volumes V and infinite volumes, respectively, are

$$\begin{aligned} f(\mathbf{x}) &= V^{-1} \sum_{\mathbf{k}} e^{i\mathbf{k} \cdot \mathbf{x}} f_{\mathbf{k}}, & f_{\mathbf{k}} &= \int_V d\mathbf{x} e^{-i\mathbf{k} \cdot \mathbf{x}} f(\mathbf{x}), & \int_V d\mathbf{x} e^{\pm i(\mathbf{k} + \mathbf{k}') \cdot \mathbf{x}} &= V \delta_{\mathbf{k}, -\mathbf{k}'}, \\ f(\mathbf{x}) &= \int \frac{d\mathbf{k}}{(2\pi)^3} e^{i\mathbf{k} \cdot \mathbf{x}} f(\mathbf{k}), & f(\mathbf{k}) &= \int d\mathbf{x} e^{-i\mathbf{k} \cdot \mathbf{x}} f(\mathbf{x}), & \int d\mathbf{x} e^{\pm i(\mathbf{k} + \mathbf{k}') \cdot \mathbf{x}} &= (2\pi)^3 \delta_D(\mathbf{k} + \mathbf{k}'). \end{aligned} \quad (1.3)$$

Here $\delta_{\mathbf{k}, -\mathbf{k}'}$ is the Kronecker delta and δ_D is the Dirac delta function. Note that the finite- and infinite-volume cases are linked by:

$$\begin{aligned} \int_{\mathbf{k}} &\longleftrightarrow \int \frac{d\mathbf{k}}{(2\pi)^3} &\longleftrightarrow \frac{1}{V} \sum_{\mathbf{k}}, \\ \delta_D(\mathbf{k} + \mathbf{k}') &\longleftrightarrow (2\pi)^3 \delta_D(\mathbf{k} + \mathbf{k}') &\longleftrightarrow V \delta_{\mathbf{k}, -\mathbf{k}'}, \end{aligned} \quad (1.4)$$

and formally $V \leftrightarrow (2\pi)^3 \delta_D(\mathbf{0})$. The first entry on each line of equation (1.4) represents the shorthand notation

$$f(\mathbf{x}) = \int_{\mathbf{k}} e^{i\mathbf{k} \cdot \mathbf{x}} f_{\mathbf{k}}, \quad f_{\mathbf{k}} = \int_{\mathbf{x}} e^{-i\mathbf{k} \cdot \mathbf{x}} f(\mathbf{x}), \quad \int_{\mathbf{x}} e^{\pm i(\mathbf{k} + \mathbf{k}') \cdot \mathbf{x}} = \delta_D(\mathbf{k} + \mathbf{k}'), \quad (1.5)$$

where the integral without the explicit measure can stand in for finite- or infinite-volume cases.

For a statistically homogeneous field f , the power spectrum P_f is defined:

$$\langle f(\mathbf{k})f(\mathbf{k}') \rangle = (2\pi)^3 P_f(\mathbf{k}) \delta_D(\mathbf{k} + \mathbf{k}'), \quad \langle f_{\mathbf{k}} f_{\mathbf{k}'} \rangle = V P_f(\mathbf{k}) \delta_{\mathbf{k}, -\mathbf{k}'}. \quad (1.6)$$

1.2 Summary of Derivation and Results

Section 2 of this paper is devoted to deriving the power spectrum P_δ of the field of density contrasts $\delta(\mathbf{x}) = [\rho(\mathbf{x}) - \bar{\rho}]/\bar{\rho}$. Here is a schematic representation of our derivation:

$$\begin{array}{c}
 P_\delta(t, k) \\
 \uparrow \\
 \underbrace{f^{(2)}(t, \mathbf{x}_1, \mathbf{x}_2, \mathbf{p}_1, \mathbf{p}_2)}_{\text{2-particle phase space distribution function}} \\
 \uparrow \\
 \underbrace{\mathcal{L}_t^{(1)} f^{(1)}(t, \mathbf{p}_1) = S[f^{(2)}], \quad \mathcal{L}_t^{(2)} f^{(2)}(t, \mathbf{x}_1, \mathbf{x}_2, \mathbf{p}_1, \mathbf{p}_2) \approx S[f^{(1)}]}_{\text{(truncated) BBGKY hierarchy}},
 \end{array} \tag{1.7}$$

where $\mathcal{L}_t^{(1,2)}$ symbolically represent time-evolution operators and $S[f^{(1,2)}]$ are source functions in the evolution equations. The input will be the initial 1-particle phase space distribution function (DF) $f^{(1)}(t_0, \mathbf{p}) = f_0(p)$, and initial adiabatic perturbations if they exist. We restrict ourselves to non-relativistic particles, clustering under Newtonian gravity in an expanding universe. While not necessary in the early parts of the derivation, the final results assume statistical homogeneity and isotropy.

The final result can be written as follows:

$$P_\delta(y, k) = \underbrace{P_{\delta_{\text{ad}}}(y_0, k) \left[\mathcal{T}_k^{\text{ad}}(y, y_0) \right]^2}_{\text{adiabatic IC + evolution}} + \frac{1}{\bar{n}} \underbrace{\left[1 + 3 \int_{y_0}^y \frac{dy'}{\sqrt{1+y'}} \mathcal{T}_k^{(a)}(y, y') \mathcal{T}_k^{(b)}(y, y') \right]}_{\text{white noise IC + evolution}}, \tag{1.8}$$

where $y = a/a_{\text{eq}}$ and y_0 is at an initial time when all wavenumber- k modes of interest are subhorizon and the “particles” of interest are non-relativistic; the initial conditions (IC) are specified at that time. Here, \bar{n} is the co-moving number density of “particles”. The three different $\mathcal{T}_k^{\text{ad},(a),(b)}$ in the above expressions are growth functions, which describe how density perturbations evolve due to gravitational clustering and free streaming. They are given by:

$$\begin{aligned}
 \mathcal{T}_k^{\text{ad}}(y, y_0) &= \mathcal{T}_k^{(a)}(y, y_0) + \frac{1}{2} \frac{d \ln P_{\delta_{\text{ad}}}(y_0, k)}{d \ln y_0} \sqrt{1+y_0} \mathcal{T}_k^{(b)}(y, y_0), \\
 \mathcal{T}_k^{(a)}(y, y') &= T_{\text{fs}}(y, y', k) + \frac{3}{2} \int_{y'}^y \frac{dy''}{\sqrt{1+y''}} \mathcal{T}_k^{(b)}(y, y'') T_{\text{fs}}(y'', y', k), \\
 \mathcal{T}_k^{(b)}(y, y') &= \mathcal{F}(y, y') T_{\text{fs}}(y, y', k) + \frac{3}{2} \int_{y'}^y \frac{dy''}{\sqrt{1+y''}} \mathcal{T}_k^{(b)}(y'', y') \mathcal{F}(y, y'') T_{\text{fs}}(y, y'', k).
 \end{aligned} \tag{1.9}$$

Here, $\mathcal{F}(y, y') = \ln [(y/y')(1 + \sqrt{1+y'})^2 / (1 + \sqrt{1+y})^2]$ captures the functional dependence of the co-moving distance traveled by non-relativistic particles during the time interval between y' and y . These equations also rely on the free-streaming “transfer function”, T_{fs} , which can be calculated based on an (isotropic) initial phase space distribution function $f_0(p)$ as

$$T_{\text{fs}}(y, y', k) = 4\pi \int dp p^2 f_0(p) \text{sinc} \left[\frac{p}{ma_{\text{eq}}} \frac{k}{k_{\text{eq}}} \sqrt{2} \mathcal{F}(y, y') \right], \tag{1.10}$$

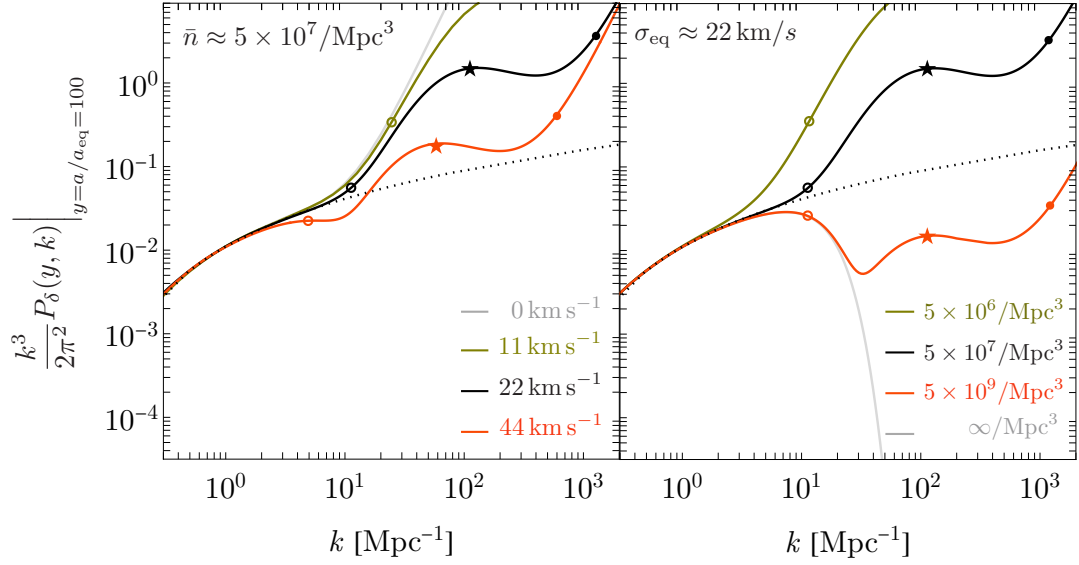


Figure 2: Small length-scale features in the dimensionless density power spectrum depend on the co-moving number \bar{n} (setting the amplitude of the white noise contribution) and 1D velocity dispersion σ_{eq} (at matter-radiation equality, which determines the free-streaming and Jeans scales). For the left panel, we keep \bar{n} fixed, whereas on the right σ_{eq} is held fixed. We show power spectra at $y = a/a_{\text{eq}} = 100$, and the filled dots indicate the Jeans scales k_J at this time, whereas the stars are the Jeans scales $k_{J,\text{eq}}$ at $y = 1$. The open circles indicate the free-streaming scale k_{fs} . The dotted curve is the “usual” cold dark matter (CDM) without any significant velocity dispersion or white noise ($\bar{n}, \sigma_{\text{eq}} \rightarrow (0, \infty)$). Existing observations in the quasi-linear regime only permit major deviations from the dotted curve for $k \gtrsim 10 \text{ Mpc}^{-1}$.

where m is the particle mass, and $\text{sinc}(x) = \sin(x)/x$.

The only equation that is nontrivial to solve is the Volterra integral equation for $\mathcal{T}_k^{(b)}$. We provide an efficient numerical algorithm for evaluating the $\mathcal{T}_k^{\text{ad},(a),(b)}$ and the power spectrum P_δ at <https://github.com/delos/warm-structure-growth>.

Our result for the scale-dependent evolution of the power spectrum exhibits the following key features:

1. A free-streaming cutoff in the adiabatic spectrum, arising due to erasure of existing correlations (such as initial adiabatic power) below the free-streaming length.
2. Suppression of gravitational growth of the initial Poisson noise below the Jeans length.

The free streaming length is the distance traveled by dark matter particles up to a given time, whereas the Jeans length is essentially the distance they travel over a Hubble time. Figure 2 shows examples of the total power spectrum that can emerge after the two aforementioned effects. Depending on the co-moving number density \bar{n} and the velocity dispersion of the dark matter, the dimensionless power spectrum can begin to dip at $k \gtrsim k_{\text{fs}}$ due to the free-streaming suppression before rising again due to the white noise (an effect

previously noticed by refs. [35, 37]). Due to the Jeans suppression, the white-noise component of the dimensionless power spectrum shallows for $k \gtrsim k_{\text{J,eq}}$ (the Jeans wavenumber at matter-radiation equality). This characteristic behavior is a consequence of delayed growth at small scales: modes with $k > k_{\text{J,eq}}$ do not begin to grow around matter-radiation equality, and their growth only begins when the Jeans wavenumber $k_{\text{J}} = k_{\text{J,eq}} \sqrt{a/a_{\text{eq}}}$ eventually rises to be of order k .²

Section 2.3.1 further details the time evolution of the adiabatic and white-noise contributions to the power spectrum (see Figs. 3 and 4). We also show in section 3 that the power spectrum we derive matches N -body simulations during radiation and matter domination as long fractional perturbations are small (see Figs. 6 and 8), and moreover, that when fractional perturbations are large, it provides a critical input to accurately calculate the abundance of dark matter halos (see Figs. 7 and 9).

On a technical note, we begin with the full BBGKY hierarchy which results from the Liouville equation (see for example [51]). The tractability of our calculation relies on assuming that the connected part (in the sense of the Mayer Cluster expansion [75]) of the 3-particle DF is negligible, and that the connected 2-particle DF is small compared to the disconnected one. The former allows us to truncate the BBGKY hierarchy, and the latter reduces the problem to a single first-order (in time) partial differential equation for the 2-particle DF. The adiabatic part of the power spectrum evolves via the homogeneous solution of this equation in Fourier space. The inhomogeneous solution yields the evolution of white noise.

2 Derivation: from Liouville Equation to Power Spectrum Evolution

For the sake of simplicity, we initially ignore cosmic expansion in the derivation. It is re-instated in the final results by appropriate transformation from physical to co-moving co-ordinates and a motivated choice of time variable.

Consider an ensemble of “systems”, each having N identical particles confined to a volume V . Each particle has the mass m . The position and momentum of the i th particle are \mathbf{x}_i and $\mathbf{p}_i = m\dot{\mathbf{x}}_i$. The particles interact via Newtonian gravity, so the force acting on the i th particle is

$$\dot{\mathbf{p}}_i = -m \sum_{j=1, j \neq i}^N \nabla_{\mathbf{x}_i} \Psi(|\mathbf{x}_i - \mathbf{x}_j|), \quad \text{where} \quad \Psi(r) = -\frac{Gm}{r}. \quad (2.1)$$

For each system, the mass density at any given time $\rho(t, \mathbf{x}) = m \sum_{i=1}^N \delta_D(\mathbf{x} - \mathbf{x}_i)$, with a Fourier transform $\rho_{\mathbf{k}}(t) = m \sum_{i=1}^N e^{-i\mathbf{k} \cdot \mathbf{x}_i}$. Our main goal is understanding the time-evolution of the two-point correlation function $\langle \rho_{\mathbf{k}}(t) \rho_{\mathbf{k}'}(t) \rangle$, where $\langle \dots \rangle$ indicate an ensemble average. This correlation function can be written as a sum of a “diagonal” and

²These scalings imply that the power spectrum for $k_{\text{J,eq}} \ll k \ll k_{\text{J}}$ would approach $P_{\delta}(k) \propto k^{-4}$ or $[k^3/(2\pi^2)]P_{\delta}(k) \propto k^{-1}$. In practice, the matter-dominated epoch is not long enough for this asymptotic scaling to emerge cleanly.

“off-diagonal” piece:

$$\frac{1}{m^2} \langle \rho_{\mathbf{k}}(t) \rho_{\mathbf{k}'}(t) \rangle = \sum_{i=1}^N \langle e^{-i(\mathbf{k}+\mathbf{k}') \cdot \mathbf{x}_i} \rangle + \sum_{i=1}^N \sum_{j=1, j \neq i}^N \langle e^{-i(\mathbf{k} \cdot \mathbf{x}_i + \mathbf{k}' \cdot \mathbf{x}_j)} \rangle. \quad (2.2)$$

Here $\langle A \rangle \equiv \int \prod_{i=1}^N d\mathbf{x}_i d\mathbf{p}_i F(t, \mathbf{x}_1, \dots, \mathbf{x}_N, \mathbf{p}_1, \dots, \mathbf{p}_N) A(t, \mathbf{x}_1, \dots, \mathbf{x}_N, \mathbf{p}_1, \dots, \mathbf{p}_N)$. Here, $F(t, \mathbf{x}_1, \dots, \mathbf{x}_N, \mathbf{p}_1, \dots, \mathbf{p}_N) \prod_{i=1}^N d\mathbf{x}_i d\mathbf{p}_i$ is the probability of a system being in a state so that particle 1 is within the phase space volume $d\mathbf{x}_1 d\mathbf{p}_1$ around the point $(\mathbf{x}_1, \mathbf{p}_1)$, particle 2 is within the phase space volume $d\mathbf{x}_2 d\mathbf{p}_2$ around the point $(\mathbf{x}_2, \mathbf{p}_2)$ and so on. Since no particle is special,

$$\frac{1}{m^2} \langle \rho_{\mathbf{k}}(t) \rho_{\mathbf{k}'}(t) \rangle = N \langle e^{-i(\mathbf{k}+\mathbf{k}') \cdot \mathbf{x}_1} \rangle + N(N-1) \langle e^{-i(\mathbf{k} \cdot \mathbf{x}_1 + \mathbf{k}' \cdot \mathbf{x}_2)} \rangle. \quad (2.3)$$

So, to evaluate the expectation values, we only need the marginalized probability densities:

$$\begin{aligned} P(t, \mathbf{x}_1) &= \int d\mathbf{p}_1 \prod_{i=2}^N d\mathbf{x}_i d\mathbf{p}_i F(t, \mathbf{x}_1, \dots, \mathbf{x}_N, \mathbf{p}_1, \dots, \mathbf{p}_N) \equiv \int d\mathbf{p}_1 \frac{f^{(1)}(t, \mathbf{x}_1, \mathbf{p}_1)}{V}, \\ P(t, \mathbf{x}_1, \mathbf{x}_2) &= \int d\mathbf{p}_1 d\mathbf{p}_2 \prod_{i=3}^N d\mathbf{x}_i d\mathbf{p}_i F(t, \mathbf{x}_1, \dots, \mathbf{x}_N, \mathbf{p}_1, \dots, \mathbf{p}_N) \equiv \int d\mathbf{p}_1 d\mathbf{p}_2 \frac{f^{(2)}(t, \mathbf{x}_1, \mathbf{x}_2, \mathbf{p}_1, \mathbf{p}_2)}{V^2}, \end{aligned} \quad (2.4)$$

where we defined the 1 and 2 particle phase-space distribution functions $f^{(1)}$ and $f^{(2)}$. These functions (or more specifically, the spatial Fourier transform) are what we need to find the two point correlation function. While it might seem that we would need the solution of the $6N$ dimensional F to calculate $f^{(1)}$ and $f^{(2)}$, it turns out that under certain approximations which hold for our system of interest, a closed set of coupled equations for $f^{(1)}$ and $f^{(2)}$ can be derived. In the following sections, we will begin with the equations for the $6N$ -dimensional F . We will then arrive at a coupled set of equations for $f^{(1)}$ and $f^{(2)}$. Indeed, it turns out that we only need the time evolution of $f^{(2)}$.

To see some of this simplification, note that under the assumption of (statistical) spatial homogeneity and isotropy, $f^{(1)}(t, \mathbf{x}_1, \mathbf{p}_1) \rightarrow f^{(1)}(t, \mathbf{p}_1)$ and $f^{(2)}(t, \mathbf{x}_1, \mathbf{x}_2, \mathbf{p}_1, \mathbf{p}_2) \rightarrow f^{(2)}(t, |\mathbf{x}_1 - \mathbf{x}_2|, \mathbf{p}_1, \mathbf{p}_2)$. In this case, evaluating the ensemble averages in eq. (2.3) yields

$$\frac{1}{\bar{\rho}^2} \langle \rho_{\mathbf{k}}(t) \rho_{\mathbf{k}'}(t) \rangle = \frac{1}{\bar{n}} \left[1 + \bar{n} \int d\mathbf{p}_1 d\mathbf{p}_2 f_k^{(2)}(t, \mathbf{p}_1, \mathbf{p}_2) \right] V \delta_{\mathbf{k}, -\mathbf{k}'}, \quad (2.5)$$

where $f_k^{(2)}(t, \mathbf{p}_1, \mathbf{p}_2) = \int_{\mathbf{y}} e^{-i\mathbf{k} \cdot \mathbf{y}} f^{(2)}(t, |\mathbf{y}|, \mathbf{p}_1, \mathbf{p}_2)$, and we defined $\bar{n} = N/V \approx (N-1)/V$ and used that $\bar{\rho} = m\bar{n}$. The first term is the Poisson noise. The second term, which contains the time evolution, is entirely determined by $f_k^{(2)}$. So our goal is to solve for the time evolution of this momentum integral of $f_k^{(2)}$. We will also need an initial condition $f_k^{(2)}(t_0, \mathbf{p}_1, \mathbf{p}_2)$. We will consider two cases: zero initial correlation, corresponding to $f_k^{(2)}(t_0, \mathbf{p}_1, \mathbf{p}_2) = 0$ (for $k > 0$), and correlations set in accordance with the initial adiabatic density power spectrum, corresponding to $\int d\mathbf{p}_1 d\mathbf{p}_2 f_k^{(2)}(t_0, \mathbf{p}_1, \mathbf{p}_2) = P_{\delta_{\text{ad}}}(t_0, k)$.

2.1 Evolution of the distribution function

2.1.1 Liouville Equation

The probability density F over the $6N$ -dimensional phase space satisfies the Liouville equation [76]:

$$\partial_t F + \sum_{i=1}^N \dot{\mathbf{x}}_i \cdot \nabla_{\mathbf{x}_i} F + \sum_{i=1}^N \dot{\mathbf{p}}_i \cdot \nabla_{\mathbf{p}_i} F = 0, \quad (2.6)$$

where $\dot{\mathbf{x}}_i = \mathbf{p}_i/m$ and $\dot{\mathbf{p}}_i$ is given by eq. (2.1). It is convenient to define the acceleration of the i th particle due to the force from the j th one as

$$\mathbf{a}_{ij} \equiv -\nabla_{\mathbf{x}_i} \Psi(|\mathbf{x}_i - \mathbf{x}_j|) = -Gm \frac{\mathbf{x}_i - \mathbf{x}_j}{|\mathbf{x}_i - \mathbf{x}_j|^3}, \quad (2.7)$$

if $i \neq j$, and $\mathbf{a}_{ii} = 0$. Then the total acceleration of the i th particle is

$$\frac{\dot{\mathbf{p}}_i}{m} = \mathbf{a}_i = \sum_{j=1}^N \mathbf{a}_{ij}, \quad (2.8)$$

and the Liouville equation becomes

$$\partial_t F + \frac{1}{m} \sum_{i=1}^N \mathbf{p}_i \cdot \nabla_{\mathbf{x}_i} F + m \sum_{i=1}^N \sum_{j=1}^N \mathbf{a}_{ij} \cdot \nabla_{\mathbf{p}_i} F = 0. \quad (2.9)$$

2.1.2 BBGKY Hierarchy

The Liouville equation is equivalent to the BBGKY hierarchy of equations for the reduced s -particle distributions:

$$\frac{f^{(s)}(\mathbf{x}_1, \dots, \mathbf{x}_s, \mathbf{p}_1, \dots, \mathbf{p}_s)}{V^s} = \int \prod_{i=s+1}^N d\mathbf{x}_i d\mathbf{p}_i F(\mathbf{x}_1, \dots, \mathbf{x}_N, \mathbf{p}_1, \dots, \mathbf{p}_N). \quad (2.10)$$

The details of this derivation can be found in textbooks; we follow ref. [50] except that we use momentum instead of velocity. For $s < N$, the evolution of the s -particle distribution depends on the $(s+1)$ -particle distribution:

$$\begin{aligned} \partial_t f^{(s)} + \frac{1}{m} \sum_{i=1}^s \mathbf{p}_i \cdot \nabla_{\mathbf{x}_i} f^{(s)} + m \sum_{i=1}^s \sum_{j=1}^s \mathbf{a}_{ij} \cdot \nabla_{\mathbf{p}_i} f^{(s)} \\ = -m \frac{(N-s)}{V} \sum_{i=1}^s \int d\mathbf{x}_{s+1} d\mathbf{p}_{s+1} \mathbf{a}_{i,s+1} \cdot \nabla_{\mathbf{p}_i} f^{(s+1)}. \end{aligned} \quad (2.11)$$

In particular, for $s = 1, 2$, we have the following equations for the reduced distributions $f^{(1)}(t, \mathbf{x}_1, \mathbf{p}_1)$ and $f^{(2)}(t, \mathbf{x}_1, \mathbf{x}_2, \mathbf{p}_1, \mathbf{p}_2)$:

$$\partial_t f^{(1)} + \frac{1}{m} \mathbf{p}_1 \cdot \nabla_{\mathbf{x}_1} f^{(1)} = -m \frac{(N-1)}{V} \int d\mathbf{x}_2 d\mathbf{p}_2 \mathbf{a}_{12} \cdot \nabla_{\mathbf{p}_1} f^{(2)}, \quad (2.12)$$

$$\begin{aligned}
& \partial_t f^{(2)} + \frac{1}{m} (\mathbf{p}_1 \cdot \nabla_{\mathbf{x}_1} + \mathbf{p}_2 \cdot \nabla_{\mathbf{x}_2}) f^{(2)} + m (\mathbf{a}_{12} \cdot \nabla_{\mathbf{p}_1} + \mathbf{a}_{21} \cdot \nabla_{\mathbf{p}_2}) f^{(2)} \\
& = -m \frac{(N-2)}{V} \int d\mathbf{x}_3 d\mathbf{p}_3 (\mathbf{a}_{13} \cdot \nabla_{\mathbf{p}_1} + \mathbf{a}_{23} \cdot \nabla_{\mathbf{p}_2}) f^{(3)}.
\end{aligned} \tag{2.13}$$

with $f^{(3)} = f^{(3)}(t, \mathbf{x}_1, \mathbf{x}_2, \mathbf{x}_3, \mathbf{p}_1, \mathbf{p}_2, \mathbf{p}_3)$. Note that this is not a closed system, since an equation for $f^{(3)}$ has not been specified in terms of $f^{(2)}$ and $f^{(1)}$.

2.1.3 Mayer Cluster Expansion

Without loss of generality, we express the reduced distributions $f^{(s)}$ using the Mayer cluster expansion [50]:

$$\begin{aligned}
f^{(1)}(1) &= f(1), \\
f^{(2)}(12) &= f(1)f(2) + g(12), \\
f^{(3)}(123) &= f(1)f(2)f(3) + f(1)g(23) + f(2)g(13) + f(3)g(12) + h(123),
\end{aligned} \tag{2.14}$$

where we have adopted the shorthand $f(1) = f(t, \mathbf{x}_1, \mathbf{p}_1)$, $g(12) = g(t, \mathbf{x}_1, \mathbf{x}_2, \mathbf{p}_1, \mathbf{p}_2)$, and so on. The function g is the connected two-particle correlation function, while h is the three-particle counterpart. We assume that these correlation functions are small: $g \ll ff$, $h \ll gf$. In particular, we will approximate $h = 0$, so that we have a closed set of equations for g and f . These assumptions are expected to hold as long as fractional density perturbations are $\ll 1$. To reduce clutter, since $N \gg 1$, we set $(N-1)/V \approx (N-2)/V \approx N/V \equiv \bar{n} = \bar{\rho}/m$.

With these assumptions, and adopting the notation $d2 = d\mathbf{x}_2 d\mathbf{p}_2$ and so on, eq. (2.12) becomes

$$\partial_t f(1) + \frac{1}{m} \mathbf{p}_1 \cdot \nabla_{\mathbf{x}_1} f(1) + \left[\bar{\rho} \int d2 \mathbf{a}_{12} f(2) \right] \cdot \nabla_{\mathbf{p}_1} f(1) = -\bar{\rho} \int d2 \mathbf{a}_{12} \cdot \nabla_{\mathbf{p}_1} g(12). \tag{2.15}$$

Similarly eq. (2.13) for $f^{(2)}$ can be converted to an equation for g (after using eq. (2.15) for $f(1)$) to get

$$\begin{aligned}
& \partial_t g(12) + \frac{1}{m} (\mathbf{p}_1 \cdot \nabla_{\mathbf{x}_1} + \mathbf{p}_2 \cdot \nabla_{\mathbf{x}_2}) g(12) + m (\mathbf{a}_{12} \cdot \nabla_{\mathbf{p}_1} + \mathbf{a}_{21} \cdot \nabla_{\mathbf{p}_2}) g(12) \\
& + \bar{\rho} \int d3 \{ \mathbf{a}_{13} \cdot \nabla_{\mathbf{p}_1} [f(1)g(23) + f(3)g(12)] + \mathbf{a}_{23} \cdot \nabla_{\mathbf{p}_2} [f(2)g(13) + f(3)g(12)] \} \\
& = -m (\mathbf{a}_{12} \cdot \nabla_{\mathbf{p}_1} + \mathbf{a}_{21} \cdot \nabla_{\mathbf{p}_2}) f(1)f(2).
\end{aligned} \tag{2.16}$$

2.1.4 Statistical Homogeneity

We assume that we are dealing with systems that are statistically homogeneous and isotropic in space. That is, we assume the following forms for f and g :

$$f(1) = f(t, \mathbf{p}_1), \quad g(12) = g(t, |\mathbf{x}_1 - \mathbf{x}_2|, \mathbf{p}_1, \mathbf{p}_2). \tag{2.17}$$

Then eq. (2.15) for $f(1)$ simplifies to

$$\partial_t f(t, \mathbf{p}_1) = -\bar{\rho} \int d2 \mathbf{a}_{12} \cdot \nabla_{\mathbf{p}_1} g(12), \tag{2.18}$$

where we used

$$\int d2 \mathbf{a}_{12} f(2) = 0, \quad (2.19)$$

which follows from statistical homogeneity.

Turning to eq. (2.16) for $g(12)$, we drop a term of order g/ff (in comparison with the “source” term on the right-hand side) and use eq. (2.19) to get

$$\begin{aligned} \partial_t g(12) + \frac{1}{m} (\mathbf{p}_1 \cdot \nabla_{\mathbf{x}_1} + \mathbf{p}_2 \cdot \nabla_{\mathbf{x}_2}) g(12) + \bar{\rho} \int d3 [g(23) \mathbf{a}_{13} \cdot \nabla_{\mathbf{p}_1} f(t, \mathbf{p}_1) + g(13) \mathbf{a}_{23} \cdot \nabla_{\mathbf{p}_2} f(t, \mathbf{p}_2)] \\ = -m (\mathbf{a}_{12} \cdot \nabla_{\mathbf{p}_1} + \mathbf{a}_{21} \cdot \nabla_{\mathbf{p}_2}) f(t, \mathbf{p}_1) f(t, \mathbf{p}_2). \end{aligned} \quad (2.20)$$

To calculate the time-evolution of the density power spectrum, we will be interested in g only; see eq. (2.23). Since the time variation of f depends on g which is supposed to be “small”, at leading order we can ignore the time variation of f in the equation for g . We will also assume that this initial f is isotropic in momentum. These considerations mean that we use $f(t, \mathbf{p}) \approx f(t_0, p) \equiv f_0(p)$ in eq. (2.20), yielding:

$$\begin{aligned} \partial_t g(12) + \frac{1}{m} (\mathbf{p}_1 \cdot \nabla_{\mathbf{x}_1} + \mathbf{p}_2 \cdot \nabla_{\mathbf{x}_2}) g(12) + \bar{\rho} \int d3 [g(23) \mathbf{a}_{13} \cdot \nabla_{\mathbf{p}_1} f_0(p_1) + g(13) \mathbf{a}_{23} \cdot \nabla_{\mathbf{p}_2} f_0(p_2)] \\ = -m (\mathbf{a}_{12} \cdot \nabla_{\mathbf{p}_1} + \mathbf{a}_{21} \cdot \nabla_{\mathbf{p}_2}) f_0(p_1) f_0(p_2). \end{aligned} \quad (2.21)$$

We expect our assumption that the time variation in f can be ignored to eventually break down when the velocity dispersion generated by gravitational clustering becomes comparable to the input velocity dispersion.

Equations and some solutions for the evolution of $f(1)$ and $g(12)$ were written down in the 1970s to understand the growth of correlations from an initially uncorrelated, statistically homogeneous and isotropic collection of point particles (see for example, [72, 73], and also [71]). However, the general form of the solutions we obtain for the evolution of the power spectrum in radiation and matter dominated eras were not provided in these works.

2.2 Power Spectrum Evolution

Recall that we wish to understand the evolution of the power spectrum of density perturbations:

$$\langle \delta_{\mathbf{k}_1}(t) \delta_{\mathbf{k}_2}(t) \rangle \equiv P_\delta(t, k_1) \delta_D(\mathbf{k}_1 + \mathbf{k}_2), \quad (2.22)$$

where $\delta_{\mathbf{k}}(t) = \rho_{\mathbf{k}}(t)/\bar{\rho}$ and $\delta_D(\mathbf{k}_1 + \mathbf{k}_2) = (2\pi)^3 \delta_D(\mathbf{k}_1 + \mathbf{k}_2) \leftrightarrow V \delta_{\mathbf{k}_1, -\mathbf{k}_2}$. The time evolution of the power spectrum can be expressed in terms of Fourier transforms of the connected

2-point correlation function $g(12)$ as

$$\begin{aligned}
P_\delta(t, k_1) \delta_D(\mathbf{k}_1 + \mathbf{k}_2) &= \frac{1}{\bar{n}} \left[1 + \bar{n} \int d\mathbf{p}_1 d\mathbf{p}_2 \tilde{g}_{k_1}(t, \mathbf{p}_1, \mathbf{p}_2) \right] \delta_D(\mathbf{k}_1 + \mathbf{k}_2), \\
&= \underbrace{\frac{1}{\bar{n}} \delta_D(\mathbf{k}_1 + \mathbf{k}_2)}_{\text{white noise}} + \underbrace{\int d\mathbf{p}_1 d\mathbf{p}_2 g_{\mathbf{k}_1 \mathbf{k}_2}(t, \mathbf{p}_1, \mathbf{p}_2)}_{\text{time evolution of correlations}}, \\
&= \underbrace{\frac{1}{\bar{n}} \delta_D(\mathbf{k}_1 + \mathbf{k}_2) + \int d\mathbf{p}_1 d\mathbf{p}_2 g_{\mathbf{k}_1 \mathbf{k}_2}^{S \neq 0}(t, \mathbf{p}_1, \mathbf{p}_2)}_{P_{\delta_{\text{wn}}}(t, k_1) \delta_D(\mathbf{k}_1 + \mathbf{k}_2)} + \underbrace{\int d\mathbf{p}_1 d\mathbf{p}_2 g_{\mathbf{k}_1 \mathbf{k}_2}^{S=0}(t, \mathbf{p}_1, \mathbf{p}_2)}_{P_{\delta_{\text{ad}}}(t, k_1) \delta_D(\mathbf{k}_1 + \mathbf{k}_2)}.
\end{aligned} \tag{2.23}$$

In the above equations, we have assumed a statistically homogeneous and isotropic ensemble (see (2.5)), where $\tilde{g}_k(t, \mathbf{p}_1, \mathbf{p}_2)$ is the Fourier transform of $g(12) = g(t, |\mathbf{x}_1 - \mathbf{x}_2|, \mathbf{p}_1, \mathbf{p}_2)$, whereas $g_{\mathbf{k}_1 \mathbf{k}_2}(t, \mathbf{p}_1, \mathbf{p}_2)$ is the Fourier transform of $g(t, \mathbf{x}_1, \mathbf{x}_2, \mathbf{p}_1, \mathbf{p}_2)$. In going from $f_k^{(2)}$ in (2.5) to \tilde{g}_k above, we used the Mayer cluster expansion for $f^{(2)}$ (see (2.14)). The reason for writing the evolution in terms of $g_{\mathbf{k}_1 \mathbf{k}_2}(t, \mathbf{p}_1, \mathbf{p}_2) \equiv \tilde{g}_{k_1}(t, \mathbf{p}_1, \mathbf{p}_2) \delta_D(\mathbf{k}_1 + \mathbf{k}_2)$ is that evolution equations are symmetrical in \mathbf{k}_1 and \mathbf{k}_2 . As seen in the third line, the total power spectrum is a sum of two contributions

$$P_\delta(t, k) = P_{\delta_{\text{wn}}}(t, k) + P_{\delta_{\text{ad}}}(t, k), \tag{2.24}$$

which will be related to the sourced and source-free solutions of $g_{\mathbf{k}_1, \mathbf{k}_2}$ respectively.

In what follows, we will derive a formal solution for $g_{\mathbf{k}_1, \mathbf{k}_2}(t, \mathbf{p}_1, \mathbf{p}_2)$ and its momentum integral. To this end, first note that the acceleration (2.7) can be written as

$$\mathbf{a}_{ij} = -4\pi Gm \int_{\mathbf{q}} \frac{i\mathbf{q}}{q^2} e^{i\mathbf{q} \cdot (\mathbf{x}_i - \mathbf{x}_j)}, \tag{2.25}$$

where $\int_{\mathbf{q}} = \int d\mathbf{q} / (2\pi)^3 = V^{-1} \sum_{\mathbf{q}}$. We can now write the equation (2.21) for $g(12)$ in terms of $g_{\mathbf{k}_1 \mathbf{k}_2}$, resulting in

$$\begin{aligned}
&\partial_t g_{\mathbf{k}_1 \mathbf{k}_2} + \frac{i}{m} (\mathbf{p}_1 \cdot \mathbf{k}_1 + \mathbf{p}_2 \cdot \mathbf{k}_2) g_{\mathbf{k}_1 \mathbf{k}_2} \\
&- 4\pi Gm \bar{\rho} \int d\mathbf{p}_3 \left[g_{\mathbf{k}_1, \mathbf{k}_2}(\mathbf{p}_2, \mathbf{p}_3) \frac{i\mathbf{k}_1}{k_1^2} \cdot \nabla_{\mathbf{p}_1} f_0(p_1) + g_{\mathbf{k}_1, \mathbf{k}_2}(\mathbf{p}_1, \mathbf{p}_3) \frac{i\mathbf{k}_2}{k_2^2} \cdot \nabla_{\mathbf{p}_2} f_0(p_2) \right] \\
&= 4\pi Gm^2 \left(\frac{i\mathbf{k}_1}{k_1^2} \cdot \nabla_{\mathbf{p}_1} + \frac{i\mathbf{k}_2}{k_2^2} \cdot \nabla_{\mathbf{p}_2} \right) f_0(p_1) f_0(p_2) \delta_D(\mathbf{k}_1 + \mathbf{k}_2),
\end{aligned} \tag{2.26}$$

where it is useful to keep in mind that $g_{\mathbf{k}_1 \mathbf{k}_2} \propto \delta_D(\mathbf{k}_1 + \mathbf{k}_2)$ and that we suppressed some or all arguments of g to reduce clutter. This equation has the form:³

$$\mathcal{D} g_{\mathbf{k}_1 \mathbf{k}_2} = \underbrace{4\pi Gm (S_{\mathbf{k}_1}^{(1)} + S_{\mathbf{k}_2}^{(2)})}_{\text{source } S} \delta_D(\mathbf{k}_1 + \mathbf{k}_2), \tag{2.27}$$

³The labels (s) that appear below do not correspond to those in the BBGKY hierarchy, i.e. they are unrelated to (s) in $f^{(s)}$.

and its general solution is of the form

$$g_{\mathbf{k}_1\mathbf{k}_2}(t, \mathbf{p}_1, \mathbf{p}_2) = g_{\mathbf{k}_1\mathbf{k}_2}^{S=0}(t, \mathbf{p}_1, \mathbf{p}_2) + g_{\mathbf{k}_1\mathbf{k}_2}^{S\neq 0}(t, \mathbf{p}_1, \mathbf{p}_2), \quad (2.28)$$

where the first term is the homogeneous solution, i.e., the solution of the source-free equation $\mathcal{D}g_{\mathbf{k}_1\mathbf{k}_2} = 0$ with non-vanishing initial condition $g_{\mathbf{k}_1\mathbf{k}_2}^{S=0}(t_0, \mathbf{p}_1, \mathbf{p}_2) \neq 0$. The second term is the particular solution consistent with the non-zero source term and vanishing initial condition $g_{\mathbf{k}_1\mathbf{k}_2}^{S\neq 0}(t_0, \mathbf{p}_1, \mathbf{p}_2) = 0$.

We first provide a formal expression for the homogeneous solution, which will then immediately allow us to construct the evolution of the power spectrum for adiabatic initial conditions (with $g_{\mathbf{k}_1\mathbf{k}_2}^{S=0}(t_0, \mathbf{p}_1, \mathbf{p}_2) \neq 0$). We will then construct $g_{\mathbf{k}_1\mathbf{k}_2}^{S\neq 0}$ via a Green's function. This will allow us to write down the power spectrum evolution for white noise initial conditions (with $g_{\mathbf{k}_1\mathbf{k}_2}^{S\neq 0}(t_0, \mathbf{p}_1, \mathbf{p}_2) = 0$). Putting these together will yield the complete evolution of the density power spectrum.

The source-free equation, $\mathcal{D}g_{\mathbf{k}_1\mathbf{k}_2} = 0$, has solutions of the form

$$g_{\mathbf{k}_1\mathbf{k}_2}(t, \mathbf{p}_1, \mathbf{p}_2) = \gamma_{\mathbf{k}_1}^{(i)}(t, \mathbf{p}_1) \gamma_{\mathbf{k}_2}^{(j)}(t, \mathbf{p}_2) \delta_D(\mathbf{k}_1 + \mathbf{k}_2), \quad (2.29)$$

where the $\gamma_{\mathbf{k}}^{(i,j)}$ are functions satisfying⁴

$$\partial_t \gamma_{\mathbf{k}} + \frac{i}{m} (\mathbf{k} \cdot \mathbf{q}) \gamma_{\mathbf{k}} - 4\pi G \bar{\rho} m \frac{i\mathbf{k}}{k^2} \cdot \nabla_q f_0(q) \int d\mathbf{p} \gamma_{\mathbf{k}}(\mathbf{p}) = 0. \quad (2.30)$$

The formal solution to eq. (2.30) can be written as

$$\gamma_{\mathbf{k}}(t, \mathbf{q}) = \gamma_{\mathbf{k}}(t_0, \mathbf{q}) e^{-i\mathbf{k} \cdot \frac{\mathbf{q}}{m}(t-t_0)} + 4\pi G m \bar{\rho} \frac{i\mathbf{k}}{k^2} \cdot \nabla_q f_0(q) \int_{t_0}^t dt'' e^{-i\mathbf{k} \cdot \frac{\mathbf{q}}{m}(t-t'')} \int d\mathbf{p} \gamma_{\mathbf{k}}(t'', \mathbf{p}). \quad (2.31)$$

An initial condition $\gamma_{\mathbf{k}}(t_0, \mathbf{q})$ is needed to proceed further.

Before proceeding, we note that equation (2.30) could have also been derived as the evolution equation for the perturbation to the 1-particle DF, if we had allowed the 1-particle DF to depend on position, as in e.g. ref. [77]. That is, if the 1-particle DF were $f(t, \mathbf{k}, \mathbf{p}) = f_0(p) + \gamma_{\mathbf{k}}(t, \mathbf{p})$, then equation (2.30) would follow from the collisionless Boltzmann equation for f at linear order in $\gamma_{\mathbf{k}}$. Consequently, the momentum integrals of the $\gamma_{\mathbf{k}}$ are precisely growth functions for warm dark matter that describe how particular realizations of the density field $\delta_{\mathbf{k}}$ evolve over time.

2.2.1 Fundamental Solutions: the Growth Functions for Warm Dark Matter

Consider the following two initial conditions:

$$\begin{aligned} (a) \quad & \gamma_{\mathbf{k}}^{(a)}(t_0, \mathbf{q}) = f_0(q), \\ (b) \quad & \gamma_{\mathbf{k}}^{(b)}(t_0, \mathbf{q}) = -m(i\mathbf{k}/k^2) \cdot \nabla_q f_0(q). \end{aligned} \quad (2.32)$$

⁴The general solution to $\mathcal{D}g_{\mathbf{k}_1\mathbf{k}_2} = 0$ would be an infinite sum $g_{\mathbf{k}_1\mathbf{k}_2} = \sum_{ij} \gamma_{\mathbf{k}_1}^{(i)} \gamma_{\mathbf{k}_2}^{(j)} \delta_D(\mathbf{k}_1 + \mathbf{k}_2)$.

The \mathbf{q} -dependence of these choices makes them pure bulk perturbations to the density and velocity,⁵ while the (\mathbf{k} -dependent) normalizations are chosen for future convenience. The product of these initial γ also matches the form of the source terms in eq. (2.26). With each initial condition, the solution $\gamma_{\mathbf{k}}^{(a,b)}(t, \mathbf{q})$ in (2.31) can be integrated over \mathbf{q} to get $T_{\mathbf{k}}^{(a,b)}(t, t_0) \equiv \int d\mathbf{q} \gamma_{\mathbf{k}}^{(a,b)}(t, \mathbf{q})$ which satisfy:

$$\begin{aligned} T_{\mathbf{k}}^{(a)}(t, t_0) &= T_{\text{fs}}(k(t - t_0)) + 4\pi G\bar{\rho} \int_{t_0}^t dt'' (t - t'') T_{\text{fs}}(k(t - t'')) T_{\mathbf{k}}^{(a)}(t'', t_0), \\ T_{\mathbf{k}}^{(b)}(t, t_0) &= (t - t_0) T_{\text{fs}}(k(t - t_0)) + 4\pi G\bar{\rho} \int_{t_0}^t dt'' (t - t'') T_{\text{fs}}(k(t - t'')) T_{\mathbf{k}}^{(b)}(t'', t_0), \end{aligned} \quad (2.33)$$

with the free-streaming effects being represented via:

$$T_{\text{fs}}(k(t - t'')) = \int d\mathbf{p} f_0(p) e^{-i\mathbf{k} \cdot \frac{\mathbf{p}}{m}(t - t'')}. \quad (2.34)$$

We will see shortly that an initial density perturbation (with zero bulk velocity) evolves in proportion with $T_{\mathbf{k}}^{(a)}$, while a pure initial velocity perturbation evolves in proportion with $T_{\mathbf{k}}^{(b)}$. That is, the $T_{\mathbf{k}}^{(a,b)}$ are growth functions for warm dark matter. They will form the building blocks for the power spectrum evolution.

Equations (2.33) are Volterra integral equations, which must be solved numerically in general. We discuss their structure in Appendix A, and we show that these equations can be put into the form:

$$\begin{aligned} T_{\mathbf{k}}^{(a)}(t, t_0) &= T_{\text{fs}}(k(t - t_0)) + 4\pi G\bar{\rho} \int_{t_0}^t dt'' T_{\mathbf{k}}^{(b)}(t, t'') T_{\text{fs}}(k(t'' - t_0)), \\ T_{\mathbf{k}}^{(b)}(t, t_0) &= (t - t_0) T_{\text{fs}}(k(t - t_0)) + 4\pi G\bar{\rho} \int_{t_0}^t dt'' T_{\mathbf{k}}^{(b)}(t, t'') (t'' - t_0) T_{\text{fs}}(k(t'' - t_0)). \end{aligned} \quad (2.35)$$

That is, $T_{\mathbf{k}}^{(a)}$ reduces to an integral over $T_{\mathbf{k}}^{(b)}$, and we only need to solve one Volterra equation for $T_{\mathbf{k}}^{(b)}$.

Conveniently, due to how the $\gamma_{\mathbf{k}}^{(a,b)}$ were normalized, $T_{\mathbf{k}}^{(a)}(t_0, t_0) = 1$ and $T_{\mathbf{k}}^{(b)}(t_0, t_0) = 0$, and their initial time derivatives are 0 and 1, respectively. It is also useful to note that the growth functions are isotropic: $T_{\mathbf{k}}^{(a,b)}(t, t_0) = T_k^{(a,b)}(t, t_0)$.

2.2.2 Evolution from Adiabatic Initial Conditions

We now consider the source-free evolution of initial correlations, with the aim of evaluating the time evolution of the adiabatic part of the power spectrum,

$$P_{\delta_{\text{ad}}}(t, k_1) \delta_D(\mathbf{k}_1 + \mathbf{k}_2) = \int d\mathbf{p}_1 d\mathbf{p}_2 g_{\mathbf{k}_1 \mathbf{k}_2}^{S=0}(t, \mathbf{p}_1, \mathbf{p}_2). \quad (2.36)$$

⁵Given an overall density shift $\delta(\mathbf{k})$ and momentum shift $\bar{\mathbf{q}}(\mathbf{k})$, the 1-particle DF becomes $f(t_0, \mathbf{k}, \mathbf{q}) = f_0(\mathbf{q} - \bar{\mathbf{q}}(\mathbf{k})) + \delta(\mathbf{k}) f_0(\mathbf{q}) \approx f_0(\mathbf{q}) + \delta(\mathbf{k}) f_0(\mathbf{q}) - \bar{\mathbf{q}}(\mathbf{k}) \cdot \nabla_{\mathbf{q}} f_0(\mathbf{q})$ at lowest order in $\bar{\mathbf{q}}(\mathbf{k})$. The \mathbf{q} -dependence in these perturbation terms matches those of $\gamma_{\mathbf{k}}^{(a)}$ and $\gamma_{\mathbf{k}}^{(b)}$ in equation (2.32).

Although $g_{\mathbf{k}_1\mathbf{k}_2}^{S=0}$ can in general involve a sum over products of solutions to eq. (2.30), its freedom is reduced if we assume that, at each \mathbf{k} , there are no initial correlations in momentum space. Then the correlation function factorizes as

$$g_{\mathbf{k}_1\mathbf{k}_2}^{S=0}(t, \mathbf{p}_1, \mathbf{p}_2) = \gamma_{\mathbf{k}_1}(t, \mathbf{p}_1) \gamma_{\mathbf{k}_2}(t, \mathbf{p}_2) \delta_D(\mathbf{k}_1 + \mathbf{k}_2) \quad (2.37)$$

for some $\gamma_{\mathbf{k}}$ satisfying eq. (2.30). The particular $\gamma_{\mathbf{k}}$ is determined when we specialize to adiabatic initial conditions, which represent overall bulk perturbations to the density and velocity.⁶ Then it must be a simple linear combination of the $\gamma_{\mathbf{k}}^{(a,b)}$ given in eq. (2.32). Given an initial adiabatic power spectrum $P_{\delta_{\text{ad}}}(t_0, k)$ and its time derivative $dP_{\delta_{\text{ad}}}(t_0, k)/dt_0$ at the time t_0 , the normalizations of the $\gamma_{\mathbf{k}}^{(a,b)}$ require the particular combination

$$\gamma_{\mathbf{k}}(t, \mathbf{p}) = \sqrt{P_{\delta_{\text{ad}}}(t_0, k)} \gamma_{\mathbf{k}}^{(a)}(t, \mathbf{p}) + \frac{d\sqrt{P_{\delta_{\text{ad}}}(t_0, k)}}{dt_0} \gamma_{\mathbf{k}}^{(b)}(t, \mathbf{p}). \quad (2.38)$$

Using this solution in equations (2.37) and (2.36), we obtain

$$\begin{aligned} P_{\delta_{\text{ad}}}(t, k) &= P_{\delta_{\text{ad}}}(t_0, k) \left[T_k^{\text{ad}}(t, t_0) \right]^2, \\ T_k^{\text{ad}}(t, t_0) &= T_k^{(a)}(t, t_0) + \frac{d \ln \sqrt{P_{\delta_{\text{ad}}}(t_0, k)}}{dt_0} T_k^{(b)}(t, t_0), \end{aligned} \quad (2.39)$$

with the $T_k^{(a,b)}$ given by equations (2.35).

There is nothing new here, and this is the usual solution expected for warm dark matter with some initial density and bulk velocity perturbations. At early times during radiation domination, one can ignore the gravitational terms proportional to G in the equations for $T_k^{(a,b)}$ (see (2.33)) and hence also in T_k^{ad} . Then T_{fs} leads to erasure of correlated fluctuations below of a free-streaming length via $P_{\delta_{\text{ad}}}(t, k) \sim P_{\delta_{\text{ad}}}(t_0, k) T_{\text{fs}}^2(k(t - t_0))$. At late times during matter domination, the G terms which correspond to gravitational clustering can dominate. In this case, T_{fs} prevents the power spectrum from growing significantly below the Jeans length.

2.2.3 Evolution of White Noise

We now focus on the evolution of the power spectrum under the ongoing influence of the sourcing terms in equation (2.26) when there are no initial correlations in position space, so the initial power spectrum is white noise. Then we can write

$$\begin{aligned} P_{\delta_{\text{wn}}}(t, k_1) \delta_D(\mathbf{k}_1 + \mathbf{k}_2) &= \frac{1}{\bar{n}} \delta_D(\mathbf{k}_1 + \mathbf{k}_2) + \int d\mathbf{p}_1 d\mathbf{p}_2 g_{\mathbf{k}_1\mathbf{k}_2}^{S \neq 0}(t, \mathbf{p}_1, \mathbf{p}_2), \\ &= \frac{1}{\bar{n}} \delta_D(\mathbf{k}_1 + \mathbf{k}_2) + \int d\mathbf{p}_1 d\mathbf{p}_2 \left[g_{\mathbf{k}_1\mathbf{k}_2}^{(1)}(t, \mathbf{p}_1, \mathbf{p}_2) + g_{\mathbf{k}_1\mathbf{k}_2}^{(2)}(t, \mathbf{p}_1, \mathbf{p}_2) \right], \end{aligned} \quad (2.40)$$

⁶However, the initially adiabatic perturbations are bulk density and velocity perturbations only to the extent that they have not yet been affected significantly by free streaming of particles. Thus, for the $\gamma_{\mathbf{k}}$ in equation (2.38) to be appropriate, in principle the initial time t_0 must be either the time that the perturbations are first sourced or the time that (non-relativistic) free streaming begins, whichever is later. See Section 4.4 for further discussion.

with the initial condition $g_{\mathbf{k}_1\mathbf{k}_2}^{S \neq 0}(t_0, \mathbf{p}_1, \mathbf{p}_2) = 0$. Here, $\mathcal{D}g_{\mathbf{k}_1\mathbf{k}_2}^{S \neq 0} = \mathcal{D} \left[g_{\mathbf{k}_1\mathbf{k}_2}^{(1)} + g_{\mathbf{k}_1\mathbf{k}_2}^{(2)} \right] = 4\pi Gm \left[S_{\mathbf{k}_1}^{(1)} + S_{\mathbf{k}_2}^{(2)} \right] \delta_D(\mathbf{k}_1 + \mathbf{k}_2)$ (cf. eq. (2.27)).

We can solve for $g_{\mathbf{k}_1\mathbf{k}_2}^{(1)}$ from:

$$\mathcal{D}g_{\mathbf{k}_1\mathbf{k}_2}^{(1)} = 4\pi Gm S_{\mathbf{k}_1}^{(1)} \delta_D(\mathbf{k}_1 + \mathbf{k}_2). \quad (2.41)$$

The solution can be written as

$$g_{\mathbf{k}_1\mathbf{k}_2}^{(1)}(t, \mathbf{p}_1, \mathbf{p}_2) = 4\pi Gm \int_{t_0}^t dt' \mathcal{G}_{\mathbf{k}_1, \mathbf{k}_2}^{(1)}(t, t', \mathbf{p}_1, \mathbf{p}_2) \delta_D(\mathbf{k}_1 + \mathbf{k}_2), \quad (2.42)$$

where $\mathcal{G}_{\mathbf{k}_1\mathbf{k}_2}^{(1)}$ is a Green's function:

$$\mathcal{G}_{\mathbf{k}_1\mathbf{k}_2}^{(1)}(t, t', \mathbf{p}_1, \mathbf{p}_2) = \gamma_{\mathbf{k}_1}^{(i)}(t, t', \mathbf{p}_1) \gamma_{\mathbf{k}_2}^{(j)}(t, t', \mathbf{p}_2) \Theta(t - t') \quad (2.43)$$

for some $\gamma_{\mathbf{k}_s}^{(i,j)}(t, t', \mathbf{p}_s)$ given by eq. (2.31) with $t_0 \rightarrow t'$. The initial conditions for $\gamma_{\mathbf{k}_s}^{(i,j)}$ needed to specify the Green's function can be determined from the defining equation for the Green's function:

$$\mathcal{D}\mathcal{G}_{\mathbf{k}_1\mathbf{k}_2}^{(1)}(t, t', \mathbf{p}_1, \mathbf{p}_2) = \delta_D(t - t') S_{\mathbf{k}_1}^{(1)}(\mathbf{p}_1, \mathbf{p}_2). \quad (2.44)$$

Note that integrating this equation for $\mathcal{G}_{\mathbf{k}_1\mathbf{k}_2}^{(1)}$ across $t = t'$, we have $\mathcal{G}_{\mathbf{k}_1\mathbf{k}_2}^{(1)}(t' + \epsilon, t', \mathbf{p}_1, \mathbf{p}_2) = S_{\mathbf{k}_1}^{(1)}(\mathbf{p}_1, \mathbf{p}_2)$ for arbitrarily small $\epsilon > 0$. This can be satisfied by choosing $\gamma_{\mathbf{k}_1}^{(i)}(t' + \epsilon, \mathbf{p}_1) = f_0(p_1)$ and $\gamma_{\mathbf{k}_2}^{(j)}(t' + \epsilon, \mathbf{p}_2) = -m(i\mathbf{k}_2/k_2^2) \cdot \nabla_{\mathbf{p}_2} f_0(p_2)$, which are the same as (2.32) with $t_0 \rightarrow t' + \epsilon$. So the general solution with these “initial” conditions is

$$g_{\mathbf{k}_1\mathbf{k}_2}^{(1)}(t, t_0, \mathbf{p}_1, \mathbf{p}_2) = 4\pi Gm \int_{t_0}^t dt' \gamma_{\mathbf{k}_1}^{(a)}(t, t', \mathbf{p}_1) \gamma_{\mathbf{k}_2}^{(b)}(t, t', \mathbf{p}_2) \delta_D(\mathbf{k}_1 + \mathbf{k}_2), \quad (2.45)$$

Integrating both sides over \mathbf{p}_1 and \mathbf{p}_2 , we have

$$\int d\mathbf{p}_1 d\mathbf{p}_2 g_{\mathbf{k}_1\mathbf{k}_2}^{(1)}(t, t_0, \mathbf{p}_1, \mathbf{p}_2) = 4\pi Gm \int_{t_0}^t dt' T_{\mathbf{k}_1}^{(a)}(t, t') T_{\mathbf{k}_2}^{(b)}(t, t') \delta_D(\mathbf{k}_1 + \mathbf{k}_2), \quad (2.46)$$

where $T_{\mathbf{k}_s}^{(a,b)}(t, t')$ are given by (2.33) or (2.35) with $t_0 \rightarrow t'$.

We repeat this exercise for $\mathcal{D}g_{\mathbf{k}_1\mathbf{k}_2}^{(2)} = 4\pi Gm S_{\mathbf{k}_2}^{(2)} \delta_D(\mathbf{k}_1 + \mathbf{k}_2)$ and find that $\int d\mathbf{p}_1 d\mathbf{p}_2 g_{\mathbf{k}_1\mathbf{k}_2}^{(2)} = \int d\mathbf{p}_1 d\mathbf{p}_2 g_{\mathbf{k}_1\mathbf{k}_2}^{(1)}$ after using $\delta_D(\mathbf{k}_1 + \mathbf{k}_2)$ to interchange \mathbf{k}_1 and \mathbf{k}_2 . Adding up the contributions from $g_{\mathbf{k}_2\mathbf{k}_2}^{(1,2)}$, we have

$$\int d\mathbf{p}_1 d\mathbf{p}_2 g_{\mathbf{k}_1\mathbf{k}_2}^{S \neq 0}(t, \mathbf{p}_1, \mathbf{p}_2) = 8\pi Gm \int_{t_0}^t dt' T_{\mathbf{k}_1}^{(a)}(t, t') T_{\mathbf{k}_1}^{(b)}(t, t') \delta_D(\mathbf{k}_1 + \mathbf{k}_2). \quad (2.47)$$

Thus, the power spectrum when we start with no existing correlations is given by

$$P_{\delta_{\text{wn}}}(t, k) = \frac{1}{\bar{n}} \left[1 + 8\pi G\bar{\rho} \int_{t_0}^t dt' T_k^{(a)}(t, t') T_k^{(b)}(t, t') \right]. \quad (2.48)$$

This is one of the main new results of our work. The $1/\bar{n}$ is the initial white noise, while the term proportional to G is the evolution of white noise. We show the diagrammatic interpretation of this expression in Appendix A.

Heuristically, at early times close to t_0 , the evolution term is $G\bar{\rho} \int dt'(t-t')T_{\text{fs}}^2(k(t-t'))$ capturing the initial growth of correlations. Unlike the white noise $1/\bar{n}$, this growth is subject to free streaming effects as is evident from T_{fs}^2 inside the integral. At late times, this term will capture growth above, and lack thereof below a Jeans length.

On a technical note, notice that the above power spectrum $P_{\delta_{\text{wn}}}$ requires an integral in time over the product of $T_k^{(a)}T_k^{(b)}$. In contrast, $P_{\delta_{\text{ad}}} \propto (T_k^{(a)} + cT_k^{(b)})^2$ with no additional time integral. Conceptually, $P_{\delta_{\text{wn}}}$ is built from density and velocity perturbations sourced at all times, whereas $P_{\delta_{\text{ad}}}$ is built from such perturbations sourced only at an initial time.

2.3 Power Spectrum Evolution in an Expanding Universe

To convert the previous results to the case of an expanding universe, we express positions, momenta, wavenumbers and densities in terms of their co-moving counterparts $\{\mathbf{x}, \mathbf{k}, \mathbf{p}\} \rightarrow \{a\mathbf{x}, \mathbf{k}/a, \mathbf{p}/a\}$ and $\{\bar{n}, \bar{\rho}, f_0(q)\} \rightarrow \{a^{-3}\bar{n}, a^{-3}\bar{\rho}, a^3f_0(q)\}$, where the variables after the arrows are co-moving quantities. We make a further change to a new time variable η which appears naturally when dealing with non-relativistic motion in an expanding universe:

$$d\eta = \frac{dt}{a^2(t)}. \quad (2.49)$$

In particular, the co-moving distance traveled by a particle with peculiar (physical) velocity $\mathbf{v}(t) = \mathbf{p}/(ma(t))$ is given by

$$l_{\text{fs}}(\mathbf{p}, t) = \int_{t_0}^t \mathbf{v}(t') \frac{dt'}{a(t')} = \frac{\mathbf{p}}{m} \int_{t_0}^t \frac{dt'}{a^2(t')} = \frac{\mathbf{p}}{m}(\eta - \eta_0). \quad (2.50)$$

This is the scale that naturally enters the free-streaming transfer function, which becomes

$$T_{\text{fs}}(k(\eta - \eta')) = \int d\mathbf{p} f_0(p) e^{-i\mathbf{k} \cdot \frac{\mathbf{p}}{m}(\eta - \eta')} = 4\pi \int dp p^2 f_0(p) \text{sinc} \left[\frac{p}{m} k(\eta - \eta') \right], \quad (2.51)$$

where $\text{sinc}(x) = \sin(x)/x$. As another example, eq. (2.30) becomes

$$\partial_\eta \gamma_{\mathbf{k}} + \frac{i}{m}(\mathbf{k} \cdot \mathbf{q}) \gamma_{\mathbf{k}} - 4\pi G \bar{\rho} a(\eta) m \frac{i\mathbf{k}}{k^2} \cdot \nabla_q f_0(q) \int d\mathbf{p} \gamma_{\mathbf{k}}(\mathbf{p}) = 0. \quad (2.52)$$

This suggests a quick replacement in the equations (2.35) for the growth functions $T^{(a,b)}$:

$$t \rightarrow \eta', \quad 4\pi G \bar{\rho} dt \rightarrow 4\pi G \bar{\rho} a(\eta) d\eta = (3/4)H^2(a_{\text{eq}})a_{\text{eq}}^3 a(\eta) d\eta. \quad (2.53)$$

Using this replacement we can find the corresponding expressions for the power spectrum evolution (eqs. (2.39) and (2.48)) in an expanding universe in terms of comoving quantities.

2.3.1 The Main Result

It is convenient to write our results in terms of dimensionless variables,

$$y = a/a_{\text{eq}}, \quad \eta - \eta' = \frac{\sqrt{2}}{a_{\text{eq}} k_{\text{eq}}} \mathcal{F}(y, y') \quad \text{with} \quad \mathcal{F}(y, y') = \ln \left[\frac{y}{y'} \left(\frac{1 + \sqrt{1 + y'}}{1 + \sqrt{1 + y}} \right)^2 \right], \quad (2.54)$$

where we plan to use $y = a/a_{\text{eq}}$ as the time variable. Then the white-noise part becomes

$$P_{\delta_{\text{wn}}}(y, k) = \frac{1}{\bar{n}} \left[1 + 3 \int_{y_0}^y \frac{dy'}{\sqrt{1 + y'}} \mathcal{T}_k^{(a)}(y, y') \mathcal{T}_k^{(b)}(y, y') \right], \quad (2.55)$$

and including adiabatic perturbations:

$$P_{\delta}(y, k) = P_{\delta_{\text{ad}}}(y_0, k) \left[\mathcal{T}_k^{\text{ad}}(y, y_0) \right]^2 + \frac{1}{\bar{n}} \left[1 + 3 \int_{y_0}^y \frac{dy'}{\sqrt{1 + y'}} \mathcal{T}_k^{(a)}(y, y') \mathcal{T}_k^{(b)}(y, y') \right], \quad (2.56)$$

where

$$\begin{aligned} \mathcal{T}_k^{\text{ad}}(y, y_0) &= \mathcal{T}_k^{(a)}(y, y_0) + \frac{1}{2} \frac{d \ln P_{\delta_{\text{ad}}}(y_0, k)}{d \ln y_0} \sqrt{1 + y_0} \mathcal{T}_k^{(b)}(y, y_0), \\ \mathcal{T}_k^{(a)}(y, y') &= T_{\text{fs}}(y, y', k) + \frac{3}{2} \int_{y'}^y \frac{dy''}{\sqrt{1 + y''}} \mathcal{T}_k^{(b)}(y, y'') T_{\text{fs}}(y'', y', k), \\ \mathcal{T}_k^{(b)}(y, y') &= \mathcal{F}(y, y') T_{\text{fs}}(y, y', k) + \frac{3}{2} \int_{y'}^y \frac{dy''}{\sqrt{1 + y''}} \mathcal{T}_k^{(b)}(y, y'') \mathcal{F}(y'', y') T_{\text{fs}}(y'', y', k). \end{aligned} \quad (2.57)$$

Here, the free-streaming transfer function is

$$T_{\text{fs}}(y, y', k) = 4\pi \int dp p^2 f_0(p) \text{sinc} \left[\frac{p}{m a_{\text{eq}}} \frac{k}{k_{\text{eq}}} \sqrt{2} \mathcal{F}(y, y') \right]. \quad (2.58)$$

If the distribution function has a characteristic momentum scale q_* , so that $f_0(q) = A(q_*)B(q/q_*)$, then a convenient dimensionless parameter

$$\alpha_k = \sqrt{2} \frac{k}{k_{\text{eq}}} \frac{q_*}{a_{\text{eq}} m}, \quad (2.59)$$

naturally appears, and the free streaming function T_{fs} becomes a function of $\alpha_k \mathcal{F}$. As a result, both $\mathcal{T}^{(a,b)}$ are functions of α_k with no further dependence on k . The behavior of these functions changes at $\alpha_k \sim 1$.

Numerical Calculation We provide efficient and fast numerical algorithms to solve the Volterra-type equations for $\mathcal{T}^{(a,b)}$ in equations (2.57) for a given T_{fs} in Appendix B. An implementation can be found at <https://github.com/delos/warm-structure-growth>. In Appendix C, we also provide simpler, approximate formulae that work well for the Maxwell-Boltzmann momentum distribution, although they can be less accurate approximations in other cases.

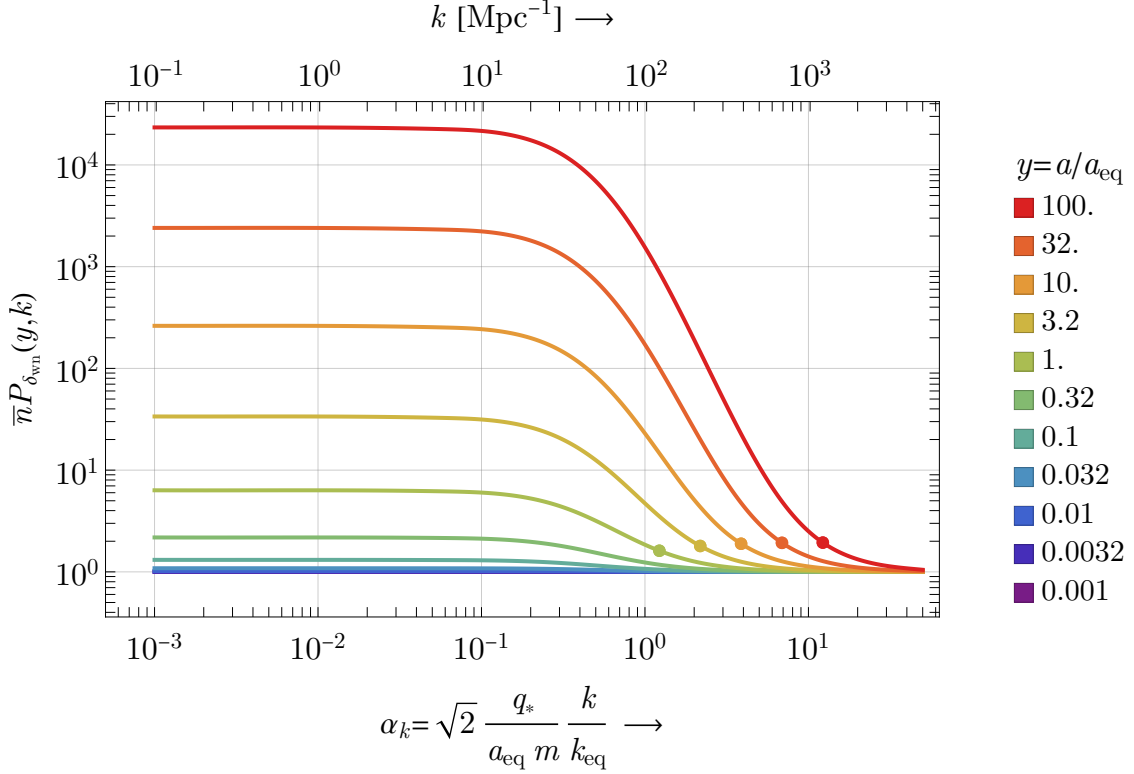


Figure 3: Evolution of the white noise power spectrum as a function of wavenumber (horizontal axis) and scale factor (colors). The colored lines are based on evaluation of our expression (2.55) for the evolution of the power spectrum. The dots indicate the co-moving Jeans scale $k_J(a)$. The left edge of the plot evolves upwards as $(1 + \frac{3}{2}y)^2$ in accordance with standard expectations, with growth at higher k being Jeans-suppressed. The above calculations are done for a Maxwellian initial momentum distribution $f_0(q) = Ae^{-q^2/2q_*^2}$, and the 1D velocity dispersion at equality is $\sigma_{\text{eq}} = q_*/a_{\text{eq}}m \approx 22 \text{ km s}^{-1}$. The dimensionless scale (α_k) on the bottom axis is converted to k in Mpc^{-1} (top axis) using this σ_{eq} . Note that in terms of α_k , the shape of $\bar{n}P_{\delta_{\text{wn}}}(y, k)$ does not depend on σ_{eq} .

Examples As concrete examples, we consider an initially Maxwellian distribution and a “top-hat” distribution function, which yield, respectively:

$$\begin{aligned}
 f_0(q) &= \frac{e^{-q^2/(2q_*^2)}}{(2\pi)^{3/2}q_*^3}, & T_{\text{fs}}(y, y', k) &= e^{-\alpha_k^2 \mathcal{F}^2/2}, & \langle q^2 \rangle &= 3q_*^2 \\
 f_0(q) &= \frac{\Theta(q_* - q)}{4\pi q_*^3/3}, & T_{\text{fs}}(y, y', k) &= \frac{3}{\alpha_k^3 \mathcal{F}^3} (\sin[\alpha_k \mathcal{F}] - \alpha_k \mathcal{F} \cos[\alpha_k \mathcal{F}]), & \langle q^2 \rangle &= \frac{3}{5}q_*^2.
 \end{aligned}
 \tag{2.60}$$

where $\mathcal{F} = \mathcal{F}(y, y')$. For the Maxwell-Boltzmann case, Fig. 3 shows the growth of the white-noise part of the power spectrum, while Fig. 4 shows the evolution of the dimensionless matter power spectrum including both the white noise and the initially adiabatic perturbations. In Appendix D, we show similar results for the uniform-sphere case.

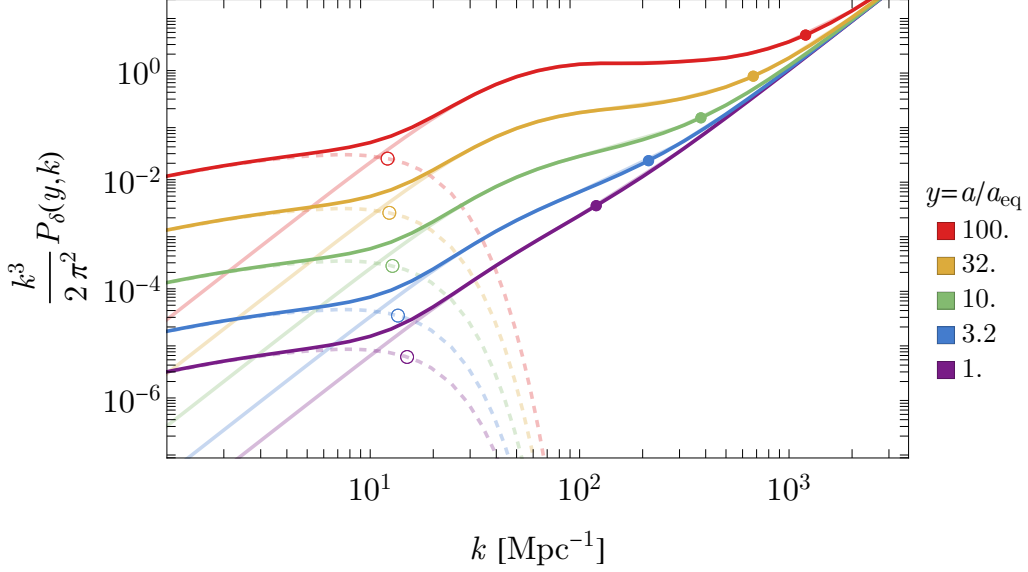


Figure 4: Evolution of the total dimensionless power spectrum (solid lines). The lighter curves are the separate adiabatic (dashed) and white-noise (solid) contributions. The open circles on the adiabatic part indicate the free-streaming wavenumber $k_{\text{fs}}(y)$, while the closed circles on the white-noise part are the Jeans wavenumber $k_{\text{J}}(y)$. We adopt a Maxwellian initial velocity distribution, with $\sigma_{\text{eq}} \approx 22 \text{ km s}^{-1}$, and $\bar{n} \approx 5 \times 10^7 / \text{Mpc}^3$. The adiabatic part has an amplitude consistent with Planck (2018) observations. The chosen parameters are motivated by ref. [35], with $k_{\text{fs}} \sim 10 / \text{Mpc}$ and $k_{\text{wn}} = (2\pi^2 \bar{n})^{1/3} \sim 10^3 / \text{Mpc}$ – at the boundary of being consistent with observations in the quasi-linear regime.

2.3.2 Relevant Scales and Range of Validity

Jeans and Free-streaming Scales: In general, there are two relevant scales for understanding the cutoff in the power spectrum at late times. These are the Jeans scale (relevant for the white-noise part) and free-streaming scale (relevant for the adiabatic part). They are defined as

$$\begin{aligned} k_{\text{J}}(y) &\equiv a(t) \sqrt{\frac{4\pi G \bar{\rho}(t)}{\sigma^2}} = \frac{\sqrt{3y}}{2} \frac{k_{\text{eq}}}{\sigma_{\text{eq}}}, \\ k_{\text{fs}}(y) &\equiv \left[\int_{t_0}^t \sigma \frac{dt'}{a(t')} \right]^{-1} = \frac{1}{\sqrt{2}\mathcal{F}(y, y_0)} \frac{k_{\text{eq}}}{\sigma_{\text{eq}}}, \end{aligned} \quad (2.61)$$

where $\sigma \equiv \langle v_{\text{p}}^2(t)/3 \rangle^{1/2}$ is the 1D peculiar velocity dispersion, and $\sigma_{\text{eq}} \equiv \langle v_{\text{eq}}^2/3 \rangle^{1/2}$ is the 1D peculiar velocity dispersion at matter radiation equality. Here the expectation values are taken using $f_0(p)$. Note that k_{J} increases as \sqrt{y} as the universe expands, whereas k_{fs} decreases as the universe expands. After equality, where $\mathcal{F}(1, y_0) \approx \ln(0.7/y_0)$, \mathcal{F} increases very slowly with y , so k_{fs} shifts only very little over time. The cutoff in the white noise part of the power spectrum typically resembles a power law in k , with suppression below $k_{\text{J}}^{\text{eq}} = k_{\text{J}}(y = 1)$. The suppression in the adiabatic part is sharper, with suppression beginning at $k_{\text{fs}}^{\text{eq}} = k_{\text{fs}}(y = 1)$. It is also worth noting that at equality, we expect $k_{\text{fs}}^{\text{eq}} \approx k_{\text{J}}^{\text{eq}} / \ln(y_0^{-1}) < k_{\text{J}}^{\text{eq}}$.

To provide a sense of the scales relevant for observations of the linear power spectrum (such as the Lyman- α forest), we note that:

$$\begin{aligned} k_{\text{fs}}(y) &\approx 15 \text{ Mpc}^{-1} \times \frac{\mathcal{F}(1, 10^{-3})}{\mathcal{F}(y, y_0)} \left(\frac{22 \text{ km s}^{-1}}{\sigma_{\text{eq}}} \right), \\ k_{\text{J}}(y) &\approx 120 \text{ Mpc}^{-1} \times \sqrt{y} \left(\frac{22 \text{ km s}^{-1}}{\sigma_{\text{eq}}} \right). \end{aligned} \quad (2.62)$$

Free streaming is associated with a longer length scale (smaller k) and so is usually expected to provide more stringent observational constraints.

Note that for the examples in the present work we chose $y_0 = 10^{-3}$, determining the instant where non-relativistic free streaming can begin. The free-streaming scale is logarithmically sensitive to this choice. As we discuss in section 4.4, non-relativistic streaming may be approximated to begin either when the dark matter becomes non-relativistic or when the initial perturbations are sourced (e.g., horizon entry), whichever is later, but a relativistic version of our calculation would be necessary to capture these considerations precisely.

Validity of Approximations: Our derivation for the power spectrum rested on two assumptions that warrant further discussion: that the two-particle correlation function is small ($g \ll ff$) and that the one-particle DF does not evolve significantly in time ($\partial_t f \approx 0$). We first discuss the $g \ll ff$ assumption. Integrating this relation over momenta yields a condition on the correlation function in position space,

$$1 \gg \xi(r) = \int d \ln k \frac{k^3}{2\pi^2} \left[P_\delta(y, k) - \frac{1}{\bar{n}} \right] \frac{\sin(kr)}{kr}. \quad (2.63)$$

This condition provides a domain of validity as a function of the length scale r and time y . It is essentially a statement that fractional density perturbations must be small, meaning that our calculation is perturbative in the same sense as standard, linear-order cosmological perturbation theory. Due to the log-measure, heuristically, requiring $(k^3/2\pi^2)[P_\delta(y, k) - \bar{n}^{-1}] \ll 1$ should typically be sufficient.

The time evolution of the 1-particle DF is a more subtle matter. For certain power spectra P_δ , velocities associated with gravitational growth of perturbations on the largest scales can easily contribute to the overall velocity variance $\langle v^2 \rangle$ at a level exceeding the input velocity dispersion σ .⁷ However, these velocities are dominated by large-scale bulk flows, which cannot affect dynamics on much smaller scales (as they can be removed with a change of reference frame). A velocity *dispersion* only develops in nonlinearly evolved systems after stream crossing. Therefore, we expect that our neglect of growth of the velocity dispersion is always valid within the small-perturbation regime corresponding to eq. (2.63). Beyond the velocity dispersion, another potential concern is that an arbitrary

⁷In the regime of small perturbations and approximating that $P_\delta(k) \propto a^2$ for $k < k_{\text{J}}$, the ratio between the velocity variance due to gravitational growth and that due to the input dispersion can be shown to be $\langle v^2 \rangle / (3\sigma^2) \approx \frac{2}{9} \int_0^{k_{\text{J}}} d \ln k (k_{\text{J}}/k)^2 [k^3/(2\pi^2)] P_\delta(k)$. If the dimensionless power spectrum $[k^3/(2\pi^2)] P_\delta(k)$ is sufficiently shallow, this integral can be dominated by low- k contributions, giving rise to $\langle v^2 \rangle \gg 3\sigma^2$ long before any nonlinear clustering occurs.

initial DF would relax toward Maxwellian due to 2-particle interactions. However, one can show using standard arguments (e.g. [51]) that the relaxation time scale is of order $t_{\text{relax}} \sim (\bar{n}/k_J^3)H^{-1}$,⁸ implying that relaxation is unimportant as long as $k_J \ll \bar{n}^{1/3}$. As this is always true when fractional perturbations longer than the Jeans scale are small, we conclude that the $\partial_t f = 0$ assumption does not add any new restriction beyond that.

In the next section, we will confirm these considerations by showing in N -body simulations that $(k^3/2\pi^2)P_\delta(y, k) \lesssim 0.1$ is sufficient for excellent agreement with analytically computed power spectra. However, we will also show that the abundance of collapsed dark matter halos can be accurately predicted by these analytically computed spectra even when $(k^3/2\pi^2)P_\delta(y, k) \gtrsim 1$, just as with standard linear-order cosmological perturbation theory.

3 Comparison with N -body Simulations

We now test our analytic results with cosmological N -body simulations. We will show that the analytic power spectrum (2.56) is accurate in the linear regime where perturbations are small. We will also show that, like the results of standard cosmological perturbation theory, our calculation is useful in the nonlinear regime because it yields accurate results when used as input to halo models.

The simulations use $N = 512^3$ particles, each with mass $780 M_\odot$, in a periodic volume of co-moving size $L_{\text{box}}^3 = (1.38 \text{ Mpc})^3$. The total mass in the simulation is about $10^{11} M_\odot$. At the starting scale factor of $a_i = 10^{-3} a_{\text{eq}}$, the particles are independently (Poisson) distributed in space and have a Maxwell-Boltzmann velocity distribution with a 1D velocity dispersion of $\sigma \equiv \langle \mathbf{v}^2/3 \rangle^{1/2} = 0.0724c = 21700 \text{ km s}^{-1}$.

We evolve the simulation volumes using a version of GADGET-4 [78] that we modified to include a homogeneous radiation component (as in ref. [79]). For simplicity, we take the white noise particles to be all of the matter. Otherwise, we adopt a cosmology in line with the Planck measurements [74]. Most relevantly, we have $a_{\text{eq}} = 2.94 \times 10^{-4}$ (where $a = 1$ today) and $k_{\text{eq}} = 1.04 \times 10^{-2} \text{ Mpc}^{-1}$.

The simulation particles represent physical dark matter particles, so it would be appropriate to run a “collisional” simulation, which fully resolves short-range gravitational interactions between the simulation particles (e.g. [80, 81]). This approach was used in a recent cosmological simulation with primordial black holes (PBHs) [82]. However, for the sake of computational efficiency, we will neglect short-range interactions by including standard GADGET-4 force softening. The co-moving softening length is taken to be $0.03\bar{n}^{-1/3}$, where \bar{n} is the co-moving number density of simulation particles. Although short-range interactions are important in simulations of cold PBHs [82], this is largely because structure formation in that scenario begins at the scale of just a few PBHs. For scenarios with warm

⁸For a given particle, an encounter with another particle with impact parameter b and relative velocity v induces a velocity kick $\Delta v = 2Gm/(bv)$. There are $dN_{\text{enc}} \sim \bar{n}_p vt_{\text{relax}} 2\pi b db$ encounters per b interval over time t_{relax} , where \bar{n}_p is the physical number density. Relaxation corresponds to $\int dN_{\text{enc}} (\Delta v)^2 \sim v^2$, which yields $t_{\text{relax}} \sim v^3/[8\pi(\ln \Lambda)(Gm)^2 \bar{n}_p]$, where $\ln \Lambda = \int db/b$ is the Coulomb logarithm. Taking $\ln \Lambda \sim 10$ and using the definition of k_J (with $v \sim \sigma$), we can obtain $t_{\text{relax}} \sim (\bar{n}/k_J^3)H^{-1}$.

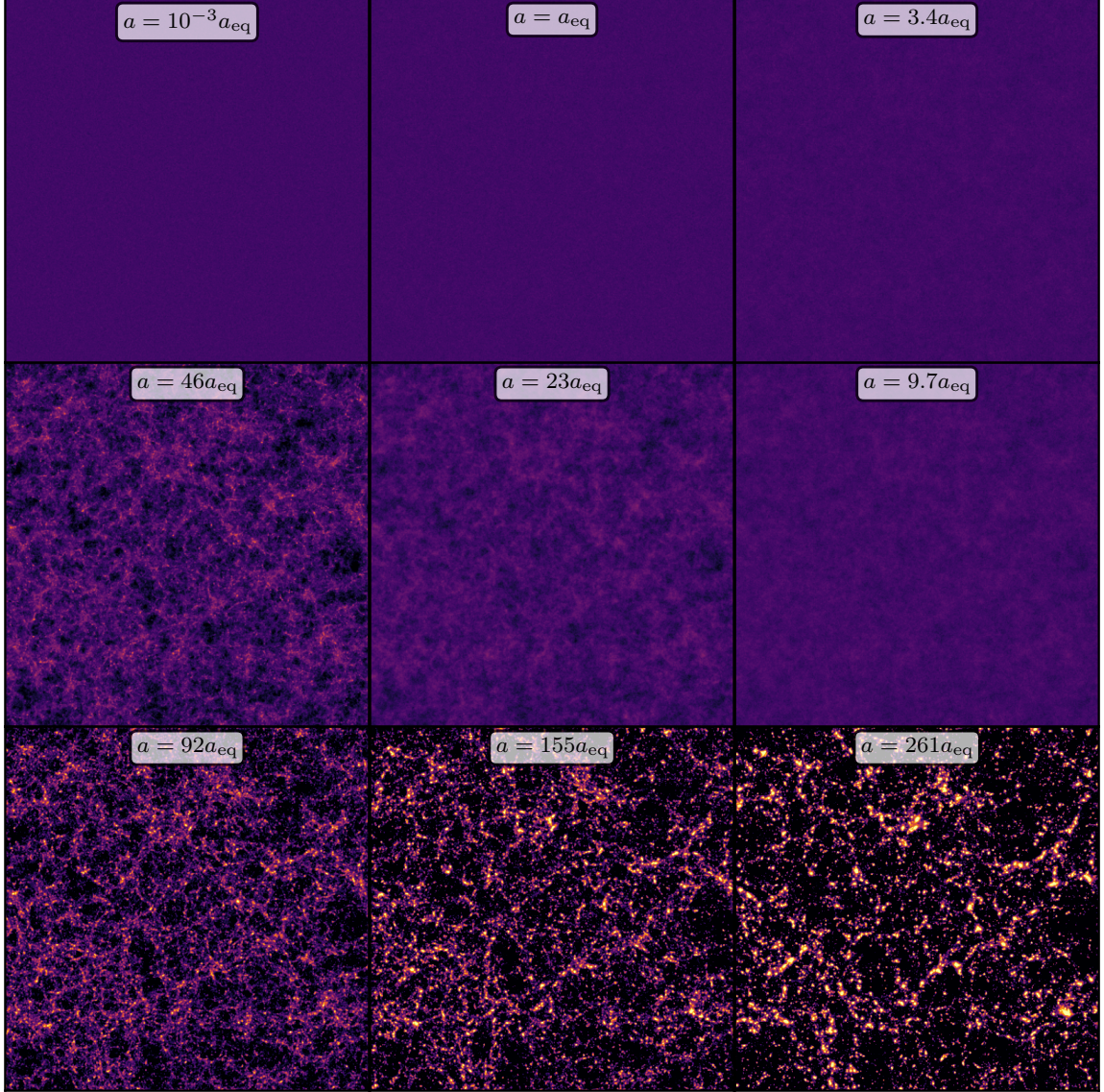


Figure 5: Gravitational clustering of a warm, Poisson distributed collection of particles (without initial adiabatic perturbations). We show, with a logarithmic color scale, the projected density across the 1.38 Mpc (co-moving) simulation volume. Note the lack of clustering during radiation domination ($a < a_{\text{eq}}$) and significant clustering during matter domination. For the scenario shown, the co-moving Jeans length during matter domination is $2\pi/k_J \approx 0.05 \text{ Mpc} \times \sqrt{a_{\text{eq}}/a}$. Clustering is suppressed below this length scale.

white noise, structure formation can begin at larger scales, since it is Jeans-suppressed at few-particle scales.

3.1 White Noise in the Linear Regime

First, we consider a scenario with no initial adiabatic power. In this case, the simulation particles are initially uniformly distributed in space with zero mean velocity. Figure 5 shows

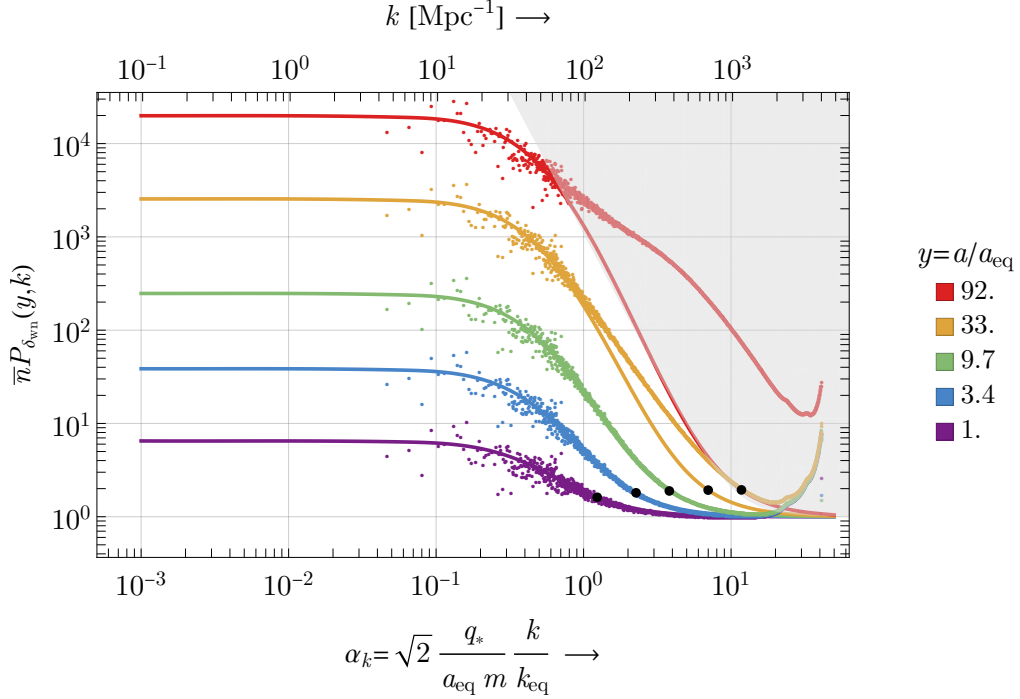


Figure 6: Comparing the analytic growth of the white-noise power spectrum with results from an N -body simulation. The solid curves are the analytic predictions, while the colored smaller dots are N -body results. The gray region marks the nonlinear regime, $(k^3/2\pi^2)[P_{\delta_{\text{wn}}}(y, k) - \bar{n}^{-1}] > 1$. The agreement between analytic and numerical results is excellent before the onset of nonlinearity. The model, initial conditions, and parameters are same as Fig. 3. The large black dots indicate the Jeans wavenumber $k_J(y)$.

the evolution of the simulation volume from these initial conditions. The Jeans wavelength at matter-radiation equality is about $2\pi/k_J \simeq 0.05$ Mpc (about $1/27$ the width of the simulation volume), and this provides a characteristic scale at which structure formation begins. Collapsed halos become abundant by about $a = 92a_{\text{eq}}$ (redshift $z = 36$).

Figure 6 compares the matter power spectrum in the simulation to our analytic calculation. At early times, when $a \lesssim 10a_{\text{eq}}$, we find good agreement (except at very low k due to cosmic variance in the simulation volume). At these times, density perturbations larger than the Jeans scale are still in the linear regime. Deviations from the analytic prediction become significant at later times as the growing density perturbations approach the nonlinear regime (indicated with gray shading).

3.2 White Noise Beyond the Linear Regime

For standard structure formation scenarios, the predictions of linear perturbation theory remain useful even deep in the nonlinear regime because they are the basis for halo models, such as Press-Schechter theory [83] and variants (e.g. [84–87]). We now show that this remains true for the analytical white noise power spectrum (2.56), and we can use it to accurately predict the halo mass function. The simplest halo models connect the halo mass

function to the linear matter power spectrum $P_\delta(k)$ through the rms density variance

$$\sigma_M^2 = \int_0^{k_{\max}} d\ln k \frac{k^3}{2\pi^2} P_\delta(k) W^2(kR_M), \quad (3.1)$$

in spheres of mass M , where $R_M \equiv [3M/(4\pi\bar{\rho})]^{1/3}$ is the radius of such a sphere and $W(z) \equiv 3(\sin z - z \cos z)/z^3$ is the spherical top-hat window function in Fourier space. Ordinarily, the upper limit of the spectral integral is taken to be $k_{\max} \rightarrow \infty$.

Figure 7 shows the halo mass function in the simulation. We use the M_{200} mass definition, which is the mass of the sphere whose enclosed density is 200 times the cosmological average.⁹ We express the halo mass function as $df/d\ln M$, the differential *fraction of dark matter* in halos of mass M (per logarithmic mass interval). Note that $df/d\ln M$ is related straightforwardly to the differential number density of halos via $dn/d\ln M = (\bar{\rho}/M)df/d\ln M$, but the differential mass fraction is often a more useful quantity because it covers a much smaller dynamic range. Figure 7 shows that over time, an increasing proportion of the dark matter comes to reside in massive halos, although the mass fraction in low-mass halos does not appear to decrease.

We compare the halo mass functions in the simulation to the predictions of the formulation of excursion set theory presented by ref. [89], which is similar to the classic Press-Schechter approach [83] but more closely follows its theoretical foundations in excursion set theory [90]. For convenience, we will employ the fitting function provided by ref. [89],

$$\frac{df}{d\ln M} = 0.658 \sigma_M^{-0.582} e^{-1.056/\sigma_M^2} \left| \frac{d\ln \sigma_M}{d\ln M} \right|, \quad (3.2)$$

which is a fit to the predictions of the excursion set theory (not a direct fit to simulations). Taking $k_{\max} \rightarrow \infty$ in equation (3.1), the dashed lines in Fig. 7 show that this model accurately predicts the halo mass function in most regimes. We have also separately verified that it is more accurate than the Press-Schechter formula.¹⁰

However, this calculation overpredicts the halo abundance at the low-mass end. This discrepancy arises because not all of the density variation associated with the white-noise power spectrum is associated with gravitational clustering. As Fig. 6 shows, the white-noise power spectrum always extends into the nonlinear regime at high enough k , but such small-scale perturbations do not necessarily contribute to gravitational clustering. Perturbations on such short length scales (below the Jeans length) are continually rearranging themselves due to random particle motion, so that the density perturbations average to zero over the long time scales relevant to gravitational clustering.

⁹We center this sphere on the minimum of the gravitational potential. Halos are first identified using a friends-of-friends algorithm [88] with a co-moving linking length of $0.2\bar{n}^{-1/3}$ and a minimum of 32 particles.

¹⁰The standard Press-Schechter formula (with $\delta_c \simeq 1.686$) is

$$\frac{df}{d\ln M} = \sqrt{\frac{2}{\pi}} \frac{\delta_c}{\sigma_M} e^{-\delta_c^2/(2\sigma_M^2)} \left| \frac{d\ln \sigma_M}{d\ln M} \right| \quad (3.3)$$

and is derived assuming density perturbations averaged on different mass scales are uncorrelated. The approach of ref. [89] accounts for the correlations, and its predictions are well fit by equation (3.2) instead.

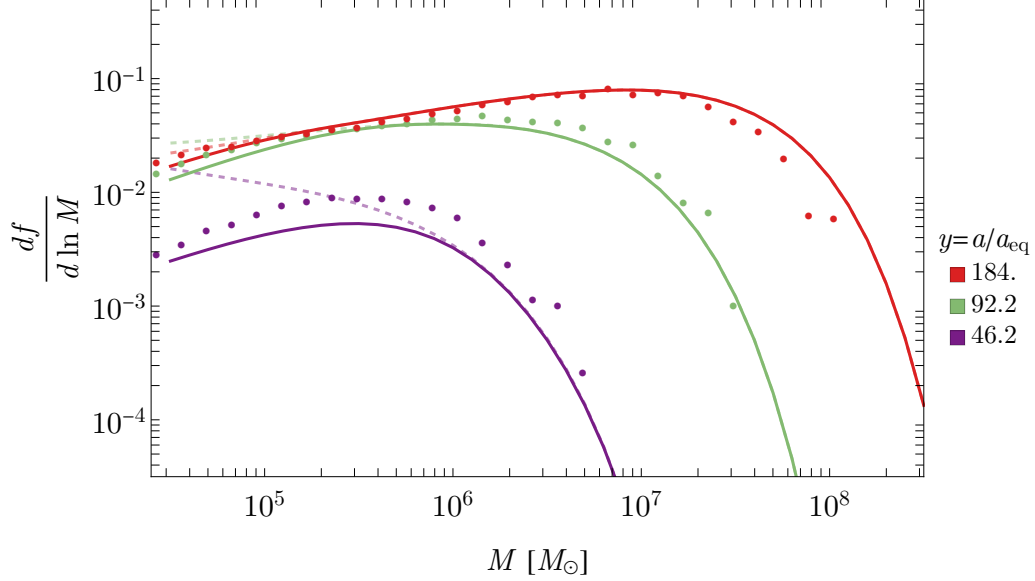


Figure 7: Comparing the halo mass function obtained using our analytically predicted power spectrum with results from an N -body simulation, for the case of white-noise initial conditions. We plot $df/d \ln M$, the differential fraction of mass in halos of mass M per logarithmic interval in M . Solid lines show analytic predictions using the halo mass function from ref. [89] with power spectrum cut off above $k_J/4$, reflecting that smaller-scale perturbations cannot contribute to gravitational clustering. The prediction closely matches results from an N -body simulation (colored dots). The lighter dashed lines show analytic predictions when no cutoff is imposed in the linear matter power spectrum.

To address this problem, we make the simple ansatz that perturbation modes with $k > k_J/4$ do not contribute to gravitational clustering, where $k_J \equiv a\sqrt{4\pi G\bar{\rho}}/\sigma$ is the (co-moving) Jeans wavenumber given in equation (2.62) (and σ is the 1D peculiar velocity dispersion). That is, we cut off the spectral integral in equation (3.1) at $k_{\max} = k_J/4$. The numerical factor of $1/4$ is not theoretically motivated, but it works well empirically. Figure 7 shows that with this ansatz, the mass functions predicted by equation (3.2) match the simulation results reasonably well at all masses and redshifts.

In Appendix D, we also consider the same simulation setup with a uniform-sphere velocity distribution instead of a Maxwell-Boltzmann velocity distribution. The analytically predicted power spectrum continues to be accurate in the linear regime for this scenario. Predicted halo mass functions are also reasonably accurate, but for the uniform-sphere scenario, the $k_{\max} = k_J/4$ ansatz somewhat overestimates the abundance of low-mass halos at early times.

3.3 White Noise with Initial Adiabatic Perturbations

We now modify the simulation initial conditions to include adiabatic density perturbations on top of the warm white noise. We use the CLASS code [91] to evaluate the cold dark matter power spectrum at redshift $z = 31$ given Planck cosmological parameters [74],

and then we extrapolate the power spectrum backward to the simulation start time ($a = 10^{-3}a_{\text{eq}}$) using a growth function from ref. [92] that is consistent with the non-relativistic, dark-matter-only physics that are present in the simulation. The purpose of this procedure is that the forward simulation evolution would then reproduce approximately the correct adiabatic modes at late times, even though the early evolution in the simulation (at $z \gtrsim 100$) is not exactly correct due to the absence of baryons.

However, even with 512^3 particles, the simulation volume has few enough particles that the white noise would completely dominate over the adiabatic power almost up to the scale of the whole box. In order to ensure that we can resolve enough adiabatic power to test our prediction in equation (2.56), we amplify the initial adiabatic power spectrum by a factor of 100 (so density perturbations are scaled by a factor of 10).

To incorporate these adiabatic perturbations, we start with the warm white noise initial conditions discussed above, in which particles have independently uniformly distributed positions and a Maxwell-Boltzmann velocity distribution with 1D dispersion $\sigma = 0.0724c$. Then we use the power spectrum to sample a random field of particle displacements and velocities (in accordance with ref. [79]). Finally, we interpolate over these fields to add bulk displacements and velocities to the white-noise particle load.

Figure 8 compares the power spectrum in this simulation to the prediction (2.56). Similarly to the white-noise-only case, here the prediction matches the simulation well at early times, $y < 10$, when the growing density perturbations are still in the linear regime. For this scenario, there is a dip in the matter power spectrum owing to the suppression of the adiabatic power due to free streaming, and this dip is followed by a rise at higher k due to the white noise.

Figure 9 shows the M_{200} halo mass function in this simulation. Compared to the pure white-noise case, the adiabatic power causes halos at the high-mass end to become abundant much earlier, and low-mass halos become correspondingly less abundant. With the $k_{\text{max}} = k_J/4$ ansatz, equation (3.2) continues to predict these halo mass functions with reasonable accuracy, although the abundance of low-mass halos is slightly overpredicted. Here, when evaluating σ_M with equation (3.1), we impose a lower limit $k_{\text{min}} = \pi/L_{\text{box}}$ on the integration over k , where L_{box} is the co-moving length of the simulation volume, since this is the smallest k that contributes to density perturbations within the simulation. We also do not accurately predict the very high-mass end of the halo mass function, likely due to low-number statistics for halos of such masses.

We now compare how structure formation with warm white noise compares to other dark matter models. In all cases, we use the same initial velocity and displacement fields sampled above, corresponding to a power spectrum boosted by a factor of 100 compared to Planck cosmological parameters [74]. We consider four models of dark matter, which are represented in the simulation as follows.

- **Cold white noise:** Particles are Poisson distributed in the initial conditions (at $y = a/a_{\text{eq}} = 10^{-3}$), but with no velocity dispersion, before being displaced in accordance with the initial velocity and displacement fields. For example, this could represent a typical primordial black hole cosmology [82, 93].

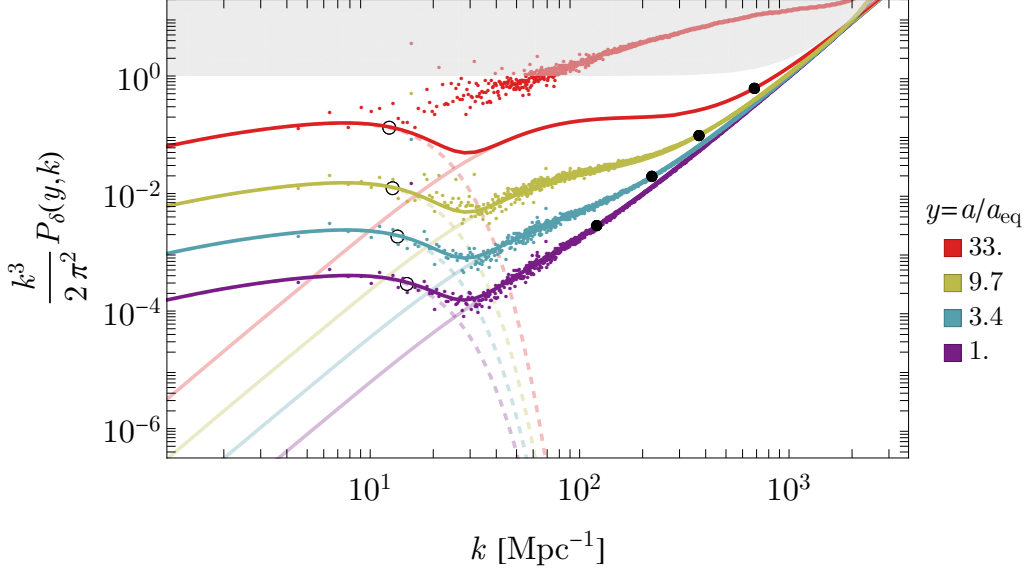


Figure 8: Comparing the analytic evolution of the dimensionless power spectrum with results from an N -body simulation for a scenario with both white noise and initial adiabatic perturbations. The solid curves are the analytic predictions, which are the sum of adiabatic (faint dashed) and white-noise (faint solid) contributions, while the colored dots are N -body results. The agreement between analytic and numerical results is excellent before the onset of nonlinearity (shaded area). Similarly to previous figures, we adopt $\sigma_{\text{eq}} = q_*/a_{\text{eq}}m \approx 22 \text{ km s}^{-1}$ and $\bar{n} \approx 5 \times 10^7 / \text{Mpc}^3$, but here the initial adiabatic spectrum has been boosted by a factor of 100 compared to Planck (2018) parameters in order to make it relevant within the $(1.38 \text{ Mpc})^3$ (co-moving) simulation volume. The open and filled black dots are the free-streaming and Jeans wavenumbers, respectively.

- **Warm white noise:** As described earlier, we start with Poisson-distributed particles with a Maxwell-Boltzmann initial velocity distribution (with 1D dispersion $\sigma = 0.0724c$) and include adiabatic perturbations.
- **Warm (no white noise):** Here the simulation particles are each supposed to represent a large number of physical dark matter particles. To suppress discreteness noise, simulation particles are initially placed on a grid before being subjected to the initial velocity and displacement fields. Additionally, we do not include a velocity dispersion, since it would induce discreteness noise. Instead, we use equation (2.56) to calculate the suppression of adiabatic perturbations at $y = 10$ due to the initial Maxwell-Boltzmann velocity distribution, and we apply that suppression to the initial velocity and displacement fields. This resembles the standard approach for simulating warm particle dark matter (e.g. [94]).
- **Cold (no white noise):** Same as the warm case without white noise, but here we omit the suppression to initial perturbations.

Figure 10 shows how structure formation proceeds for these different models. As is

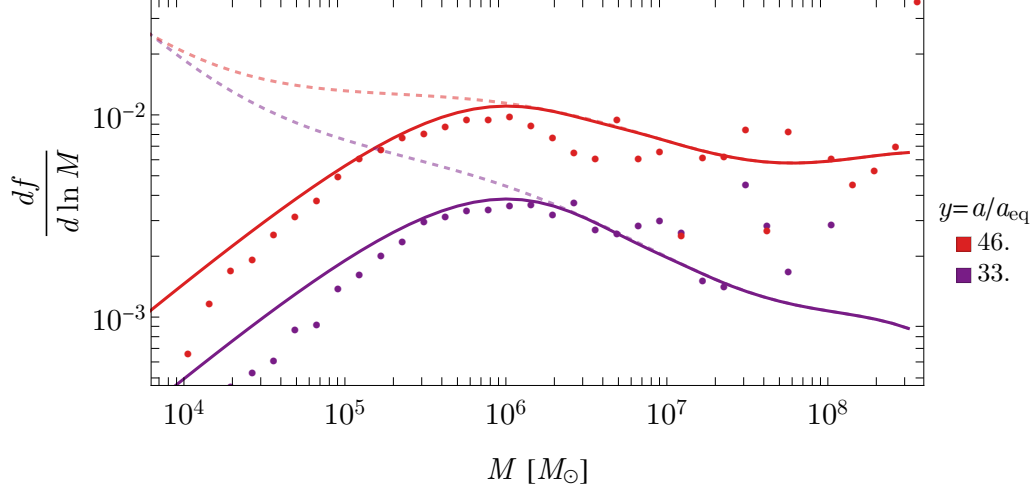


Figure 9: Halo mass functions for a scenario with both white noise and adiabatic initial perturbations. We show $df/d \ln M$, the differential fraction of mass in halos of mass M per logarithmic interval in M . The colored points are from an N -body simulation, while the solid lines are the mass function from ref. [89] evaluated using the analytic power spectrum cut off above $k_J/4$ (as in Fig. 7), reflecting inability of smaller-scale modes to contribute to gravitational clustering. This analytic prediction generally matches the N -body results well. The lighter dashed curves are analytic predictions with no cutoff imposed in the power spectrum.

well known (e.g. [95]), the cold white noise scenario produces an abundance of very small, dense structures. These structures turn out to be absent in the warm white noise case due to the Jeans scale. Note however that our cold white noise simulation does not properly include short-range gravitational interactions, which tend to suppress the abundance and internal density of the smallest structures [82].

Meanwhile, the warm dark matter scenario without white noise produces no structure at all at very small scales. Compared to this, the particle noise in the warm white noise simulation introduces structure at smaller scales. Indeed, the warm white noise scenario turns out to make a pattern of structures that is similar to that produced by cold dark matter without white noise. However, this is largely a coincidence owing to the similarity between the analytically predicted power spectrum in figure 8 and a cold dark matter power spectrum. For example, if the adiabatic power were not boosted by a factor of 100, then the cold dark matter scenario without white noise would produce nonlinear structures significantly later than would the warm white noise.

3.4 Halo Internal Structures

Finally, we provide a brief discussion of the internal structures of dark matter halos in the different scenarios considered in this section. Figure 11 compares the density profiles of the largest halo from each simulation at the time $y = 46$. For all of the simulations with adiabatic power, this halo has a mass of about $M_{200} \approx 10^9 M_\odot$ (1% of the total

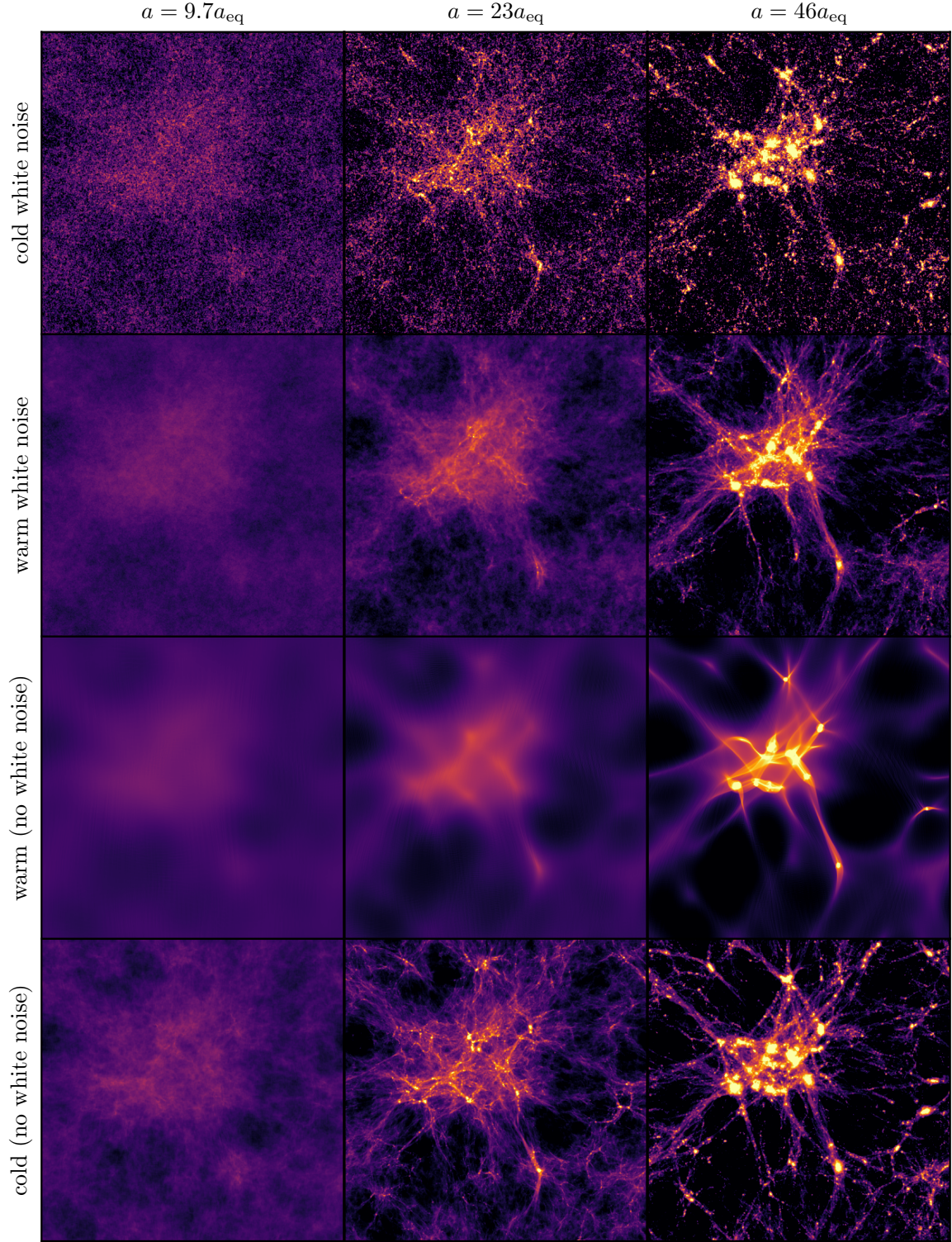


Figure 10: Comparing structure formation with warm white noise (second row from top) to other dark matter models; see the text for details. In all cases the adiabatic power is boosted by a factor of 100 compared to Planck cosmological parameters [74]. We show, with a logarithmic color scale, the density projected across the $(1.38 \text{ Mpc})^3$ co-moving box.

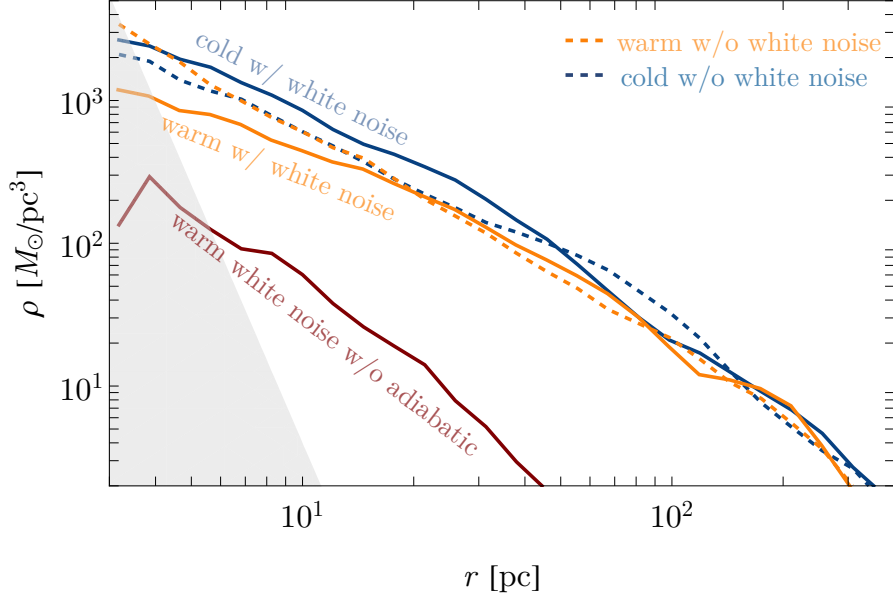


Figure 11: Comparing density profiles of a halo of mass $M \approx 10^9 M_\odot$ at $y = a/a_{\text{eq}} = 46$ in the different sets of simulations for cold and warm dark matter (blue and orange curves) shown in Fig. 10. Their initial conditions include $100\times$ boosted adiabatic power with and without white noise. The maroon curve is for a halo of $M \approx 5 \times 10^6 M_\odot$ at $y = 46$ from the warm white noise simulation in Fig. 5, which does not include initial adiabatic perturbations. This halo is approximately representative of what would be expected to arise in a realistic warm white noise cosmology without the boost to adiabatic power. The shaded region marks the boundary of maximum density based on phase space considerations for the warm dark matter cases – increased resolution would reveal a shallow central core.

mass in the simulation). This halo has a similar internal structure in all cases, owing to the dominance of the $100\times$ boosted adiabatic power spectrum at this mass scale, but there are still noteworthy differences. As seen in Fig. 11, warm white noise (solid orange) produces a less internally dense structure than does warm dark matter (without white noise, dashed orange) with the same velocity distribution. This outcome is somewhat surprising given that the warm white noise power spectrum matches or exceeds at all k the power spectrum of warm dark matter without white noise. The usual expectation is that more power leads to earlier halo formation and thus more internally dense halos [96–99]. However, this difference in outcome is likely related to prompt cusp formation in the warm case without white noise [100–103]. This prompt cusp formation has been shown in simulations to produce a compact $\rho \propto r^{-1.5}$ density cusp on the scale at which the matter power spectrum cuts off due to free streaming [79, 98, 99, 104–113]. The halo in our warm simulation without white noise indeed possesses a precisely $\rho \propto r^{-1.5}$ density profile (dashed orange). For warm white noise (solid orange), on the other hand, the white-noise contribution to the matter power spectrum appears to prevent prompt cusp formation from occurring.

The warm white noise halo is also less internally dense than the halos that form in both of the cold dark matter simulations (with and without white noise, solid and dashed blue). This outcome is unsurprising because the power spectra of cold dark matter and cold white noise lie above the power spectrum of warm white noise at all k , leading to earlier halo formation. Note however that, as we discussed above, the cold white noise simulation does not resolve short-range interactions that can be important in this scenario [82]. Also, the high halo density in the simulations without white noise is an artificial consequence of our $100\times$ boosted adiabatic power spectrum. Without that boost, we expect warm white noise to produce denser halos than would dark matter without white noise, as we show next.

The maroon line in Fig. 11 shows the largest halo at the same time, $y = 46$, in the warm white noise simulation without adiabatic power (sections 3.1 and 3.2). This halo has mass $M_{200} \approx 5 \times 10^6 M_\odot$. Note that $y = 46$ corresponds to the redshift $z \approx 72$, which is largely before halos would form from standard adiabatic fluctuations. Consequently, this halo is fairly representative of what would actually arise in a warm white noise cosmology. It reaches an internal density of $\sim 100 M_\odot \text{pc}^{-3}$, a significantly higher value than would arise comparably deep inside standard cold or warm dark matter halos. Without the boost to adiabatic power, our simulations without white noise would not have even produced a halo by $y = 46$.

Note that the density within the warm white noise halo is not expected to increase further at (unresolved) smaller radii, because it already saturates the phase-space limit (shaded region) discussed by ref. [99]. The initial velocity dispersion of the dark matter sets a maximum phase-space density at early times, and this density cannot be exceeded inside collapsed systems later. A halo’s cold central density cusp should shallow into a finite-density core once it crosses into the shaded area.

Finally, we note that although our simulations do not resolve short-range gravitational interactions, we expect that these interactions would eventually give rise to gravo-thermal core collapse [114] inside warm white noise halos, greatly boosting the central density. Core collapse has been suggested to arise in halos of primordial black holes (cold white noise) [115–117], but this process may be forestalled by the abundance of tightly bound binary systems that arise in this scenario prior to halo formation [82]. For warm white noise, however, the velocity dispersion should largely prevent the formation of binary systems outside of halos, so they should not present an obstacle to core collapse.

4 Generalizations

4.1 Warm Wave Dark Matter

We can translate our results to wave dark matter as follows. Suppose that we begin with a field ϕ with a mass m_ϕ , with its initial power spectrum $q^3 P_\phi(t_0, q)$ peaked at a $q = k_*$ such that $a(t_0)H(t_0) < k_* < a(t_0)m_\phi$.¹¹ Then, $\sigma_{\text{eq}} \sim k_*/m_\phi a_{\text{eq}}$ and $\bar{n} \sim k_{\text{wn}}^3 \sim k_*^3$. Here k_*^{-1} is the de Broglie length scale which characterizes the comoving size and separation

¹¹Such peaked spectra without a significant zero mode in the dark matter field can arise from post-inflationary/causal production mechanisms. For example, see refs. [118–126]. For inflationary production, such spectra arise for vector dark matter (e.g. [127, 128]), and for some cases in scalars, e.g. [34, 129].

of the quasi-particles as well as the velocity dispersion. Note that m used in the present work would be the mass of the quasi-particle, i.e., the mass within a de Broglie volume: $m \sim \bar{\rho}_{a=1}/k_*^3 \gg m_\phi$, and the momentum would be $q_* \sim (m/m_\phi)k_* \gg k_*$. For fiducial parameters used here and in ref. [35], we have $(m_\phi, k_*) \sim (10^{-19}, 10^{-26}) \text{ eV}$.¹² The free-streaming and Jeans scales (2.62) in this scenario are determined by k_* . These scales are different from the scale of the cutoff ($k \sim a\sqrt{mH}$ [52]) in the power spectrum for cold wave dark matter (dominated by a zero mode of the field). Also see the discussions in refs. [35–37]. We expect our framework to be applicable to wave dark matter as long as we restrict ourselves to length scales larger than k_*^{-1} .

In an upcoming work [130], results of cosmological Schrödinger-Poisson simulations and corresponding analytic calculations for structure formation in warm wave dark matter will be provided. Results consistent with the present work are seen in those simulations (above the de Broglie scale). In particular, the power spectrum shows: (i) a scale-dependent growth of the white-noise-like part during matter domination along with a Jeans suppression, and (ii) free-streaming suppression of the adiabatic part. The initial conditions relevant for these simulations, and evolution during radiation domination, are discussed in detail in ref. [37].

A detailed derivation of a single- and multi-component Boltzmann-like equation appropriate for non-relativistic wave dynamics inside a halo is provided in ref. [131]. One of the key results there was the time-scale of soliton formation [131, 132]. It is not possible to get this time-scale directly in the current work. It would be interesting to merge the two approaches, which we leave for future work. Furthermore, the impact of non-standard expansion histories [38] and non-minimal couplings [133] can also be considered. While our focus here is on dark matter, we note at the end of inflation, peaked field spectra in the inflaton field are naturally generated via self-resonance [134]. It would be possible to apply our formalism to gravitational clustering in those very-early-universe scenarios once the field becomes non-relativistic, e.g. [135, 136], and/or if the field fragments into solitons (e.g. [135, 137, 138]).

4.2 Non-gravitational Interactions

Inclusion of non-gravitational interactions is possible within our framework. This requires us to consider acceleration due to forces other than gravity. That is, the acceleration of particle i due to particle j now becomes

$$\mathbf{a}_{ij} = \mathbf{a}_{ij}^{\text{grav}} + \mathbf{a}_{ij}^{\text{int.}}. \quad (4.1)$$

If $\mathbf{a}_{ij}^{\text{int.}} = a^{-1}(t)\nabla_{\mathbf{x}_i} V_{ij}^{\text{int.}}(a(t)|\mathbf{x}_i - \mathbf{x}_j|)$, then the derivation proceeds almost identically to before. For example, the additional interaction potential could be of Yukawa type,

$$V^{\text{int.}}(r) = -\alpha_\chi \frac{e^{-\mu r}}{r}. \quad (4.2)$$

Instead of equation (2.25), the acceleration due to this potential would be

$$\mathbf{a}_{ij}^{\text{int.}} = -4\pi G m \alpha_\chi \int_{\mathbf{q}} \frac{i\mathbf{q}}{q^2 + \mu^2} e^{i\mathbf{q} \cdot (\mathbf{x}_i - \mathbf{x}_j)}. \quad (4.3)$$

¹²Note that $k_*/\text{eV} \approx 6.4 \times 10^{-30} k_*/\text{Mpc}^{-1}$.

This interaction is expected to affect the power spectrum for $k > \mu a(t)$. This type of additional interaction has been the focus of intense study to understand the small-scale structure in dark matter [139, 140], and warrants careful exploration. As special cases, this interaction also includes point or hard-sphere scattering type interactions [141].

Generalizing further, if the differential cross section is available, we can relate this interaction potential to it via $d\sigma_{ij}/d\Omega \propto |\tilde{V}_{ij}^{\text{int.}}(\mathbf{q})|^2$ (under the Born Approximation in the non-relativistic regime). Here, $\tilde{V}_{ij}^{\text{int.}}(\mathbf{q})$ is the Fourier transform of the interaction potential. Hence, such interactions can also be included in the framework we have. Such non-gravitational interactions can also be included for wave dark matter discussed earlier [135, 142–146].

As has been appreciated for a long time, the equations for Newtonian gravitational dynamics of dark matter (or stellar systems) are similar to those for plasmas where electric fields are included but magnetic fields are ignored. If dark gauge fields are included, and the dark electric and magnetic fields are also relevant, one can imagine using the plasma physics literature to read off some results for the dark sector.

4.3 Subdominant Fractions

Gravitational microlensing and stellar dynamics place strong constraints on scenarios in which all of the dark matter is in macroscopically massive “particles” [147, 148]. Therefore, it would be natural to extend our treatment to scenarios in which these particles comprise a small fraction of the dark matter. In general, for particles with differential number density dn/dm per mass interval and co-moving spatial volume, the initial white-noise power spectrum is

$$P_{\delta_{\text{wn}}}(y_0, k) = \frac{1}{\bar{\rho}^2} \int dm m^2 \frac{dn}{dm}. \quad (4.4)$$

If a fraction f of the dark matter mass is in massive “particles” of a single mass m , with the remainder being microscopic particle dark matter, then

$$P_{\delta_{\text{wn}}}(y_0, k) = \frac{fm}{\bar{\rho}} = \frac{f^2}{\bar{n}}, \quad (4.5)$$

where $\bar{n} = f\bar{\rho}/m$ is the co-moving number density of the massive particles. In these expressions we take $\bar{\rho}$ to be the co-moving matter density.

This means that, for sufficiently high particle masses, a small fraction of the dark matter can still give rise to a significant white-noise contribution. However, the growth of structure with fractional warm white noise will differ from what we have calculated. We leave this calculation for future work. For example, the massive “particles” under consideration could be oscillons/Q-balls/solitons/boson stars (e.g. [135, 149–156]), miniclusters (e.g. [40, 157–159]), primordial black holes (e.g. [147, 148, 160–164]), or substructure arising from enhanced primordial power at small scales (e.g. [16, 43, 79, 110, 165–170]). Hence such dynamics would find quite general applicability.

4.4 Relativistic Physics

We have focused on the regime of non-relativistic motion and Newtonian gravity. The relativistic regime complicates an analytical treatment in two main ways:

1. Relativistic motion couples kinematics in different directions, because the distance covered along some axis depends not only on the velocity component along that axis but also on the velocity magnitude.
2. Relativistic gravity depends not only on position but also on velocity.

Relativistic physics are important for properly describing the early evolution of the adiabatic perturbations. The non-relativistic growth functions $\mathcal{T}_{\mathbf{k}}^{(a,b)}(y, y')$ that we have derived describe perturbation growth that begins at some preset initial time y' , and although the precise value of y' is not important, the general order of magnitude must be picked carefully. In particular, the $y' \rightarrow 0$ limit is not meaningful. Roughly speaking, Newtonian free streaming at some scale k begins either at horizon entry ($k \sim aH$), which is when the perturbation is sourced, or when the streaming motion becomes non-relativistic – whichever is later. But a relativistic version of our derivation would be needed to account for these effects precisely. A relativistic description would also be needed to describe a fraction of the dark matter that is still relativistic at the time of matter-radiation equality. In the context of wave dark matter, some of these relativistic effects are included in the Klein-Gordon simulations of ref. [37].

5 Summary & Conclusions

We have investigated the evolution of density perturbations in warm dark matter including the effect of a finite number density, which gives rise to an (initially) white-noise contribution to the power spectrum of density perturbations. Observationally accessible examples of such white-noise spectra (at $k \gtrsim 10/\text{Mpc}$) with significant velocity dispersion can arise when light wave dark matter is produced after inflation. White-noise-related effects are also present for heavy primordial black holes, solitons, etc. composing (a fraction of) the total dark matter. The power spectrum enhancement on small scales due to white noise can have important consequences, such as accelerating early galaxy formation (e.g. [171–173]). To understand the growth of structure on small scales in these scenarios, we derive a formalism, based on solving the truncated BBGKY hierarchy, that provides the shape and time-evolution of the power spectrum.

We provide efficient code to numerically evaluate the results of our formalism, which are expressed as time integrals of solutions to a linear Volterra equation. These results include several key features. An initially white-noise power spectrum remains approximately constant in time during the radiation era, because it cannot be erased by free streaming of particles. During the matter-dominated era, self-gravity causes that power spectrum to grow below the Jeans wavenumber k_J , but growth remains suppressed above k_J . The formalism also naturally includes the contribution from initial adiabatic perturbations, for which we recover the standard growth and free-streaming suppression.

Our calculations of the matter power spectrum agree precisely with the results of numerical simulations as long as fractional density perturbations remain small. In the regime of large perturbations, we also used the predicted power spectra to estimate halo mass functions. In most regimes, the results agree well with the halo distributions that

arise in numerical simulations of the same cosmological scenarios. At the smallest mass scales, the accuracy of our predicted halo mass functions is improved by making the ansatz that perturbations on wavenumbers $k > k_J/4$ do not contribute to halo formation.

Beyond observations, we expect that our results can be useful for interpreting cosmological N -body simulations, in which warm white noise emerges as a discreteness artifact. Ordinarily, simulations are initialized to minimize white noise in the initial conditions, but it would still emerge during nonlinear evolution. In some cases, artificial warm white noise can also be relevant in the linear regime, for example if the simulation were initialized with a velocity dispersion (e.g. [174]) or if a velocity dispersion were to arise dynamically (e.g. [175]).

Moreover, our framework includes traditional warm and cold dark matter models. In most cases, microscopic particle dark matter is far too warm for the Poissonian particle noise to give rise to any gravitational clustering. However, for some models, such as that proposed by refs. [176–178], the dark matter is sufficiently cold and heavy that gravitational clustering can be relevant on scales on which the power spectrum is boosted by white noise. Moreover, even if the particle noise is not relevant, our results supply an alternative way to evaluate the effect of free streaming on the matter power spectrum, which is faster and simpler than the usual approach of integrating the Boltzmann hierarchy (e.g. [179]). This aspect of our calculation is similar to the approach suggested by ref. [180] but is much simpler because we focus on the non-relativistic regime.

We expect that the formalism can be generalized in multiple ways, which we discussed but did not work out in detail. (1) It is possible to include fractional amounts of dark matter in a warm and/or white-noise component. (2) We can accommodate non-gravitational interactions between the dark matter particles. (3) We are working on a generalization to wave dark matter, where we expect the present results to hold above the de Broglie length. (4) It would be useful to incorporate relativistic physics and the effects of baryons. Alternatively, it would be worthwhile to consider inclusion of the effects discussed here in existing numerical codes (e.g. [91, 181, 182]), which already account for relativistic effects and baryonic physics.

Acknowledgements

MA is supported by a DOE award DE-SC0021619. Part of this research was supported by grant NSF PHY-2309135 to the Kavli Institute for Theoretical Physics (KITP). Simulations for this work were carried out on the OBS HPC computing cluster at the Observatories of the Carnegie Institution for Science. We thank Fabian Schmidt for important insights regarding the analytic results. We also gratefully acknowledge access to simulation results of warm wave dark matter carried out by Simon May as well as conversations with him. We thank Adrienne Erickcek, Mudit Jain, Andrew Long, Siyang Ling, and Moira Venegas for helpful discussions.

References

- [1] M. Cirelli, A. Strumia and J. Zupan, *Dark Matter*, [2406.01705](#).
- [2] D.J.E. Marsh, D. Ellis and V.M. Mehta, *Dark Matter: Evidence, Theory, and Constraints*, Princeton Series in Astrophysics, Princeton University Press (10, 2024), [10.1515/9780691249711](#).
- [3] A. Drlica-Wagner et al., *Report of the Topical Group on Cosmic Probes of Dark Matter for Snowmass 2021*, [2209.08215](#).
- [4] C. Mondino, A.-M. Taki, K. Van Tilburg and N. Weiner, *First Results on Dark Matter Substructure from Astrometric Weak Lensing*, *Phys. Rev. Lett.* **125** (2020) 111101 [[2002.01938](#)].
- [5] N. Sabti, J.B. Muñoz and D. Blas, *New Roads to the Small-scale Universe: Measurements of the Clustering of Matter with the High-redshift UV Galaxy Luminosity Function*, *Astrophys. J. Lett.* **928** (2022) L20 [[2110.13161](#)].
- [6] D. Gilman, A. Benson, J. Bovy, S. Birrer, T. Treu and A. Nierenberg, *The primordial matter power spectrum on sub-galactic scales*, *Mon. Not. Roy. Astron. Soc.* **512** (2022) 3163 [[2112.03293](#)].
- [7] M.S. Delos and F. Schmidt, *Stellar streams and dark substructure: the diffusion regime*, *Mon. Not. Roy. Astron. Soc.* **513** (2022) 3682 [[2108.13420](#)].
- [8] M. Boylan-Kolchin, *Stress testing Λ CDM with high-redshift galaxy candidates*, *Nature Astron.* **7** (2023) 731 [[2208.01611](#)].
- [9] D.J.H. Chung, M. Münchmeyer and S.C. Tadepalli, *Search for isocurvature with large-scale structure: A forecast for Euclid and MegaMapper using EFTofLSS*, *Phys. Rev. D* **108** (2023) 103542 [[2306.09456](#)].
- [10] V. Iršič et al., *Unveiling dark matter free streaming at the smallest scales with the high redshift Lyman-alpha forest*, *Phys. Rev. D* **109** (2024) 043511 [[2309.04533](#)].
- [11] M.S. Delos, *An analytical description of substructure-induced gravitational perturbations in stellar systems*, *Mon. Not. Roy. Astron. Soc.* **529** (2024) 2349 [[2312.13338](#)].
- [12] I. Esteban, A.H.G. Peter and S.Y. Kim, *Milky Way satellite velocities reveal the dark matter power spectrum at small scales*, *Phys. Rev. D* **110** (2024) 123013 [[2306.04674](#)].
- [13] E.O. Nadler, V. Gluscevic, T. Driskell, R.H. Wechsler, L.A. Moustakas, A. Benson et al., *Forecasts for Galaxy Formation and Dark Matter Constraints from Dwarf Galaxy Surveys*, *Astrophys. J.* **967** (2024) 61 [[2401.10318](#)].
- [14] H. Xiao, L. Dai and M. McQuinn, *Detecting dark matter substructures on small scales with fast radio bursts*, *Phys. Rev. D* **110** (2024) 023516 [[2401.08862](#)].
- [15] L. Ji and L. Dai, *Effects of Subhalos on Interpreting Highly Magnified Sources Near Lensing Caustics*, [2407.09594](#).
- [16] J. de Kruijf, E. Vanzan, K.K. Boddy, A. Raccanelli and N. Bartolo, *Searching for blue-tilted power spectra in the dark ages*, *Phys. Rev. D* **111** (2025) 063507 [[2408.04991](#)].
- [17] M.R. Buckley, P. Du, N. Fernandez and M.J. Weikert, *General Constraints on Isocurvature from the CMB and Ly- α Forest*, [2502.20434](#).

- [18] V.K. Narayanan, D.N. Spergel, R. Dave and C.-P. Ma, *Constraints on the mass of warm dark matter particles and the shape of the linear power spectrum from the Ly α forest*, *Astrophys. J. Lett.* **543** (2000) L103 [[astro-ph/0005095](#)].
- [19] S.H. Hansen, J. Lesgourgues, S. Pastor and J. Silk, *Constraining the window on sterile neutrinos as warm dark matter*, *Mon. Not. Roy. Astron. Soc.* **333** (2002) 544 [[astro-ph/0106108](#)].
- [20] A. Lewis and A. Challinor, *Evolution of cosmological dark matter perturbations*, *Phys. Rev. D* **66** (2002) 023531 [[astro-ph/0203507](#)].
- [21] A.M. Green, S. Hofmann and D.J. Schwarz, *The power spectrum of SUSY - CDM on sub-galactic scales*, *Mon. Not. Roy. Astron. Soc.* **353** (2004) L23 [[astro-ph/0309621](#)].
- [22] M. Viel, J. Lesgourgues, M.G. Haehnelt, S. Matarrese and A. Riotto, *Constraining warm dark matter candidates including sterile neutrinos and light gravitinos with WMAP and the Lyman-alpha forest*, *Phys. Rev. D* **71** (2005) 063534 [[astro-ph/0501562](#)].
- [23] J. Lesgourgues and S. Pastor, *Massive neutrinos and cosmology*, *Phys. Rept.* **429** (2006) 307 [[astro-ph/0603494](#)].
- [24] M. Viel, G.D. Becker, J.S. Bolton, M.G. Haehnelt, M. Rauch and W.L.W. Sargent, *How cold is cold dark matter? Small scales constraints from the flux power spectrum of the high-redshift Lyman-alpha forest*, *Phys. Rev. Lett.* **100** (2008) 041304 [[0709.0131](#)].
- [25] A. Boyarsky, J. Lesgourgues, O. Ruchayskiy and M. Viel, *Lyman-alpha constraints on warm and on warm-plus-cold dark matter models*, *JCAP* **05** (2009) 012 [[0812.0010](#)].
- [26] A.L. Erickcek and K. Sigurdson, *Reheating Effects in the Matter Power Spectrum and Implications for Substructure*, *Phys. Rev. D* **84** (2011) 083503 [[1106.0536](#)].
- [27] L. Lancaster, F.-Y. Cyr-Racine, L. Knox and Z. Pan, *A tale of two modes: Neutrino free-streaming in the early universe*, *JCAP* **07** (2017) 033 [[1704.06657](#)].
- [28] V. Iršič et al., *New Constraints on the free-streaming of warm dark matter from intermediate and small scale Lyman- α forest data*, *Phys. Rev. D* **96** (2017) 023522 [[1702.01764](#)].
- [29] V. Iršič et al., *New Constraints on the free-streaming of warm dark matter from intermediate and small scale Lyman- α forest data*, *Phys. Rev. D* **96** (2017) 023522 [[1702.01764](#)].
- [30] C. Miller, A.L. Erickcek and R. Murgia, *Constraining nonthermal dark matter's impact on the matter power spectrum*, *Phys. Rev. D* **100** (2019) 123520 [[1908.10369](#)].
- [31] A.L. Erickcek, P. Ralegankar and J. Shelton, *Cannibalism's lingering imprint on the matter power spectrum*, *JCAP* **01** (2022) 017 [[2106.09041](#)].
- [32] G. Ballesteros, M.A.G. Garcia and M. Pierre, *How warm are non-thermal relics? Lyman- α bounds on out-of-equilibrium dark matter*, *JCAP* **03** (2021) 101 [[2011.13458](#)].
- [33] A.K. Sarkar, K.L. Pandey and S.K. Sethi, *Using the redshift evolution of the Lyman- α effective opacity as a probe of dark matter models*, *JCAP* **10** (2021) 077 [[2101.09917](#)].
- [34] M.A.G. Garcia, M. Pierre and S. Verner, *New window into gravitationally produced scalar dark matter*, *Phys. Rev. D* **108** (2023) 115024 [[2305.14446](#)].
- [35] M.A. Amin and M. Mirbabayi, *A Lower Bound on Dark Matter Mass*, *Phys. Rev. Lett.* **132** (2024) 221004 [[2211.09775](#)].

- [36] R. Liu, W. Hu and H. Xiao, *Warm and fuzzy dark matter: Free streaming of wave dark matter*, *Phys. Rev. D* **111** (2025) 023535 [2406.12970].
- [37] S. Ling and M.A. Amin, *Free streaming in warm wave dark matter*, *JCAP* **02** (2025) 025 [2408.05591].
- [38] A.J. Long and M. Venegas, *Free streaming of warm wave dark matter in modified expansion histories*, **2412.14322**.
- [39] A.M. Green and B.J. Kavanagh, *Primordial Black Holes as a dark matter candidate*, *J. Phys. G* **48** (2021) 043001 [2007.10722].
- [40] D. Ellis, D.J.E. Marsh, B. Eggemeier, J. Niemeyer, J. Redondo and K. Dolag, *Structure of axion miniclusters*, *Phys. Rev. D* **106** (2022) 103514 [2204.13187].
- [41] S.-Y. Zhou, *Non-topological solitons and quasi-solitons*, **2411.16604**.
- [42] D.E. Kaplan, X. Luo and S. Rajendran, *Probing long-range forces between neutrinos with cosmic structures*, *Phys. Rev. D* **111** (2025) 055019 [2412.20766].
- [43] P.W. Graham and H. Ramani, *Constraints on dark matter from dynamical heating of stars in ultrafaint dwarfs. II. Substructure and the primordial power spectrum*, *Phys. Rev. D* **110** (2024) 075012 [2404.01378].
- [44] H. Ramani, T. Trickle and K.M. Zurek, *Observability of Dark Matter Substructure with Pulsar Timing Correlations*, *JCAP* **12** (2020) 033 [2005.03030].
- [45] V.S.H. Lee, A. Mitridate, T. Trickle and K.M. Zurek, *Probing Small-Scale Power Spectra with Pulsar Timing Arrays*, *JHEP* **06** (2021) 028 [2012.09857].
- [46] V.S.H. Lee, S.R. Taylor, T. Trickle and K.M. Zurek, *Bayesian Forecasts for Dark Matter Substructure Searches with Mock Pulsar Timing Data*, *JCAP* **08** (2021) 025 [2104.05717].
- [47] M.S. Delos and T. Linden, *Dark matter microhalos in the solar neighborhood: Pulsar timing signatures of early matter domination*, *Phys. Rev. D* **105** (2022) 123514 [2109.03240].
- [48] L. Dai and J. Miralda-Escudé, *Gravitational Lensing Signatures of Axion Dark Matter Minihalos in Highly Magnified Stars*, *Astron. J.* **159** (2020) 49 [1908.01773].
- [49] N. Blinov, M.J. Dolan, P. Draper and J. Shelton, *Dark Matter Microhalos From Simplified Models*, *Phys. Rev. D* **103** (2021) 103514 [2102.05070].
- [50] D.R.D.R. Nicholson, *Introduction to plasma theory / Dwight R. Nicholson.*, Wiley series in plasma physics, Wiley, New York (1983 - 1983).
- [51] J. Binney and S. Tremaine, *Galactic dynamics* (1987).
- [52] W. Hu, R. Barkana and A. Gruzinov, *Cold and fuzzy dark matter*, *Phys. Rev. Lett.* **85** (2000) 1158 [astro-ph/0003365].
- [53] B.V. Church, P. Mocz and J.P. Ostriker, *Heating of Milky Way disc stars by dark matter fluctuations in cold dark matter and fuzzy dark matter paradigms*, *MNRAS* **485** (2019) 2861 [1809.04744].
- [54] B. Bar-Or, J.-B. Fouvry and S. Tremaine, *Relaxation in a Fuzzy Dark Matter Halo*, *ApJ* **871** (2019) 28 [1809.07673].
- [55] N. Dalal, J. Bovy, L. Hui and X. Li, *Don't cross the streams: caustics from Fuzzy Dark Matter*, *JCAP* **03** (2021) 076 [2011.13141].

- [56] B. Bar-Or, J.-B. Fouvry and S. Tremaine, *Relaxation in a Fuzzy Dark Matter Halo. II. Self-consistent Kinetic Equations*, *ApJ* **915** (2021) 27 [2010.10212].
- [57] P. Mocz, M. Vogelsberger, V.H. Robles, J. Zavala, M. Boylan-Kolchin, A. Fialkov et al., *Galaxy formation with BECDM – I. Turbulence and relaxation of idealized haloes*, *Mon. Not. Roy. Astron. Soc.* **471** (2017) 4559 [1705.05845].
- [58] E.G.M. Ferreira, *Ultra-light dark matter*, *Astron. Astrophys. Rev.* **29** (2021) 7 [2005.03254].
- [59] L. Hui, *Wave Dark Matter*, *Ann. Rev. Astron. Astrophys.* **59** (2021) 247 [2101.11735].
- [60] S. May and V. Springel, *Structure formation in large-volume cosmological simulations of fuzzy dark matter: impact of the non-linear dynamics*, *Mon. Not. Roy. Astron. Soc.* **506** (2021) 2603 [2101.01828].
- [61] M.A. Amin, M. Jain, R. Karur and P. Mocz, *Small-scale structure in vector dark matter*, *JCAP* **08** (2022) 014 [2203.11935].
- [62] M. Gosenca, A. Eberhardt, Y. Wang, B. Eggemeier, E. Kendall, J.L. Zagorac et al., *Multifield ultralight dark matter*, *Phys. Rev. D* **107** (2023) 083014 [2301.07114].
- [63] D.M. Powell, S. Vegetti, J.P. McKean, S.D.M. White, E.G.M. Ferreira, S. May et al., *A lensed radio jet at milli-arcsecond resolution – II. Constraints on fuzzy dark matter from an extended gravitational arc*, *Mon. Not. Roy. Astron. Soc.* **524** (2023) L84 [2302.10941].
- [64] A. Eberhardt, Q. Liang and E.G.M. Ferreira, *de Broglie scale time delays in pulsar networks for ultralight dark matter*, **2411.18051**.
- [65] K.K. Boddy, J.A. Dror and A. Lam, *Ultralight Dark Matter Statistics for Pulsar Timing Detection*, **2502.15874**.
- [66] A. Eberhardt, E. Ferreira, W. Luo, S. Lin and Y. Li, *Stochastic lensing of stars by ultralight dark matter halos*, **2502.20697**.
- [67] H.N. Luu et al., *Diverse dark matter haloes in Two-field Fuzzy Dark Matter*, **2408.00827**.
- [68] J.H. Jeans, *On the theory of star-streaming and the structure of the universe*, *MNRAS* **76** (1915) 70.
- [69] M. Henon, *Vlasov equation*, *A&A* **114** (1982) 211.
- [70] K.S. Thorne and R.D. Blandford, *Plasma Physics. Volume 4 of Modern Classical Physics*, vol. 4 (2021).
- [71] I.H. Gilbert, *Collisional Processes in Stellar Systems (Papers appear in the Proceedings of IAU Colloquium No. 10 Gravitational N-Body Problem (ed. by Myron Lecar), R. Reidel Publ. Co. , Dordrecht-Holland.)*, *Ap&SS* **14** (1971) 3.
- [72] S.M. Fall and G. Severne, *Correlation dynamics in an expanding universe.*, *MNRAS* **174** (1976) 241.
- [73] S.M. Fall and W.C. Saslaw, *The growth of correlations in an expanding universe and the clustering of galaxies.*, *ApJ* **204** (1976) 631.
- [74] PLANCK collaboration, *Planck 2018 results. VI. Cosmological parameters*, *Astron. Astrophys.* **641** (2020) A6 [1807.06209].
- [75] J. Mayer and M. Mayer, *Statistical Mechanics*, J. Wiley & sons, Incorporated (1948).

- [76] J.W. Gibbs, *On the Fundamental Formula of Statistical Mechanics, with Applications to Astronomy and Thermodynamics*, in *Proceedings of the American Association for the Advancement of Science*, vol. 33, pp. 57–58, 1884.
- [77] R. Brandenberger, N. Kaiser and N. Turok, *Dissipationless clustering of neutrinos around a cosmic-string loop*, *Phys. Rev. D* **36** (1987) 2242.
- [78] V. Springel, R. Pakmor, O. Zier and M. Reinecke, *Simulating cosmic structure formation with the gadget-4 code*, *Mon. Not. Roy. Astron. Soc.* **506** (2021) 2871 [2010.03567].
- [79] M.S. Delos, A.L. Erickcek, A.P. Bailey and M.A. Alvarez, *Density profiles of ultracompact minihalos: Implications for constraining the primordial power spectrum*, *Phys. Rev. D* **98** (2018) 063527 [1806.07389].
- [80] L. Wang, M. Iwasawa, K. Nitadori and J. Makino, *PETAR: a high-performance N-body code for modelling massive collisional stellar systems*, *MNRAS* **497** (2020) 536 [2006.16560].
- [81] A. Rantala, T. Naab, F.P. Rizzuto, M. Mannerkoski, C. Partmann and K. Lautenschütz, *BIFROST: simulating compact subsystems in star clusters using a hierarchical fourth-order forward symplectic integrator code*, *Mon. Not. Roy. Astron. Soc.* **522** (2023) 5180 [2210.02472].
- [82] M.S. Delos, A. Rantala, S. Young and F. Schmidt, *Structure formation with primordial black holes: collisional dynamics, binaries, and gravitational waves*, *JCAP* **12** (2024) 005 [2410.01876].
- [83] W.H. Press and P. Schechter, *Formation of galaxies and clusters of galaxies by selfsimilar gravitational condensation*, *Astrophys. J.* **187** (1974) 425.
- [84] R.K. Sheth and G. Tormen, *An Excursion Set Model of Hierarchical Clustering : Ellipsoidal Collapse and the Moving Barrier*, *Mon. Not. Roy. Astron. Soc.* **329** (2002) 61 [astro-ph/0105113].
- [85] J.L. Tinker, A.V. Kravtsov, A. Klypin, K. Abazajian, M.S. Warren, G. Yepes et al., *Toward a halo mass function for precision cosmology: The Limits of universality*, *Astrophys. J.* **688** (2008) 709 [0803.2706].
- [86] B. Diemer, *Universal at last? The splashback mass function of dark matter halos*, *Astrophys. J.* **903** (2020) 87 [2007.10346].
- [87] L. Ondaro-Mallea, R.E. Angulo, M. Zennaro, S. Contreras and G. Aricò, *Non-universality of the mass function: dependence on the growth rate and power spectrum shape*, *Mon. Not. Roy. Astron. Soc.* **509** (2021) 6077 [2102.08958].
- [88] M. Davis, G. Efstathiou, C.S. Frenk and S.D.M. White, *The Evolution of Large Scale Structure in a Universe Dominated by Cold Dark Matter*, *Astrophys. J.* **292** (1985) 371.
- [89] M.S. Delos, *Accurate halo mass functions from the simplest excursion set theory*, *Mon. Not. Roy. Astron. Soc.* **528** (2024) 1372 [2311.17986].
- [90] J.R. Bond, S. Cole, G. Efstathiou and N. Kaiser, *Excursion set mass functions for hierarchical Gaussian fluctuations*, *Astrophys. J.* **379** (1991) 440.
- [91] D. Blas, J. Lesgourgues and T. Tram, *The Cosmic Linear Anisotropy Solving System (CLASS) II: Approximation schemes*, *JCAP* **07** (2011) 034 [1104.2933].
- [92] W. Hu and N. Sugiyama, *Small scale cosmological perturbations: An Analytic approach*, *Astrophys. J.* **471** (1996) 542 [astro-ph/9510117].

- [93] D. Inman and Y. Ali-Haïmoud, *Early structure formation in primordial black hole cosmologies*, *Phys. Rev. D* **100** (2019) 083528 [[1907.08129](#)].
- [94] P. Bode, J.P. Ostriker and N. Turok, *Halo formation in warm dark matter models*, *Astrophys. J.* **556** (2001) 93 [[astro-ph/0010389](#)].
- [95] N. Afshordi, P. McDonald and D.N. Spergel, *Primordial black holes as dark matter: The Power spectrum and evaporation of early structures*, *Astrophys. J. Lett.* **594** (2003) L71 [[astro-ph/0302035](#)].
- [96] N. Dalal, Y. Lithwick and M. Kuhlen, *The Origin of Dark Matter Halo Profiles*, [1010.2539](#).
- [97] A.D. Ludlow, J.F. Navarro, M. Boylan-Kolchin, P.E. Bett, R.E. Angulo, M. Li et al., *The Mass Profile and Accretion History of Cold Dark Matter Halos*, *Mon. Not. Roy. Astron. Soc.* **432** (2013) 1103 [[1302.0288](#)].
- [98] M.S. Delos, M. Bruff and A.L. Erickcek, *Predicting the density profiles of the first halos*, *Phys. Rev. D* **100** (2019) 023523 [[1905.05766](#)].
- [99] M.S. Delos and S.D.M. White, *Inner cusps of the first dark matter haloes: formation and survival in a cosmological context*, *Mon. Not. Roy. Astron. Soc.* **518** (2022) 3509 [[2207.05082](#)].
- [100] S.D.M. White, *Prompt cusp formation from the gravitational collapse of peaks in the initial cosmological density field*, *Mon. Not. Roy. Astron. Soc.* **517** (2022) L46 [[2207.13565](#)].
- [101] M.S. Delos and S.D.M. White, *Prompt cusps and the dark matter annihilation signal*, *JCAP* **10** (2023) 008 [[2209.11237](#)].
- [102] M.S. Delos, *Massive prompt cusps: a new signature of warm dark matter*, *Mon. Not. Roy. Astron. Soc.* **522** (2023) L78 [[2302.03040](#)].
- [103] A. Del Popolo and S. Fakhry, *On the effect of angular momentum on the prompt cusp formation via the gravitational collapse*, *Phys. Dark Univ.* **41** (2023) 101259 [[2305.19817](#)].
- [104] T. Ishiyama, J. Makino and T. Ebisuzaki, *Gamma-ray Signal from Earth-mass Dark Matter Microhalos*, *Astrophys. J. Lett.* **723** (2010) L195 [[1006.3392](#)].
- [105] D. Anderhalden and J. Diemand, *Density Profiles of CDM Microhalos and their Implications for Annihilation Boost Factors*, *JCAP* **04** (2013) 009 [[1302.0003](#)].
- [106] T. Ishiyama, *Hierarchical Formation of Dark Matter Halos and the Free Streaming Scale*, *Astrophys. J.* **788** (2014) 27 [[1404.1650](#)].
- [107] E. Polisensky and M. Ricotti, *Fingerprints of the initial conditions on the density profiles of cold and warm dark matter haloes*, *Mon. Not. Roy. Astron. Soc.* **450** (2015) 2172 [[1504.02126](#)].
- [108] G. Ogiya, D. Nagai and T. Ishiyama, *Dynamical evolution of primordial dark matter haloes through mergers*, *Mon. Not. Roy. Astron. Soc.* **461** (2016) 3385 [[1604.02866](#)].
- [109] R.E. Angulo, O. Hahn, A. Ludlow and S. Bonoli, *Earth-mass haloes and the emergence of NFW density profiles*, *Mon. Not. Roy. Astron. Soc.* **471** (2017) 4687 [[1604.03131](#)].
- [110] M.S. Delos, A.L. Erickcek, A.P. Bailey and M.A. Alvarez, *Are ultracompact minihalos really ultracompact?*, *Phys. Rev. D* **97** (2018) 041303 [[1712.05421](#)].
- [111] T. Ishiyama and S. Ando, *The Abundance and Structure of Subhaloes near the Free Streaming Scale and Their Impact on Indirect Dark Matter Searches*, *Mon. Not. Roy. Astron. Soc.* **492** (2020) 3662 [[1907.03642](#)].

- [112] S. Colombi, *Phase-space structure of protohalos: Vlasov versus Particle-Mesh*, *Astron. Astrophys.* **647** (2021) A66 [2012.04409].
- [113] L. Ondaro-Mallea, R.E. Angulo, J. Stücker, O. Hahn and S.D.M. White, *Phase-space simulations of prompt cusps: simulating the formation of the first haloes without artificial fragmentation*, *Mon. Not. Roy. Astron. Soc.* **527** (2023) 10802 [2309.05707].
- [114] D. Lynden-Bell and R. Wood, *The gravo-thermal catastrophe in isothermal spheres and the onset of red-giant structure for stellar systems*, *Mon. Not. Roy. Astron. Soc.* **138** (1968) 495.
- [115] V. Vaskonen and H. Veermäe, *Lower bound on the primordial black hole merger rate*, *Phys. Rev. D* **101** (2020) 043015 [1908.09752].
- [116] V. Stasenko and K. Belotsky, *Influence of early dark matter haloes on the primordial black holes merger rate*, *Mon. Not. Roy. Astron. Soc.* **526** (2023) 4308 [2307.12924].
- [117] V. Stasenko, *Redshift evolution of primordial black hole merger rate*, *Phys. Rev. D* **109** (2024) 123546 [2403.11325].
- [118] P. Agrawal, N. Kitajima, M. Reece, T. Sekiguchi and F. Takahashi, *Relic Abundance of Dark Photon Dark Matter*, *Phys. Lett. B* **801** (2020) 135136 [1810.07188].
- [119] V. Iršič, H. Xiao and M. McQuinn, *Early structure formation constraints on the ultralight axion in the postinflation scenario*, *Phys. Rev. D* **101** (2020) 123518 [1911.11150].
- [120] M. Gorghetto, E. Hardy and G. Villadoro, *More axions from strings*, *SciPost Phys.* **10** (2021) 050 [2007.04990].
- [121] M. Buschmann, J.W. Foster, A. Hook, A. Peterson, D.E. Willcox, W. Zhang et al., *Dark matter from axion strings with adaptive mesh refinement*, *Nature Commun.* **13** (2022) 1049 [2108.05368].
- [122] C.A.J. O’Hare, G. Pierobon, J. Redondo and Y.Y.Y. Wong, *Simulations of axionlike particles in the postinflationary scenario*, *Phys. Rev. D* **105** (2022) 055025 [2112.05117].
- [123] P. Adshead, K.D. Lozanov and Z.J. Weiner, *Dark photon dark matter from an oscillating dilaton*, *Phys. Rev. D* **107** (2023) 083519 [2301.07718].
- [124] D. Cyncynates and Z.J. Weiner, *Detectable, defect-free dark photon dark matter*, **2310.18397**.
- [125] K. Saikawa, J. Redondo, A. Vaquero and M. Kaltschmidt, *Spectrum of global string networks and the axion dark matter mass*, *JCAP* **10** (2024) 043 [2401.17253].
- [126] R. Petrossian-Byrne and G. Villadoro, *Open String Axiverse*, **2503.16387**.
- [127] P.W. Graham, J. Mardon and S. Rajendran, *Vector Dark Matter from Inflationary Fluctuations*, *Phys. Rev. D* **93** (2016) 103520 [1504.02102].
- [128] E.W. Kolb and A.J. Long, *Completely dark photons from gravitational particle production during the inflationary era*, *JHEP* **03** (2021) 283 [2009.03828].
- [129] M. Redi and A. Tesi, *Meso-inflationary QCD axion*, *Phys. Rev. D* **107** (2023) 095032 [2211.06421].
- [130] M.A. Amin and S. May, *Growth of structure in warm wave dark matter, (in progress)* (2025) .
- [131] M. Jain, M.A. Amin, J. Thomas and W. Wanichwecharungruang, *Kinetic relaxation and*

- Bose-star formation in multicomponent dark matter*, *Phys. Rev. D* **108** (2023) 043535 [2304.01985].
- [132] D.G. Levkov, A.G. Panin and I.I. Tkachev, *Gravitational Bose-Einstein condensation in the kinetic regime*, *Phys. Rev. Lett.* **121** (2018) 151301 [1804.05857].
 - [133] J. Chen and H.-Y. Zhang, *Novel structures and collapse of solitons in nonminimally gravitating dark matter halos*, 2407.09265.
 - [134] M.A. Amin, R. Easther, H. Finkel, R. Flauger and M.P. Hertzberg, *Oscillons After Inflation*, *Phys. Rev. Lett.* **108** (2012) 241302 [1106.3335].
 - [135] M.A. Amin and P. Mocz, *Formation, gravitational clustering, and interactions of nonrelativistic solitons in an expanding universe*, *Phys. Rev. D* **100** (2019) 063507 [1902.07261].
 - [136] B. Eggemeier, B. Schwabe, J.C. Niemeyer and R. Easther, *Gravitational Collapse in the Post-Inflationary Universe*, 10, 2021.
 - [137] K.D. Lozanov and V. Takhistov, *Enhanced Gravitational Waves from Inflaton Oscillons*, *Phys. Rev. Lett.* **130** (2023) 181002 [2204.07152].
 - [138] K.D. Lozanov, M. Sasaki and V. Takhistov, *Universal gravitational wave signatures of cosmological solitons*, *JCAP* **01** (2025) 094 [2304.06709].
 - [139] S. Tulin and H.-B. Yu, *Dark Matter Self-interactions and Small Scale Structure*, *Phys. Rept.* **730** (2018) 1 [1705.02358].
 - [140] E.O. Nadler, D. Kong, D. Yang and H.-B. Yu, *SIDM Concerto: Compilation and Data Release of Self-interacting Dark Matter Zoom-in Simulations*, 2503.10748.
 - [141] D.N. Spergel and P.J. Steinhardt, *Observational evidence for selfinteracting cold dark matter*, *Phys. Rev. Lett.* **84** (2000) 3760 [astro-ph/9909386].
 - [142] M. Jain, W. Wanichwecharungruang and J. Thomas, *Kinetic relaxation and nucleation of Bose stars in self-interacting wave dark matter*, *Phys. Rev. D* **109** (2024) 016002 [2310.00058].
 - [143] P. Mocz et al., *Cosmological structure formation and soliton phase transition in fuzzy dark matter with axion self-interactions*, *Mon. Not. Roy. Astron. Soc.* **521** (2023) 2608 [2301.10266].
 - [144] C.A. Painter, M. Boylan-Kolchin, P. Mocz and M. Vogelsberger, *An attractive model: simulating fuzzy dark matter with attractive self-interactions*, *Mon. Not. Roy. Astron. Soc.* **533** (2024) 2454 [2402.16945].
 - [145] K. Kirkpatrick, A.E. Mirasola and C. Prescod-Weinstein, *Analysis of Bose-Einstein condensation times for self-interacting scalar dark matter*, 2110.08921.
 - [146] J. Chen, X. Du, E.W. Lentz, D.J.E. Marsh and J.C. Niemeyer, *New insights into the formation and growth of boson stars in dark matter halos*, 2011.01333.
 - [147] B. Carr, K. Kohri, Y. Sendouda and J. Yokoyama, *Constraints on primordial black holes*, *Rept. Prog. Phys.* **84** (2021) 116902 [2002.12778].
 - [148] P. Mróz et al., *No massive black holes in the Milky Way halo*, *Nature* **632** (2024) 749 [2403.02386].
 - [149] E.J. Copeland, M. Gleiser and H.R. Muller, *Oscillons: Resonant configurations during bubble collapse*, *Phys. Rev. D* **52** (1995) 1920 [hep-ph/9503217].

- [150] A. Kusenko and M.E. Shaposhnikov, *Supersymmetric Q balls as dark matter*, *Phys. Lett. B* **418** (1998) 46 [[hep-ph/9709492](#)].
- [151] M. Gorghetto, E. Hardy and G. Villadoro, *More axion stars from strings*, *JHEP* **08** (2024) 126 [[2405.19389](#)].
- [152] P. Adshead and K.D. Lozanov, *Self-gravitating Vector Dark Matter*, *Phys. Rev. D* **103** (2021) 103501 [[2101.07265](#)].
- [153] M. Jain and M.A. Amin, *Polarized solitons in higher-spin wave dark matter*, *Phys. Rev. D* **105** (2022) 056019 [[2109.04892](#)].
- [154] P.-H. Chavanis, *Mass-radius relation of newtonian self-gravitating bose-einstein condensates with short-range interactions. i. analytical results*, *Physical Review D* **84** (2011) .
- [155] J. Eby, M. Leembruggen, L. Street, P. Suranyi and L.R. Wijewardhana, *Global view of QCD axion stars*, *Phys. Rev. D* **100** (2019) 063002 [[1905.00981](#)].
- [156] L. Visinelli, S. Baum, J. Redondo, K. Freese and F. Wilczek, *Dilute and dense axion stars*, *Phys. Lett. B* **777** (2018) 64 [[1710.08910](#)].
- [157] K.M. Zurek, C.J. Hogan and T.R. Quinn, *Astrophysical Effects of Scalar Dark Matter Miniclusters*, *Phys. Rev. D* **75** (2007) 043511 [[astro-ph/0607341](#)].
- [158] H. Xiao, I. Williams and M. McQuinn, *Simulations of axion minihalos*, *Phys. Rev. D* **104** (2021) 023515 [[2101.04177](#)].
- [159] L. Visinelli and J. Redondo, *Axion Miniclusters in Modified Cosmological Histories*, *Phys. Rev. D* **101** (2020) 023008 [[1808.01879](#)].
- [160] B. Liu, S. Zhang and V. Bromm, *Effects of stellar-mass primordial black holes on first star formation*, *Mon. Not. Roy. Astron. Soc.* **514** (2022) 2376 [[2204.06330](#)].
- [161] B. Carr, S. Clesse, J. Garcia-Bellido, M. Hawkins and F. Kuhnel, *Observational evidence for primordial black holes: A positivist perspective*, *Phys. Rept.* **1054** (2024) 1 [[2306.03903](#)].
- [162] I. Musco, K. Jedamzik and S. Young, *Primordial black hole formation during the QCD phase transition: Threshold, mass distribution, and abundance*, *Phys. Rev. D* **109** (2024) 083506 [[2303.07980](#)].
- [163] S. Zhang, V. Bromm and B. Liu, *How Do Primordial Black Holes Change the Halo Mass Function and Structure?*, *Astrophys. J.* **975** (2024) 139 [[2405.11381](#)].
- [164] S. Zhang, B. Liu, V. Bromm, J. Jeon, M. Boylan-Kolchin and F. Kuhnel, *How do Massive Primordial Black Holes Impact the Formation of the First Stars and Galaxies?*, [2503.17585](#).
- [165] M. Gosenca, J. Adamek, C.T. Byrnes and S. Hotchkiss, *3D simulations with boosted primordial power spectra and ultracompact minihalos*, *Phys. Rev. D* **96** (2017) 123519 [[1710.02055](#)].
- [166] M.S. Delos and J. Silk, *Ultradense dark matter haloes accompany primordial black holes*, *Mon. Not. Roy. Astron. Soc.* **520** (2023) 4370 [[2210.04904](#)].
- [167] M.S. Delos and G. Franciolini, *Lensing constraints on ultradense dark matter halos*, *Phys. Rev. D* **107** (2023) 083505 [[2301.13171](#)].
- [168] S. Fakhry, M. Farhang and A. Del Popolo, *Toward more realistic mass functions for ultradense dark matter halos*, *Phys. Dark Univ.* **46** (2024) 101544 [[2311.15307](#)].

- [169] A. Dekker and A. Kravtsov, *Constraints on blue and red tilted primordial power spectra using dwarf galaxy properties*, *Phys. Rev. D* **111** (2025) 063516 [2407.04198].
- [170] S. Kumar and N. Weiner, *Early Galaxies from Rare Inflationary Processes and JWST Observations*, **2502.08701**.
- [171] G. Hütsi, M. Raidal, J. Urrutia, V. Vaskonen and H. Veermäe, *Did JWST observe imprints of axion miniclusters or primordial black holes?*, *Phys. Rev. D* **107** (2023) 043502 [2211.02651].
- [172] P. Parashari and R. Laha, *Primordial power spectrum in light of JWST observations of high redshift galaxies*, *Mon. Not. Roy. Astron. Soc.* **526** (2023) L63 [2305.00999].
- [173] F. Iocco and L. Visinelli, *Compatibility of JWST results with exotic halos*, *Phys. Dark Univ.* **44** (2024) 101496 [2403.13068].
- [174] A.V. Maccio, S. Paduroiu, D. Anderhalden, A. Schneider and B. Moore, *Cores in warm dark matter haloes: a Catch 22 problem*, *Mon. Not. Roy. Astron. Soc.* **424** (2012) 1105 [1202.1282].
- [175] H. Ganjoo and M.S. Delos, *Simulations of gravitational heating due to early matter domination*, *JCAP* **04** (2024) 015 [2306.14961].
- [176] L. Boyle, K. Finn and N. Turok, *CPT-Symmetric Universe*, *Phys. Rev. Lett.* **121** (2018) 251301 [1803.08928].
- [177] L. Boyle, K. Finn and N. Turok, *The Big Bang, CPT, and neutrino dark matter*, *Annals Phys.* **438** (2022) 168767 [1803.08930].
- [178] N. Turok and L. Boyle, *A Minimal Explanation of the Primordial Cosmological Perturbations*, **2302.00344**.
- [179] J. Lesgourgues and T. Tram, *The Cosmic Linear Anisotropy Solving System (CLASS) IV: efficient implementation of non-cold relics*, *J. Cosmology Astropart. Phys.* **2011** (2011) 032 [1104.2935].
- [180] L. Ji, M. Kamionkowski and J.L. Bernal, *Cosmological perturbations: Noncold relics without the Boltzmann hierarchy*, *Phys. Rev. D* **106** (2022) 103531 [2201.11129].
- [181] D. Grin, D.J.E. Marsh and R. Hlozek, *axionCAMB: Modification of the CAMB Boltzmann code*, .
- [182] R. Liu, W. Hu and D. Grin, *Accurate method for ultralight axion CMB and matter power spectra*, **2412.15192**.
- [183] E. Bertschinger, *The Effects of Cold Dark Matter Decoupling and Pair Annihilation on Cosmological Perturbations*, *Phys. Rev. D* **74** (2006) 063509 [astro-ph/0607319].

A Diagrammatic Interpretation of the Growth Functions

The warm dark matter growth functions are expressed as solutions to Volterra integral equations (2.33), which may be written as

$$\begin{aligned} T_{\mathbf{k}}^{(a)}(t, t_0) &= T_{\mathbf{k}}^{(A)}(t, t_0) + \int_{t_0}^t 4\pi G \bar{\rho} dt' T_{\mathbf{k}}^{(B)}(t, t') T_{\mathbf{k}}^{(a)}(t', t_0), \\ T_{\mathbf{k}}^{(b)}(t, t_0) &= T_{\mathbf{k}}^{(B)}(t, t_0) + \int_{t_0}^t 4\pi G \bar{\rho} dt' T_{\mathbf{k}}^{(B)}(t, t') T_{\mathbf{k}}^{(b)}(t', t_0), \end{aligned} \quad (\text{A.1})$$

where we define

$$\begin{aligned} T_{\mathbf{k}}^{(A)}(t, t_0) &= T_{\text{fs}}(k(t - t_0)), \\ T_{\mathbf{k}}^{(B)}(t, t_0) &= (t - t_0) T_{\text{fs}}(k(t - t_0)). \end{aligned} \quad (\text{A.2})$$

Similar expressions may be written for an expanding universe. The physical meaning of these functions is that $T_{\mathbf{k}}^{(A)}(t, t_0)$ and $T_{\mathbf{k}}^{(B)}(t, t_0)$ evolve initial density or velocity perturbations, respectively, from t_0 to t in the absence of self-gravity. Meanwhile, $T_{\mathbf{k}}^{(a)}(t, t_0)$ and $T_{\mathbf{k}}^{(b)}(t, t_0)$ do the same while accounting for self-gravity. The intuition for the integral in each of equations (A.1) is that, via the $T_{\mathbf{k}}^{(B)}(t, t')$ factor, it sums over the velocity perturbations induced at all times t' by the self-gravity of the perturbation $T_{\mathbf{k}}^{(a,b)}(t', t_0)$.

The mathematical structure of these equations is clearest in a diagrammatic form. For some fixed \mathbf{k} , let us define

$$\begin{aligned} T_{\mathbf{k}}^{(A)}(t, t_0) &\equiv \left. \begin{array}{c} t \\ \text{ } \\ \text{ } \\ \text{ } \\ t_0 \end{array} \right\} A, & T_{\mathbf{k}}^{(B)}(t, t_0) &\equiv \left. \begin{array}{c} t \\ \text{ } \\ \text{ } \\ \text{ } \\ t_0 \end{array} \right| B, \\ T_{\mathbf{k}}^{(a)}(t, t_0) &\equiv \left. \begin{array}{c} t \\ \text{ } \\ \text{ } \\ \text{ } \\ t_0 \end{array} \right\} a, & T_{\mathbf{k}}^{(b)}(t, t_0) &\equiv \left. \begin{array}{c} t \\ \text{ } \\ \text{ } \\ \text{ } \\ t_0 \end{array} \right\| b. \end{aligned} \quad (\text{A.3})$$

We may now write equations (A.1) as

$$\begin{aligned} \left. \begin{array}{c} t \\ \text{ } \\ \text{ } \\ \text{ } \\ t_0 \end{array} \right\} a &= \left. \begin{array}{c} t \\ \text{ } \\ \text{ } \\ \text{ } \\ t_0 \end{array} \right\} A + \left. \begin{array}{c} t \\ \text{ } \\ \text{ } \\ \text{ } \\ t_0 \end{array} \right\} \begin{array}{c} B \\ \text{ } \\ \text{ } \\ \text{ } \\ t' \\ \text{ } \\ \text{ } \\ \text{ } \\ a \end{array}, & \left. \begin{array}{c} t \\ \text{ } \\ \text{ } \\ \text{ } \\ t_0 \end{array} \right\| b &= \left. \begin{array}{c} t \\ \text{ } \\ \text{ } \\ \text{ } \\ t_0 \end{array} \right| B + \left. \begin{array}{c} t \\ \text{ } \\ \text{ } \\ \text{ } \\ t_0 \end{array} \right\| \begin{array}{c} B \\ \text{ } \\ \text{ } \\ \text{ } \\ t' \\ \text{ } \\ \text{ } \\ \text{ } \\ b \end{array}. \end{aligned} \quad (\text{A.4})$$

Here we introduce another convention: the circle corresponds to an “internal” time vertex t' , which is to be integrated out between the time vertices immediately above and below it (so that $t_0 < t' < t$ in this case) with the measure $4\pi G \bar{\rho} dt'$.

To reduce clutter, we will suppress the time vertex labels. By successive substitutions, we may now write out $T_{\mathbf{k}}^{(a,b)}(t, t_0)$ explicitly as the infinite sums

$$\begin{aligned}
\text{wavy } a &= \text{wavy } A + \begin{array}{c} B \\ \circ \\ \text{wavy } A \end{array} + \begin{array}{c} B \\ \circ \\ B \\ \circ \\ \text{wavy } A \end{array} + \begin{array}{c} B \\ \circ \\ B \\ \circ \\ B \\ \circ \\ \text{wavy } A \end{array} + \begin{array}{c} B \\ \circ \\ B \\ \circ \\ B \\ \circ \\ B \\ \circ \\ \text{wavy } A \end{array} + \dots, \\
\text{double } b &= B + \begin{array}{c} B \\ \circ \\ B \end{array} + \begin{array}{c} B \\ \circ \\ B \\ \circ \\ B \end{array} + \begin{array}{c} B \\ \circ \\ B \\ \circ \\ B \\ \circ \\ B \end{array} + \dots.
\end{aligned} \tag{A.5}$$

Note that each “internal” time vertex (indicated with a circle) contributes a factor of $G\bar{\rho}$, so the i -th term on the right-hand side of each of these equations is proportional to $(G\bar{\rho})^{i-1}$. The interpretation is that the first term in each of these equations does not account for gravity (as we noted above), and each successive term adds a correction due to the gravitational influence of the previous term. Symbolically, these series expansions correspond to

$$\begin{aligned}
T_{\mathbf{k}}^{(a)}(t, t_0) &= T_{\mathbf{k}}^{(A)}(t, t_0) + \sum_{s=1}^{\infty} (4\pi G\bar{\rho})^s \int \left(\prod_{i=1}^s dt_i \right) T_{\mathbf{k}}^{(B)}(t, t_s) \left[\prod_{i=2}^s T_{\mathbf{k}}^{(B)}(t_i, t_{i-1}) \right] T_{\mathbf{k}}^{(A)}(t_1, t_0), \\
T_{\mathbf{k}}^{(b)}(t, t_0) &= T_{\mathbf{k}}^{(B)}(t, t_0) + \sum_{s=1}^{\infty} (4\pi G\bar{\rho})^s \int \left(\prod_{i=1}^s dt_i \right) T_{\mathbf{k}}^{(B)}(t, t_s) \left[\prod_{i=1}^s T_{\mathbf{k}}^{(B)}(t_i, t_{i-1}) \right],
\end{aligned} \tag{A.6}$$

where we enforce the appropriate time ordering by defining $T_{\mathbf{k}}^{(A)}(t, t') = T_{\mathbf{k}}^{(B)}(t, t') = 0$ if $t < t'$ (or equivalently, we multiply each integrand by a function that is 1 if $t > t_s > t_{s-1} > \dots > t_0$ and 0 otherwise).

Now from equations (A.5), it is clear that

$$\text{wavy } a = \text{wavy } A + \begin{array}{c} \text{double } b \\ \circ \\ \text{wavy } A \end{array}, \quad \text{double } b = B + \begin{array}{c} \text{double } b \\ \circ \\ B \end{array}, \tag{A.7}$$

or symbolically,

$$\begin{aligned}
T_{\mathbf{k}}^{(a)}(t, t_0) &= T_{\mathbf{k}}^{(A)}(t, t_0) + \int_{t_0}^t 4\pi G\bar{\rho} dt' T_{\mathbf{k}}^{(b)}(t, t') T_{\mathbf{k}}^{(A)}(t', t_0), \\
T_{\mathbf{k}}^{(b)}(t, t_0) &= T_{\mathbf{k}}^{(B)}(t, t_0) + \int_{t_0}^t 4\pi G\bar{\rho} dt' T_{\mathbf{k}}^{(b)}(t, t') T_{\mathbf{k}}^{(B)}(t', t_0),
\end{aligned} \tag{A.8}$$

proving equations (2.35) and implying that there is no need to solve a separate Volterra equation for $T_k^{(a)}$. The expression for $T_k^{(b)}$ here is still a Volterra equation, but we include it because it nicely mirrors the expression for $T_k^{(a)}$. Intuition for equations (A.8) is that perturbation growth with self-gravity ($T^{(a,b)}$) can be represented as the evolution of the same perturbation without self-gravity ($T^{(A,B)}$) plus the sum over all of the new perturbations $T^{(b)}$ that are sourced by the gravity of the original perturbation, where the new perturbations are themselves evolved subject to their own self-gravity.

Finally, we note that the white noise power spectrum in equation (2.48) can be written in this notation as well, if we define the power spectrum of pure Poisson noise to be

$$\frac{1}{\bar{n}} \equiv \text{---} \quad . \quad (\text{A.9})$$

Now the white noise power spectrum $P_{\delta_{\text{wn}}}(t, k)$ may be written

$$P_{\delta_{\text{wn}}}(t, k) = \text{---} + 2 \text{---} \quad . \quad (\text{A.10})$$

As before, upper “external” vertices correspond to the final time t . Intuitively, the interpretation is that the $1/\bar{n}$ white noise “floor” of the power spectrum continuously sources perturbations of both “initial displacement” and “initial velocity” type, and their product contributes to the power spectrum.

B Numerically Evaluating the Growth Functions

The time evolution of the power spectrum relies on the “initial velocity” growth function $\mathcal{T}^{(b)}(y, y', k)$ which satisfies a Volterra equation (2.57). This growth function may be efficiently evaluated using an iterative scheme that is closely related to the series expansion in equation (A.5) or (A.6). For $i \geq 0$, we define $\mathcal{T}_k^{(b,i)}(y, y')$ as

$$\begin{aligned} \mathcal{T}_k^{(b,0)}(y, y') &= \mathcal{F}(y, y') T_{\text{fs}}(y, y', k), \\ \mathcal{T}_k^{(b,i+1)}(y, y') &= \mathcal{T}_k^{(b,0)}(y, y') + \frac{3}{2} \int_{y'}^y \frac{dy''}{\sqrt{1+y''}} \mathcal{T}_k^{(b,i)}(y, y'') \mathcal{T}_k^{(b,0)}(y'', y'). \end{aligned} \quad (\text{B.1})$$

Then $\mathcal{T}_k^{(b)}(y, y') = \lim_{i \rightarrow \infty} \mathcal{T}_k^{(b,i)}(y, y')$. Note that $\mathcal{T}_k^{(b,i)}$ corresponds to the series expansion (A.5) or (A.6) truncated after the $(i+1)$ th term. In practice, we find that extremely good convergence is achieved up to the time $y = 10^3$ with $i \approx 10$ iterations. Fewer iterations are needed to integrate over shorter periods of matter domination. To carry out the integral in equation (B.1), we find that integration time steps as coarse as $\Delta \ln y \approx 0.2$ are sufficient. We provide an implementation of this iterative calculation in the PYTHON language at <https://github.com/delos/warm-structure-growth>. This implementation can accurately evaluate the white-noise power spectrum in just a few seconds on a personal computer.

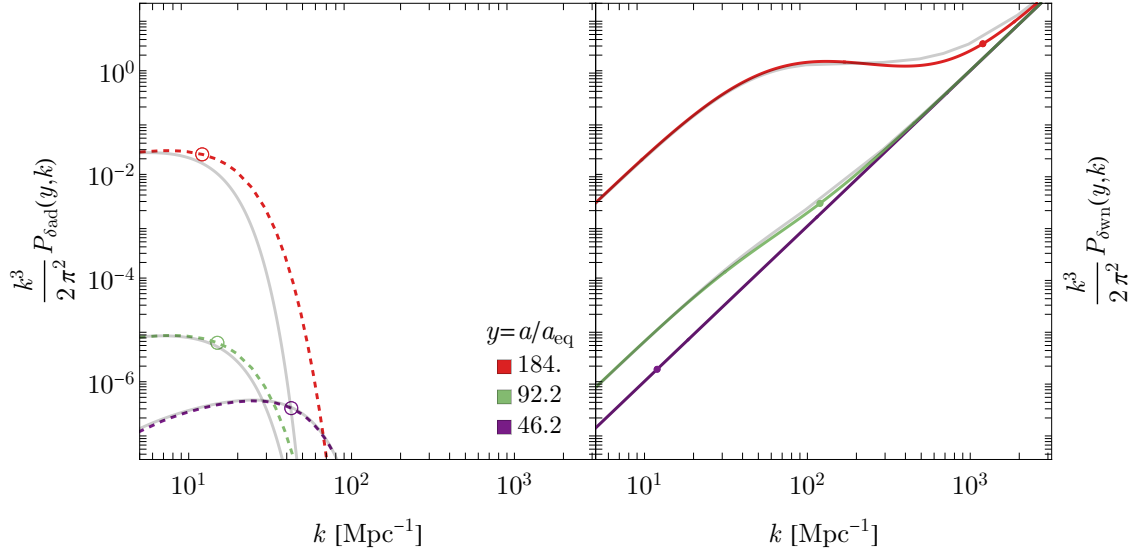


Figure 12: The colored lines are the power spectra from solving the Volterra equations, while the grey lines are based on the simplified ansatz provided in Appendix C. For the left panel, note that the ansatz $P_{\delta_{\text{ad}}}^{\text{CDM}} T_{\text{fs}}^2$ works well in radiation domination (as expected). Deep in the matter era, the ansatz leads to a 10-30% error regarding the characteristic length scale where the power spectrum is suppressed. The error is smaller for colder dark matter.

Beyond warm white noise, we also point out that this computation and code may be used more generally as a fast alternative to a full Boltzmann solver such as CLASS [179] to study the effect of non-cold relics on the matter power spectrum, at least in the non-relativistic regime. Our iterative approach is similar to that suggested by ref. [180].

C Fitting Functions and Approximate Evaluation of Power Spectrum

To a good approximation, $\mathcal{T}_k^{(a,b)}(y, y')$ appearing inside the integral in the evolution of the white noise spectrum (2.55) can be replaced by (this is empirical, rather than a controlled expansion)

$$\mathcal{T}_k^{(a)}(y, y') \mathcal{T}_k^{(b)}(y, y') \rightarrow T_0^{(a)}(y, y') T_0^{(b)}(y, y') T_{\text{fs}}(y, y', k), \quad (\text{C.1})$$

where

$$\begin{aligned} T_0^{(a)}(y, y') &= \left(1 + \frac{3}{2}y\right) (1 + 3y') - \frac{3}{2}y' \sqrt{1+y'} \left[3\sqrt{1+y} - \left(1 + \frac{3}{2}y\right) \ln\left(\frac{x}{x'}\right)\right], \\ T_0^{(b)}(y, y') &= 3 \left(1 + \frac{3}{2}y\right) \left(1 + \frac{3}{2}y'\right) \left[\frac{\sqrt{1+y}}{1 + \frac{3}{2}y} - \frac{\sqrt{1+y'}}{1 + \frac{3}{2}y'} - \frac{1}{3} \ln(x/x')\right], \end{aligned} \quad (\text{C.2})$$

with $x \equiv \frac{\sqrt{1+y}+1}{\sqrt{1+y}-1}$ and $x' \equiv \frac{\sqrt{1+y'}+1}{\sqrt{1+y'}-1}$. This ansatz eliminates the need for solving Volterra equations for $T_k^{(a)}$ and $T_k^{(b)}$. Given a $f_0(p)$, we can get an expression for T_{fs} , which then yields $P_{\delta_{\text{wn}}}$.

The adiabatic part of the power spectrum can be approximated as

$$P_{\delta_{\text{ad}}}(y, k) \approx P_{\delta_{\text{ad}}}^{\text{CDM}}(y, k) T_{\text{fs}}^2(y, y_0, k), \quad (\text{C.3})$$

where $P_{\delta_{\text{ad}}}^{\text{CDM}}(y, k)$ is the power spectrum for cold dark matter (CDM). This expression is exact during radiation domination but loses some accuracy during the matter era. For $y \gg 1$, it overestimates the length scale at which the power spectrum is suppressed by around 10-30% (with less error for colder dark matter). The CDM power spectrum $P_{\delta_{\text{ad}}}^{\text{CDM}}$ may be computed using standard methods (e.g. [91]), but on scales that are sufficiently subhorizon at matter-radiation equality ($k \gtrsim \text{Mpc}^{-1}$), we may write it as

$$P_{\delta_{\text{ad}}}(y, k) \approx 36 P_{\mathcal{R}}(k) \left[\left(1 + \frac{3}{2}y \right) \ln \left(0.15 \frac{k}{k_{\text{eq}}} \right) + 3\sqrt{1+y} - \left(1 + \frac{3}{2}y \right) \ln \left(\frac{\sqrt{1+y}+1}{\sqrt{1+y}-1} \right) \right]^2, \quad (\text{C.4})$$

where $P_{\mathcal{R}}(k)$ is the primordial curvature power spectrum. This expression is derived assuming that dark matter is all of the matter. To account for baryons, at late times $z \lesssim 100$, equation (C.4) should be scaled by a factor of about $1/2$.¹³

In order to set initial conditions for evolution of adiabatic perturbations, it is also useful to note that at $y = y_0 \ll 1$,

$$P_{\delta_{\text{ad}}}(y_0, k) \approx 36 P_{\mathcal{R}}(k) \left[3 + \ln \left(0.15 \frac{k}{k_{\text{eq}}} \right) - \ln \left(\frac{4}{y_0} \right) \right]^2. \quad (\text{C.5})$$

D Example: the Uniform-Sphere Momentum Distribution

The calculations in this work are valid for any isotropic initial momentum distribution $f_0(q)$, but in the main text, we focused on the Maxwell-Boltzmann distribution, $f_0(q) \propto e^{-(q/q_*)^2/2}$. Here we show results for a uniform-sphere momentum distribution, $f_0(q) \propto \Theta(q_* - q)$. Figure 13 shows the predicted matter power spectrum evolution at late times for a model with this momentum distribution, along with the separate adiabatic and white noise contributions. Compared with the Maxwell-Boltzmann case (Fig. 4), here the momentum distribution gives rise to oscillations in the adiabatic spectrum (dashed lines), although these do not significantly contribute to the total power spectrum.

In Fig. 14, we compare the analytically predicted white noise power spectrum to the results from an N -body simulation. This simulation is initialized with a uniform-sphere momentum distribution and no initial (adiabatic) perturbations. As in section 3, the particles have mass $780 M_{\odot}$, and the 1D velocity dispersion at matter-radiation equality is $\sigma_{\text{eq}} \approx 22 \text{ km s}^{-1}$. The predicted power spectrum (solid curves) generally matches the simulation results (dots). Deviations only arise at low k due to cosmic variance in the 1.38-Mpc simulation box and at late times, when the density perturbations are approaching the nonlinear regime (gray shaded area).

Figure 15 compares the halo mass function in the simulation with the mass function predicted analytically as in section 3.2. With the mass variance σ_M evaluated from equation (3.1) with $k_{\text{max}} = k_J/4$ (the same ansatz that worked well for the Maxwell-Boltzmann

¹³Baryons remain coupled to the cosmic microwave background until $a \approx 1/125$ (e.g. [183]), which leads to slower growth of dark matter perturbations for $a_{\text{eq}} \lesssim a \lesssim 1/125$.

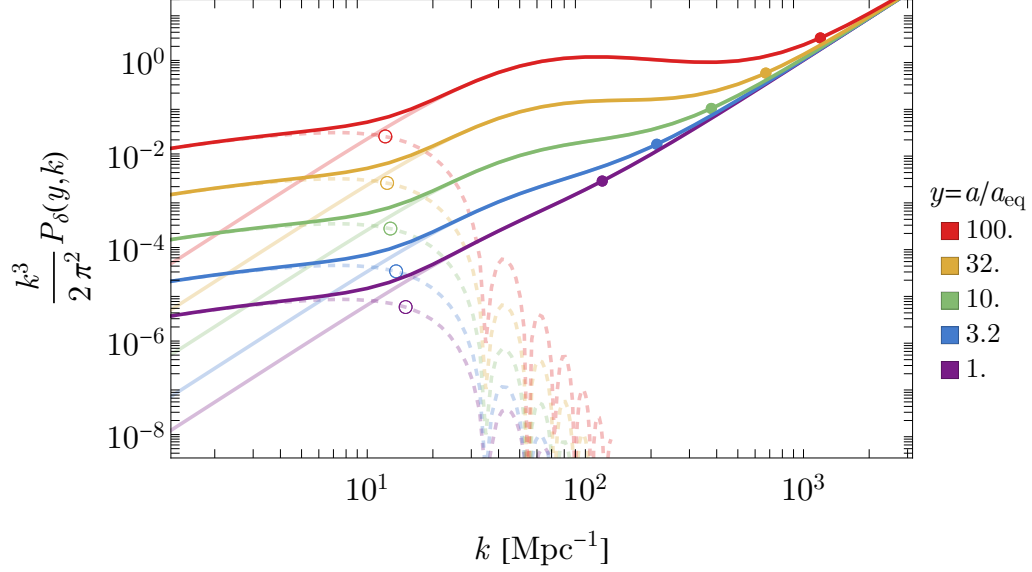


Figure 13: Evolution of the matter power spectrum (solid lines) for the case of a uniform-sphere initial velocity distribution. The lighter curves are the separate adiabatic (dashed) and white-noise (solid) contributions. The open circles on the adiabatic part indicate the free-streaming wavenumber $k_{\text{fs}}(y)$, and solid circles on the white noise part are the Jeans wavenumber $k_{\text{J}}(y)$. Here we set $\sigma_{\text{eq}} \approx 22 \text{ km s}^{-1}$ and $\bar{n} \approx 5 \times 10^7 / \text{Mpc}^3$, and the adiabatic part has an amplitude consistent with Planck 2018 observations. Compare Fig. 4 for the Maxwellian distribution.

momentum distribution), the prediction matches the simulation result generally well, although the abundance of low-mass halos is somewhat overpredicted at early times. Without that ansatz (so $k_{\text{max}} \rightarrow \infty$), the abundance of low-mass halos is overpredicted to a much greater degree.

Finally, we note that the approximation in appendix C does not work as well for the uniform-sphere momentum distribution as it does for the Maxwell-Boltzmann case. For the uniform sphere, it predicts significantly less power at $\alpha_k \gtrsim 1$ than does the exact calculation, leading to a lower predicted halo abundance.

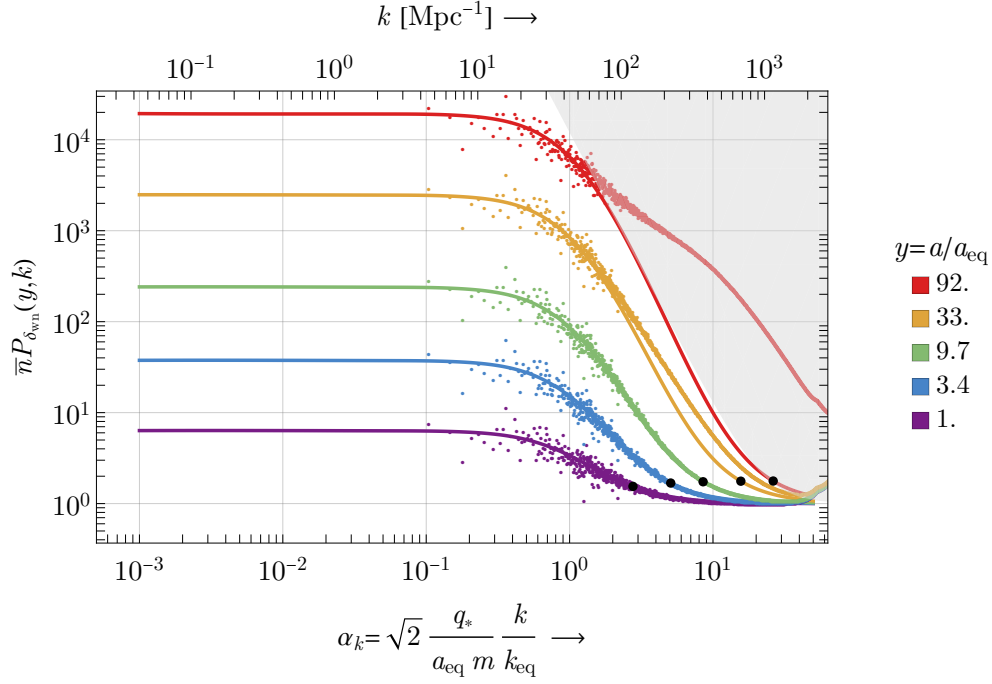


Figure 14: Comparing analytically predicted power spectra (solid curves) with results from an N -body simulation (colored points) for the case of the uniform-sphere momentum distribution. The gray region marks the nonlinear regime, while the black dots mark the Jeans wavenumber k_J . Compare Fig. 6 for the Maxwellian distribution.

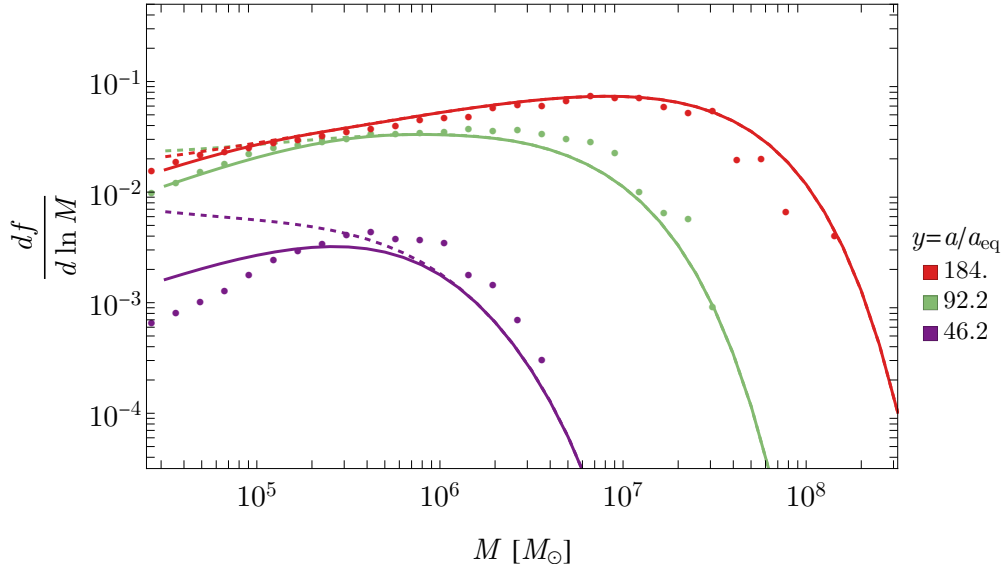


Figure 15: Comparing analytically predicted halo mass functions (solid curves) with results from an N -body simulation (points) for the uniform-sphere momentum distribution. We show the differential fraction of mass (per logarithmic mass interval) in halos of mass M . We evaluate the analytic predictions with the $k_{\text{max}} = k_J/4$ ansatz; the dashed lines show the predictions without that ansatz. Compare Fig. 7 for the Maxwellian distribution.